IO: A GLOBAL GEOLOGIC MAP AND ITS SULFUR VOLCANISM COMPARED TO TERRESTRIAL ANALOGS

By Jessica A. Yff

A Thesis

Submitted in Partial Fulfillment

of the Requirements for the Degree of

Master of Science

in Geology

Northern Arizona University

December 2009

Approved:

_____

Michael H. Ort, Ph.D., Chair

_____

David M. Best, Ph.D.

_____

Laszlo P. Keszthelyi, Ph.D

ABSTRACT

IO: A GLOBAL GEOLOGIC MAP AND ITS SULFUR VOLCANISM COMPARED TO TERRESTRIAL ANALOGS

Jessica A. Yff

Io, the innermost of the four Galilean satellites of the planet Jupiter, is the most volcanically active body in the Solar System. Some intriguing volcanic processes appear to occur on the surface of Io, including possible sulfur flows and dramatic plumes of gas-rich material erupting from volcanic features. The map presented here provides a characterization of the surface features present on Io using the best resolution images available from the Voyager and Galileo spacecraft, that each visited the Jovian system in the 1970s and 1990s, respectively.

Although general models as to the nature of sulfur volcanism on Io have been addressed, very little is known about the character of specific sulfur-rich paterae. This poorly understood type of volcanism is the focus of my second task. To do this, I studied high-resolution imaging of Emakong paterae, to which I compared Volcán Poás in Costa Rica, my terrestrial analog. Volcán Poás is one of the better documented volcanoes with a crater lake/sulfur lake system present at certain stages in its eruptive cycle, and so provides an intriguing comparison to volcanoes on Io. Determining the similarities between the nature of sulfur volcanism on Io and that of a terrestrial analog can provide better models of sulfur volcanism on Io and an overall better understanding of this moon.

ACKNOWLEDGEMENTS

Many thanks to Michael Ort and David Best (NAU). Particular thanks to Laszlo Keszthelyi (USGS) for his continuous stream of ideas and guiding me through this whole process.

Thanks to Ashley, Josh, and Sara who were with me through it all. Special thanks to my mother and sister, who have given me endless support and encouragement. I wouldn't be where I am today without them. And to my Jon, the love of my life, without whom I couldn't have finished this thesis.

TABLE OF CONTENTS

LIST OF TABLES

LIST OF FIGURES

LIST OF PLATES

CHAPTER 1

INTRODUCTION AND SCOPE OF THESIS

1.1 Introduction

Io, the innermost of the four Galilean satellites of the planet Jupiter, is the most volcanically active body in the Solar system. Io currently radiates ~10^{14} W above the background heat flow (Veeder et al., 1994), with about 500 active volcanic centers, approximately 150 of which are erupting at any one time, generating roughly 500 km^3/yr of silicate melts (Radebaugh et al., 2001). Several spacecraft have studied the surface of this moon, notably *Voyager* and *Galileo*, whose imagery has allowed scientists to create a global mosaic of the surface and detect active silicate and sulfur-rich eruptions. For this work, I focused on mapping the surface of Io using mosaics of such images. The map I present here provides a characterization of the surface features present on Io using the best resolution images available. Attention will then be turned to studying the nature of sulfur volcanism seen on the surface with the use of a terrestrial analog, Poás volcano in Costa Rica.

Io orbits Jupiter at a distance of 421,700 km from the planet's center and 350,000 km from its cloudtops. It has a radius of 1821.3 km (0.286 Earths), and is 84.3 km larger in radius than Earth's moon, with a surface area of 41,910,00 km^2 (0.082 Earths). Io takes about 42.5 hours to make one complete revolution around Jupiter, and it is tidally locked so that only one side faces Jupiter. This same situation is present in our own Earth-Moon system. Tidal heating over the course of Io's history due to the strong gravitational pull of Jupiter and nearby moons has produced partially molten conditions within the interior, producing an enhanced internal heat flow that results in volcanic

plumes (Anderson et al., 1996). Other than Earth, Io is the most colorful object in the Solar system. Its color palette is produced by the complex interaction of sulfur-bearing materials with silicates in the intense radiation environment at and near the surface.

The lack of impact craters on Io in spacecraft images at any resolution attests to the high resurfacing rate (0.1 – 1.0 cm/yr) and the dominant role of active volcanism in shaping the surface (Johnson et al., 1979). Io is covered by flows of sulfur, sulfur compounds, and silicates. Its mean density of 3.57 g/cm^3 (Burns, 1986) and rugged topography suggest an interior composed of silicates, similar to the interiors of the Earth and its moon.

Due to the presence of very high temperature lavas on Io, significant implications for Io's interior can be deduced. If, for the past 4 billion years, Io has been as volcanically active as it is today, erupting ~550 km^3/yr of lava (Blaney et al., 1995), it has produced a volume of lava equivalent to approximately 140 times the volume of Io. The interior could therefore be extremely differentiated by multiple episodes of partial melting. Indeed, *Galileo* measurements of Io's mass, radius, and gravitational field suggest that its interior is differentiated between an outer silicate-rich crust and mantle, and an inner iron- or iron sulfide-rich core (Anderson et al., 1996). Models of Io's interior density derived from gravitational data indicate a metallic core, which makes up approximately 20 percent of Io's mass (Anderson et al., 1996). Depending on the amount of sulfur in the core, which is not yet known, the core has a radius between 350 and 650 km if it is composed almost entirely of iron, or between 550 and 900 km for a core consisting of an iron-sulfur mix (Kivelson et al., 2001).

Several scientists have published theories on the thickness of Io's lithosphere, which is composed of basalt and sulfur deposited by many eruptions (e.g. O'Reilly and Davies, 1981; Jaeger et al., 2003; Schenk and Bulmer, 1998). According to Jaeger et al. (2003), the lithosphere is at least 12 km thick and 30 km is a reasonable thickness.

Many new discoveries were made from the wide range of *Galileo* observations. Study of the distribution of different colored materials in *Galileo* SSI images provide insight into the styles of volcanic eruptions that occur on Io (Geissler et al., 1999, 2004). The geologic map presented here will provide the characterization of surface features and their distribution, observations that will have profound implications for future work conducted on the nature of Io's surface and interior, as well as the development of models of Io's geologic evolution to its present state (e.g., Keszthelyi et al., 2004, 2007; Anderson et al., 2001).

With the more accurate color data obtained by *Galileo*, scientists combined the *Galileo* and *Voyager* image datasets to produce a series of high quality grayscale and color global mosaics (Williams et al., submitted). This set of 1 km/pixel global mosaics made it possible for the United States Geological Survey (USGS) to complete the mapping of Io.

1.2 Outline of thesis and justification

I carried out two main projects: the first, and larger, project involved the global geologic mapping of Io. The second involved studying the sources of sulfur volcanism on Io (paterae) and comparing these to a terrestrial analog for sulfur volcanism.

I undertook the global mapping work as part of a collaborative effort led by Dr. David Williams of the School of Earth and Space Exploration, Arizona State University,

(Phoenix, AZ). The project involved several other researchers, including Drs. Laszlo Keszthelyi, Windy Jaeger, Paul Geissler and Tammy Becker of the USGS (Flagstaff, AZ), Dr. David Crown of the Planetary Science Institute (Tucson, AZ), and Dr. Paul Schenk of the Lunar and Planetary Institute (Houston, TX). I mapped Io using ArcGIS software to assess the types and abundances of process-related geologic materials and structures. The map, which is in publication, is a collaborative effort and my own mapping is being incorporated in the final product (Williams et al., submitted). The conclusions and descriptions presented here are built upon those in the submitted manuscript. My mapping allowed me to become familiar with the surface of Io, which was the springboard for the additional work I conducted on Io's volcanism.

Although general models as to the nature of sulfur volcanism on Io have been addressed (e.g. McEwen at al., 2000; Williams et al., 2004, 2005: Lopes at al., 2004), very little is known about the character of specific sulfur-rich paterae. This poorly understood type of volcanism is the focus of my second task. I studied high-resolution imaging of Emakong paterae, to which I compared Volcán Poás, my terrestrial analog. The appearance of sulfur lakes at Volcán Poás following dessication of its crater lake may mimic to some extent the evolution of sulfur volcanism on Io (Oppenheimer and Stevenson, 1989). Volcán Poás is also one of the better documented volcanoes with a crater lake/sulfur lake system present at certain stages in its eruptive cycle, and so provides an intriguing comparison to volcanoes on Io.

Unlike Earth, Io has no water, which is the primary volcanic volatile in the volcanic system of Volcán Poás. Sulfur is ubiquitous on Io, and the dominant volcanic volatile is sulfur dioxide (SO_2). Determining the similarities between the nature of sulfur

volcanism on Io and that of a terrestrial analog can provide better models of sulfur volcanism on Io and an overall better understanding of this moon.

CHAPTER 2

GEOLOGIC MAPPING OF IO

2.1 Previous Work

The first attempts at a global geologic map of Io (e.g., Schaber 1980, 1982; Crown et al., 1992; Figure 1) were based solely on coverage obtained from the 1979 *Voyager* flybys, which imaged approximately one-quarter of the moon and focused on the subjovian hemisphere (the side of Io that always faces Jupiter), and therefore had a limited extent (Schaber, 1980). Regional maps have also been made (e.g., Williams et al., 2002, 2004) from high resolution pictures taken by *Galileo*. These maps were important for gaining experience and determining the most effective mapping procedure for Io, one that has been outlined in detail (e.g. Williams et al., submitted).

The *Voyager* flybys obtained good coverage of Io's subjovian hemisphere at ≤500 m/pixel to 2 km/pixel, and most of the remainder of Io at 5-20 km/pixel (Smith et al., 1979a,b). The extended *Galileo* mission (1998-2002) obtained complementary coverage of Io's antijovian hemisphere (the side of Io that always faces away from Jupiter) in order to study specific features and geologic activity (McEwen et al., 2000; Keszthelyi et al., 2001; Turtle et al., 2004) (Figure 2). The resolution for these flybys ranged from 5 m/pixel to 1.4 km/pixel (McEwen et al, 2000; Keszthelyi et al., 2001; Turtle et al., 2004). As stated in Chapter 1, *Voyager* 1 and 2 covered about one-fourth of the surface of Io and focused on the subjovian hemisphere. Thus, the decision to merge the *Voyager* and *Galileo* data sets was in order to enable the characterization of the whole surface of the satellite at a consistent resolution (Williams et al., submitted).

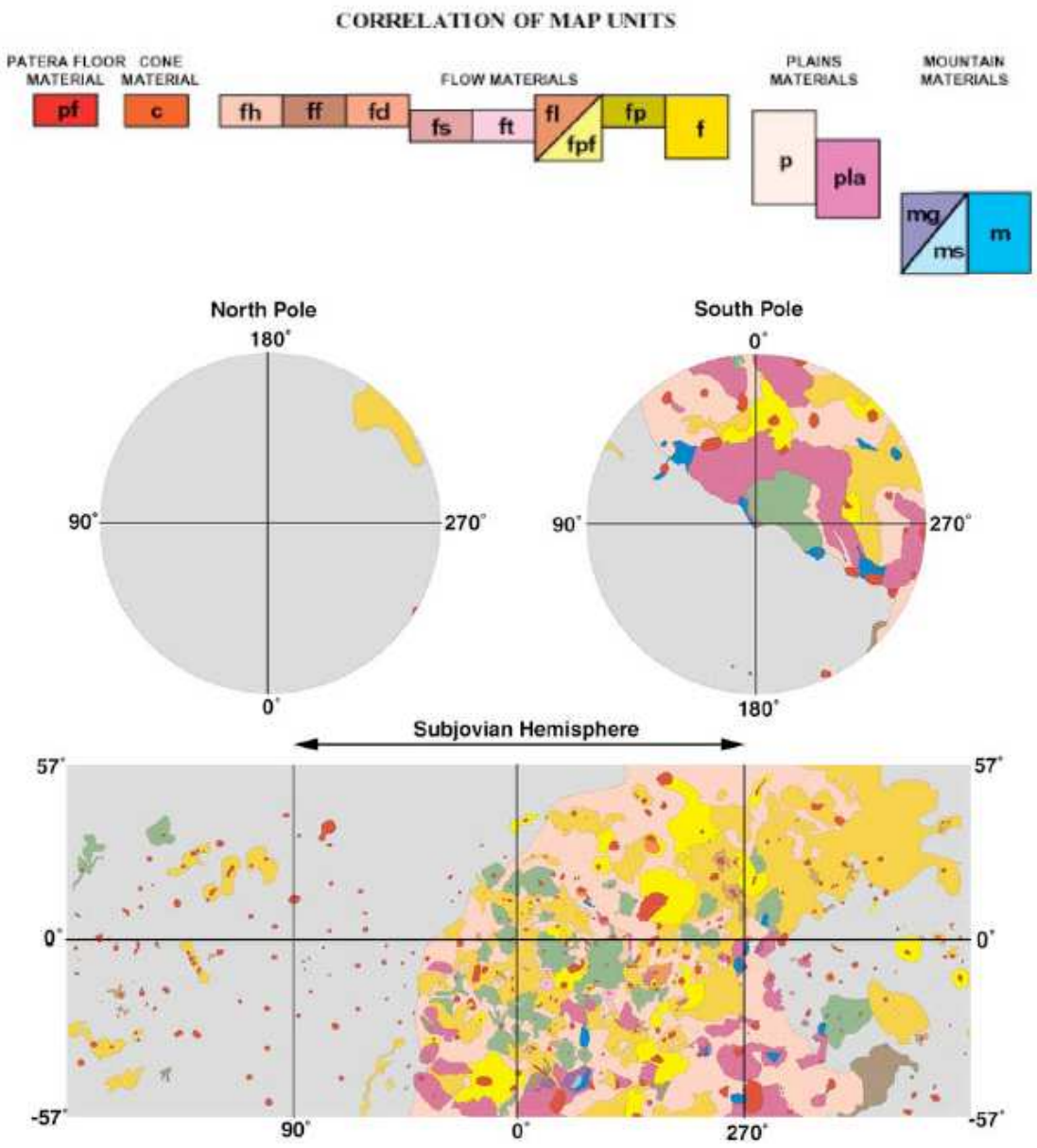

Figure 1: Simplified digital version of the *Voyager*-era global geologic map of Io by Crown et al. (1992). Most of the mapping is concentrated in the subjovian hemisphere, which was well imaged. In contrast, *Galileo* obtained excellent regional and high-resolution coverage of the antijovian hemisphere (Figure 2). By combining the best imaging of *Galileo* and *Voyager*, an improved and more useful global geologic map of Io can be produced. Map digitized by USGS, Flagstaff. Units: pf = patera floor materials; c = cone materials; fh = hummocky flow materials; ff = fissure flow materials; fd = digitate flow materials; fs = shield materials; ft = tholus material; fl = lobate flow materials; fpf = plains-forming materials; fp = patera materials; f = undivided flow materials; p = interpatera plains materials; pla = layered plains materials; mg = grooved mountain materials; ms = smooth mountain materials; m = undivided mountain materials.

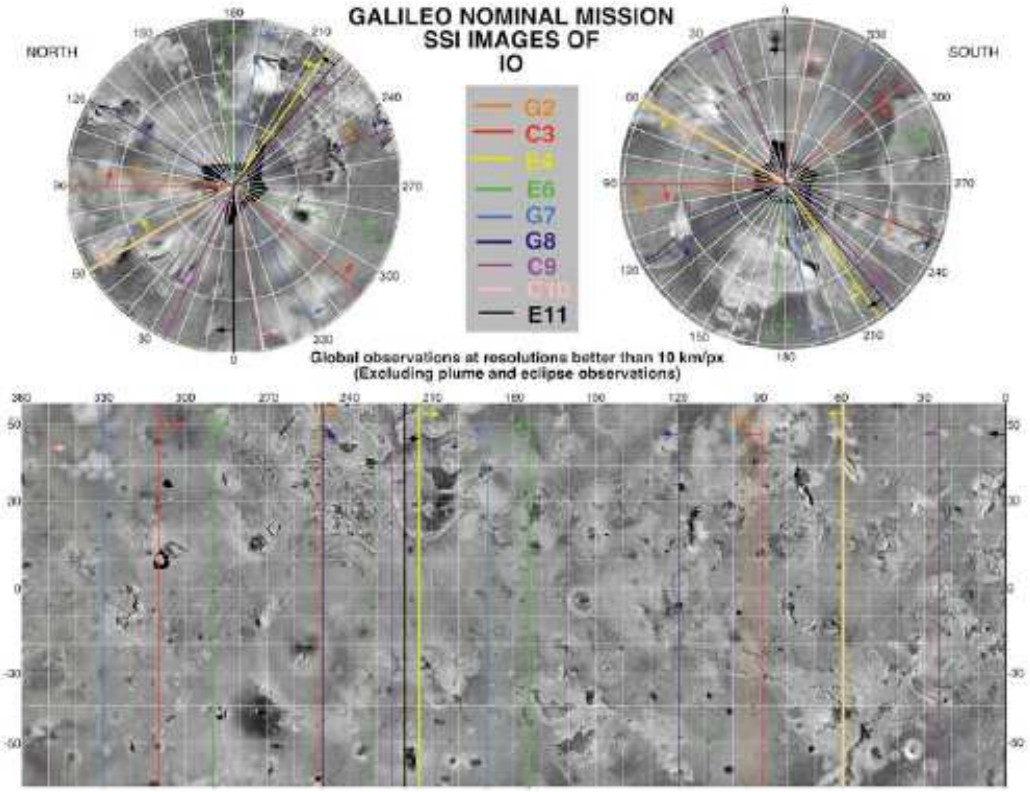
GALILEO NOMINAL MISSION
SSI IMAGES OF
IO
NORTH
SOUTH
G2
C3
E6
G7
G8
C9
E11
Global observations at resolutions better than 10 km/px
(Excluding plume and eclipse observations)

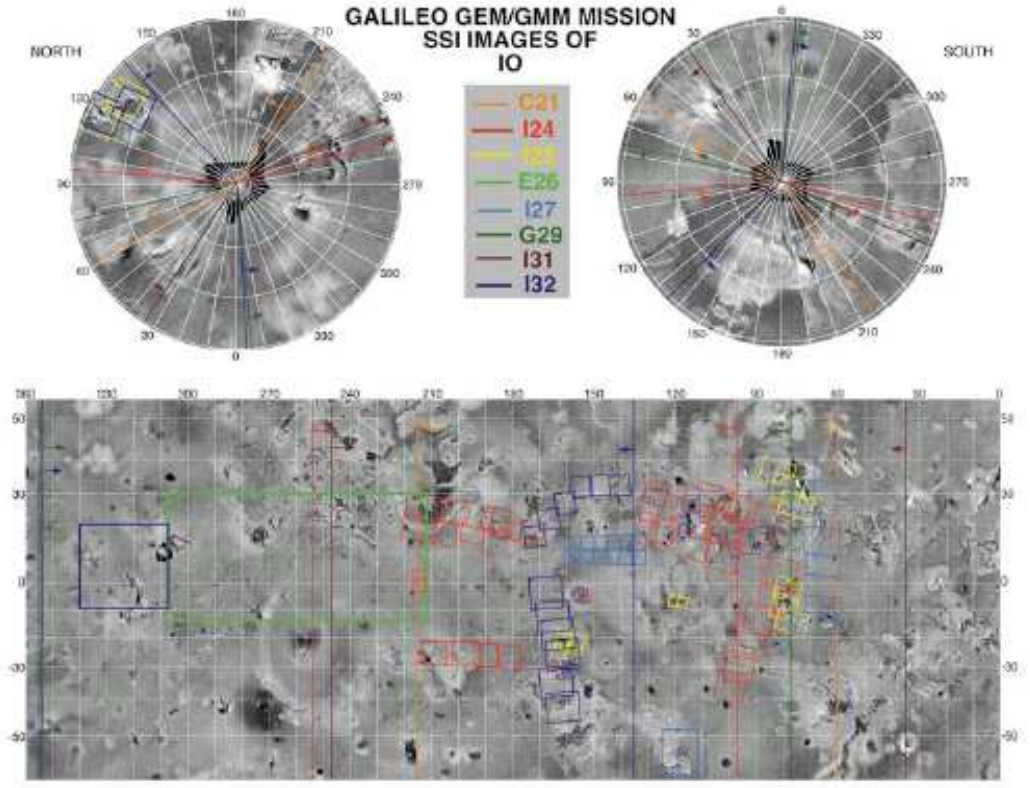
GALILEO GEM/GMM MISSION
SSI IMAGES OF
IO
NORTH
SOUTH
C21
I24
E26
I27
G29
I31
I32

Figure 2: *Galileo* Solid-State Imager (SSI) coverage of Io: (top) Nominal mission coverage; (bottom) Extended mission coverage. The *Galileo* spacecraft obtained multiple global views of Io's surface between 1996-2002, as well as extensive high-resolution coverage of the antijovian hemisphere, which was poorly imaged by *Voyager* (Williams, submitted; Williams et al., in press).

Scientists were able to combine these two image datasets to produce a series of high quality grayscale and color global mosaics with an overall resolution of 1 km/pixel. These mosaics, produced by the U.S. Geological Survey, are now the definitive global image products for Io (Williams et al., in press) (Figure 3).

2.2 Significance

A systematic characterization of surface features and their distribution in time and space is essential for identifying the volcanic and tectonic processes working on and within any planetary body (Williams et al., submitted). Such a map of Io will serve as a fundamental tool that shows the locations, distributions, and timing of the range of material units and the processes that are interpreted to have formed and modified the surface. The term *material unit* refers to the subdivision of geologic units that have been established for Io (Schaber 1980b, 1982). There are four principal classes: mountain materials, plains materials, volcanic flows, and patera floor material (Crown et al., 1992). Other notable features include diffuse deposits, and topographic features (e.g. scarps, ridges, etc.). The mapping I conducted will assist in defining and characterizing surface features into process-related material units and structures, placing them within their stratigraphic context, and enabling recognition of the geologic evolution of areas on varying scales (Shoemaker and Hackman, 1962; Wilhelms, 1972, 1990; Tanaka et al., 1994). The map of Io will also provide a geologic context for mapping of other *Galileo*

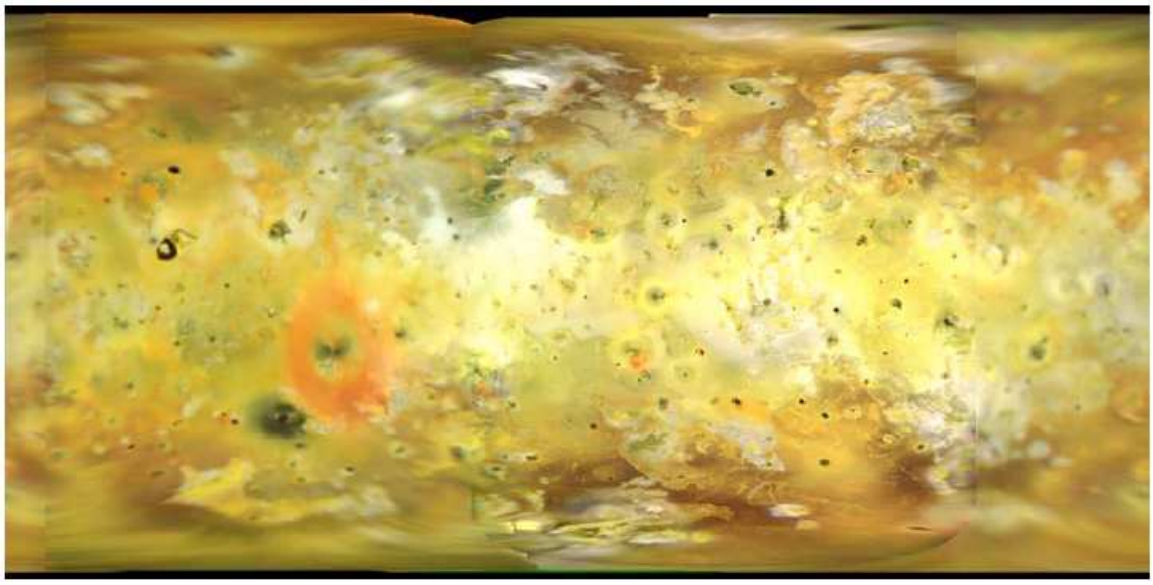

Figure 3a

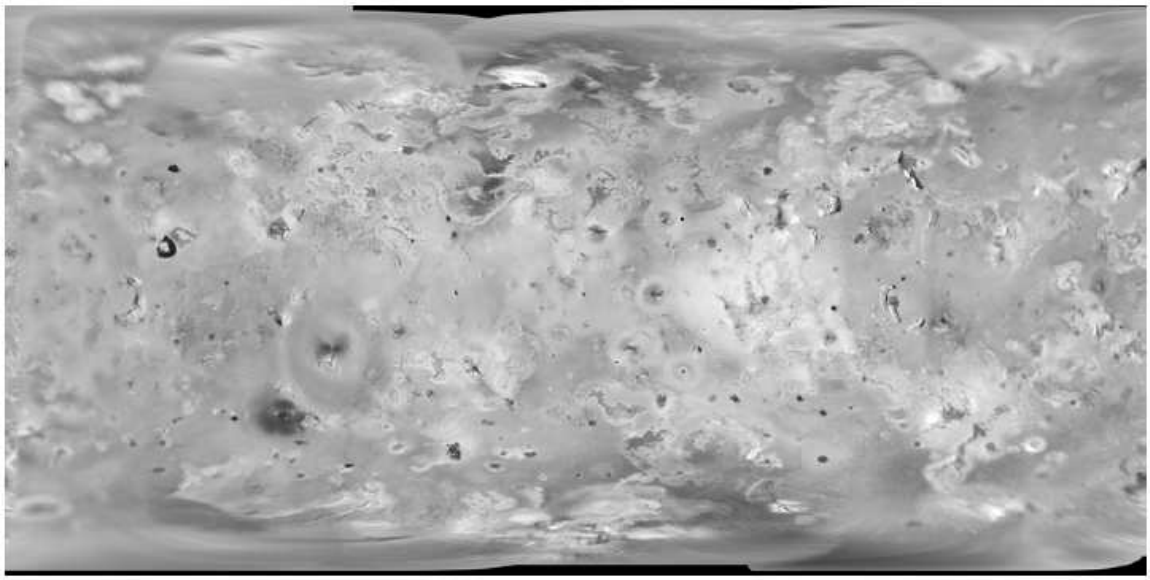

Figure 3b

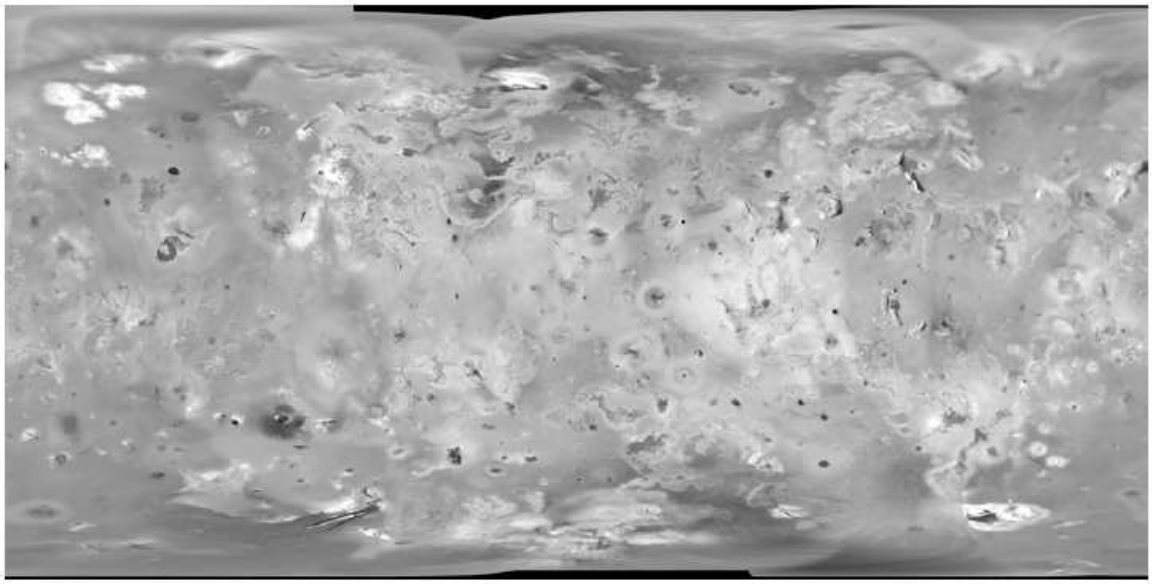

Figure 3c

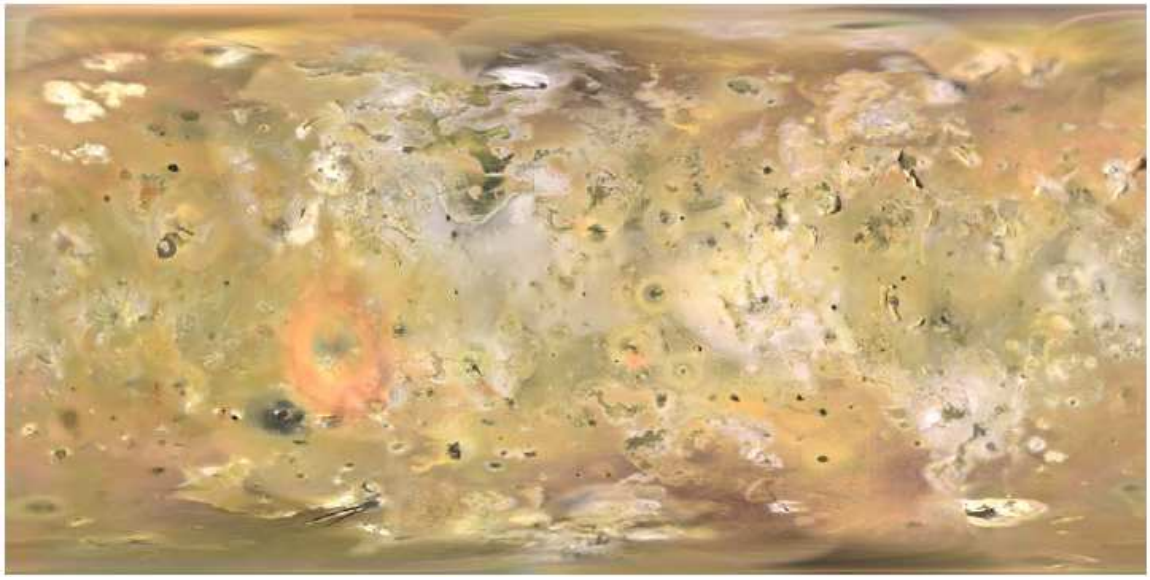

Figure 3d

Figure 3: New global mosaics of Io, produced by the U.S. Geological Survey. 4a: *Galileo* SSI low-phase (4°) color mosaic. 4b: Best resolution *Galileo* SSI monochrome images. 4c: Best *Galileo* SSI coverage of the antijovian hemisphere (right) merged with best *Voyager* Imaging Science Subsystem coverage monochrome images. 4d: Merged product combining *Galileo* images with the higher resolution monochrome mosaic. All mosaics are simple cylindrical projections centered on 180° longitude, with spatial resolutions of 1 km/pixel (Williams, submitted; Williams et al., in press).

observations of Io at regional and local scales, and will reveal potential areas for targeting on future missions.

2.3 Instrumentation

Io has been studied by six spacecraft that have been sent to, or through, the Jovian system: Pioneer 10 (December 1973), *Voyager* 1 (March 1979), *Voyager* 2 (July 1979), *Galileo* (during 34 Galilean satellite flybys: 1995-2002), Cassini (December 2000), and New Horizons (February 2007), each with different instrumental payloads (Table 1).

Spacecraft	Time Period	Instrument	Abbreviation
Voyager	March, July 1979	Imagine Science Subsystem	ISS
		Infrared Interferometer Spectrometer	IRIS
		Photopolarimeter Subsystem	PPS
Galileo	1996-2002	Solid State Imaging Camera	SSI
		Near-Infrared Mapping Spectrometer	NIMS
		Photopolarimeter-Radiometer	PPR
Cassini	December 2000	Imaging Science Subsystem	ISS
New Horizons	September 2006-February 2007	Long Range Reconnaissance Imager	LORRI
		Ultraviolet Imaging Spectrometer	Alice
		Visible and Infrared Imager/Spectrometer	Ralph

Table 1: Geologically relevant instrument payloads of the NASA spacecraft that have visited the Jovian system (Williams et al., in press).

The initial reconnaissance of Io took place during the *Voyager* 1 and 2 flybys in 1979, covering approximately one-quarter of the moon at high resolution and focusing on the subjovian hemisphere. These data allowed for preliminary geologic mapping that led to the production of four regional geologic maps and a global geologic map (Figure 2) (Moore, 1987; Greeley et al., 1988; Crown et al., 1992). These maps were not a complete global picture of the surface, but they succeeded in focusing the debate on important issues regarding the nature of Io's volcanism that were addressed during and after the *Voyager* mission. These included the relative roles of sulfur vs. silicate lavas (Sagan, 1979; Pieri et al., 1984; Carr, 1986), explosive styles of plume eruptions and their volatile sources (Kieffer, 1982; Johnson et al., 1995), the distribution of hot spots and mountains and the implications for Io's crust and mantle (O'Reilly and Davies, 1981; Johnson et al., 1984; McEwen et al., 1985), as well as the sources of Io's high heat flow (Matson et al., 1981; Veeder et al., 1994).

The *Galileo* spacecraft was launched in October 1989, and entered orbit around Jupiter in December 1995; it completed 34 orbits in the nominal (June 1996 – December 1997) and three extended missions (Turtle et al., 2004), collecting many images of the surface of Io. The mission ended with *Galileo* plummeting into Jupiter's atmosphere in September 2003. The nominal mission acquired global coverage of Io three times, and included five close flybys of Io, focusing mostly on the antijovian hemisphere, to study specific features and processes (McEwen et al., 2000; Keszthelyi et al., 2001, Turtle et al., 2001, 2004) (Figure 3). This imaging enabled intensive study of specific volcanic and tectonic features, producing many new insights into Io's geologic activity (e.g., McEwen et al., 1998b, 2000; Keszthelyi et al., 2001; Turtle et al., 2004).

Keszthelyi et al. (2004) summarizes the instrument complement of the *Galileo* spacecraft, which covered most of the electromagnetic spectrum. Of particular interest to Io investigations were the gravity and magnetometer experiments, as well as a set of remote sensing instruments: the Solid State Imager (SSI), Near Infrared Mapping Spectrometer (NIMS), and Photopolarimeter–Radiometer (PPR). SSI collected 800 x 800 pixel images between 0.4 and 1.0 μm using eight color filters. Image resolutions varied from tens of kilometers per pixel to 5 m/pixel (Turtle et al., 2004). NIMS covered between 0.7 and 5.2 μm and built up images in vertical strips (Lopes-Gautier et al., 2000). NIMS spatial resolution varied between hundreds of kilometers per pixel to hundreds of meters per pixel (Lopes et al., 2004). PPR took broadband observations, from visible wavelengths to 100 μm, and built up images by scanning across the target. Much of the data was collected at 17 and 21 μm and images ranged in resolution from hundreds of kilometers per pixel to a few kilometers per pixel (Spencer et al., 2000a; Rathbun et al., 2004; Keszthelyi et al., 2004).

2.4 Constraints involved in Io mapping

2.4.1 Nature of Flyby Imaging

Certain limitations are inherent in imaging another planetary body. One major consideration is the variety of phase angles at which images were taken. The *Galileo* and *Voyager* missions at Io occurred as a series of flybys, and the images that were obtained have a wide range of phase angles, lighting conditions, and image resolutions. Varying phase angles are the result of images taken with spacecraft at different positions during the flybys. Also, the varying times of 'day' at which images are taken and differing distance from the surface (i.e. angles) give various lighting condition. This lack of

uniformity in Io imaging coverage (i.e., much global (>1 km/pixel) imaging, limited regional (>100 m/ pixel - <1 km/ pixel) imaging, and rare local (<100 m/ pixel) imaging) placed limits on the level of detail of the mapping that was possible.

2.4.2. Nature of Io's Activity

As noted by Geissler et al. (1999, 2004), the bulk of the surface changes on Io due to volcanism are caused by eruptions from a few very active vents. The initial analysis of *Galileo* global images shows that large areas of the surface (~83 percent) had no discernable changes between the *Voyager* and *Galileo* missions (Geissler et al., 2004). The observation that changes in Io's surface activity are related to localized volcanic sources rather than large-scale global processes has implications for a mapping approach using the global mosaics. Specifically, an approach centered on formations (i.e. sets of related geologic units focused on a specific source of activity, such as patera, mountains, etc.) may be indicated. The planned GIS database will allow linkage of multiple *Galileo* observations showing surface changes to our base map, in order to help users gain more insight into geologic activity at specific locations.

2.4.3 Role of Color

Interpreting colors on Io has been significant in trying to understand the geologic activity occurring there (e.g., Geissler et al., 1999; Phillips, 2000; Spencer et al., 2000). In using color, however, it is important to recognize some issues that are intrinsic to the remote collection of images on another planetary body. Several instruments were used for color images (Table 2), most notably the SSI (solid state imaging camera). This instrument used various filters and different wavelengths to obtain all the colors we see (and use for mapping) in the mosaic. The Solid State Imaging (SSI) camera on the

Galileo spacecraft used an 800 x 800 pixel charge coupled device (CCD) as its detector (Klaasen et al., 2003). Exposure time, gain state, filter, summation mode, and compression mode were the primary parameters that could be adjusted. For Io, the filters used were primarily the violet (413 nm), green (559 nm), red (665 nm), near-IR (756 nm), 1 μm (> 968 nm). In addition, a clear filter composed of a broad wavelength filter with

Mosaic	Filter-Wavelengths Used	Phase angle (°)	Data Sources	Comments
Galileo SSI-only low-phase color	765nm-GRN-VIO	4	57 images from *Galileo* orbits G2, E6, C9, C21, I31	Use for mapping colorful diffuse deposits
Galileo SSI-only monochrome	CLR, GRN, 756nm	Various	32 images from *Galileo* orbits G1, G2, C3, E6, G7, C9, C10, E11, C21, C22, I24	Use for mapping surface morphology-Antijovian hemisphere
Combined Galileo-Voyager monochrome	GLL: CLR, GRN, 756nm; VGR: CLR, BLU	Various	50 *Voyager 1* images, 32 *Galileo* images (see above)	Use for mapping surface morphology-Subjovian hemisphere
Merged *Galileo-Voyager* monochrome and SSI low-phase color	See above	Various, Color = 4°	See above	Use for correlating mapped features with color-compositional relationships

Table 2: List of the new Io global mosaics produced by the USGS, combining *Galileo* and *Voyager* images. All mosaics have a spatial resolution of 1 km/pixel (*Williams et al.*, in press).

an effective wavelength of 652 nm that was used for the majority of the high-resolution images. The violet filter was most useful for detecting SO_2-rich plumes and deposits. The green and red filters, in combination with the violet filter, provided the best "true-color" data from Io. The 756 nm filter was often used in place of the red filter to provide enhanced discrimination of color variations. The 1 μm and clear filters, in combination, provided the best constraints on the temperatures of active lavas (e.g., McEwen et al., 1998b; Radebaugh et al., 2004; Turtle et al., 2004).

1) *Galileo* SSI color images of Io are only an approximation of the "true" color that would be seen by the unaided human eye.

2) Surface colors on Io change their hues with variations in lighting conditions (e.g., Geissler et al., 2000). These optical property changes can cause problems for color interpretation due to the widely different geometries of the *Galileo* spacecraft's various encounters with Io (Geissler et al., 1999, 2000). Thus, for consistency in geologic mapping, it is important to use color images that were obtained at a single, preferably low, phase angle.

3) Io's heavy radiation environment causes the colors of some surficial deposits to change as they age. Dark materials tend to brighten with time, as they develop coatings of sulfurous materials from plume deposits (Nash et al., 1986). In contrast, bright materials tend to darken over time, as they interact with underlying or superposed materials (e.g., Williams et al., 2002). Kargel et al. (1999) studied the effects of these processes on sulfurous materials, which indicated that these color changes occur on timescales geologically important for Io, on the order of days to years (Williams et al., 2002). Kargel et al. (1999) went further to study the possibilities that minor and trace components (i.e. impurities) in elemental sulfur also affect Io's reflectance and alter the physical properties of sulfur.

2.5 Mapping Process

2.5.1 Background

The mosaics, compiled by the USGS, consist of the best images (spatial resolution ~1 km/pixel), in both black and white and color, compiled from the *Voyager* and *Galileo*

missions. The Io mosaic is a set of four global mosaics at a spatial resolution of 1 km/pixel (Becker et al., 2005), released in February 2005. Four distinct image products were created by the USGS, and were used in this mapping project: (1) a global mosaic of *Galileo* Solid State Imager (SSI) color images; (2) a global mosaic of the best resolution *Galileo* SSI monochrome images; (3) a global mosaic of the best resolution *Voyager* Imaging Science Subsystem (ISS) and *Galileo* SSI monochrome images; and (4) a merged product combining *Galileo* color images with the higher resolution monochrome mosaic (Williams et al., submitted; Figure 3).

Poor overall resolution of some areas (especially the north pole) made it difficult to definitively determine what some features were. The final USGS publication, therefore, is the product of two additional mapping efforts: David Williams (Arizona State University, Phoenix AZ) and David Crown (Planetary Science Institute, Tucson AZ) also conducted their own mapping of the surface, and the final map is a compilation of our interpretations, agreements being reached on those features that were equivocal.

The global mapping of Io was performed following standard principles for the geological mapping of planetary surfaces (Shoemaker and Hackman, 1962; Wilhelms, 1972, 1990; Tanaka et al., 1994), building on the experience gained from work on the *Voyager*-era Io map (Crown et al., 1992) and on local mapping from high-resolution *Galileo* images (e.g. Williams et al., 2002, 2004). This approach allowed the spatial co-registration and comparison of all geographically referenced data sets. For example, NIMS and PPR hotspot locations were accurately correlated with volcanic features seen in SSI images (Williams et al., in press), and mountain locations were confirmed from limb measurements. Io lacks a significant atmosphere, and so limb measurements of

mountains are the most accurate measure of location and height of mountains on the surface. A prime element of *Galileo*'s instrument payload was the SSI, a slow-scan planetary imaging system, consisting of an 800- by 800-pixel solid-state camera consisting of an array of silicon sensors called a 'charge-coupled device' (CCD). The optical portion of the camera was built as a Cassegrain (reflecting) telescope. Light was collected by the primary mirror and directed to a smaller secondary mirror that channels it through a hole in the center of the primary mirror and onto the CCD (Clary et al., 1979). The CCD imaging from many different longitudes has provided data of highly accurate relative measurements in a plane. When these measurements are of an object that is assumed to be ellipsoidal (which Io is), they provide a shape and size measurement of features on the surface (Thomas et al., 1998). Mountain locations and heights of Io's mountains were obtained in this manner.

2.5.2 Description of units and mapping

A detailed description of the units that I mapped follows along with interpretations. In ArcGIS, the globe is divided into three sections, or group layers. The first group layer contains the mosaics of the equatorial region, which spans -50 to 50 degrees longitude. The other two group layers contain the mosaics for the north and south poles, respectively. In mapping each group of features, discussed below, I started with the equatorial region and systematically visually mapped 30-degree longitudinal slices of the mosaic. I mapped five different groupings of geomorphologic features, each of which I will expand upon in the following section. I first mapped diffuse deposit contacts, after which I focused on lava flows and volcanic features. I then mapped topographic features (mountains, scarps, etc.), and then finally plains features, which

consisted of those areas left over after the mapping of the preceding three features. The areal coverage of each material unit as a percentage of Io's surface area was then determined (Table 3, 4; Figure 4).

Material Unit	Area (km^2)	Area (%)	Material Unit	Area (km^2)	Area (%)
Red-brown plains	1.41E7	33.4	Bright patera floors	1.84E5	0.4
Bright (yellow) plains	7.68E6	18.4	Dark patera floors	1.93E5	0.5
White plains	3.75E6	8.9	Undivided patera floors	6.75E5	1.6
Layered plains	1.84E6	4.4	*Total Patera Floors*	1.05E6	**2.5**
Region of poor resolution (Likely R-b plains)	7.20E5	1.7			
			Bright lava flows	1.80E6	4.3
Total Plains	2.81E7	**66.6**	Dark lava flows	1.23E6	2.9
			Undivided lava flows	8.70E6	20.6
Lineated mountains	6.40E5	1.5	*Total Lava Flows*	1.17E7	**27.8**
Mottled mountains	8.05E4	0.2			
Undivided mountains	5.54E5	1.3	Bright (yellow) diffuse dep.	8.76E5	2.1
Tholi (domes)	5.25E4	0.1	White diffuse deposits	2.90E6	6.9
Total Mountains	1.33E6	**3.1**	Red diffuse deposits	3.61E6	8.6
			Dark diffuse deposits	2.68E5	0.6
			Green diffuse deposits	4.09E3	0.01

Note: Diffuse deposits are superposed on all other materials, and cover 18.2% of Io's surface.

Table 3: Distribution of geologic material units as a percentage of Io's surface area (Williams et al., submitted).

2.5.2.1 Diffuse Deposits

The first round of mapping focused on diffuse deposit contacts. These deposits are concentrated in areas where paterae are present, consistent with them being the product of volcanic eruptions. The color of the diffuse deposits indicates their relative age, since sulfur, once exposed to surface conditions, gets lighter with age and exposure to vacuum weathering on Io (e.g. Nash and Moses, 1988). The north polar region has plentiful diffuse deposits, but a large portion was not imaged well by any of the spacecraft sent to image Io, so much of the north polar region cannot be mapped with certainty. The south pole is generally well-imaged and also has extensive diffuse deposits.

The more accurate color imaging and higher resolution of the *Galileo* SSI has been invaluable in recognizing the diversity of diffuse deposits on Io's surface. The five

Map Unit	Abbreviation	Coordinates
Yellow Bright Plains	p_{by}	-25°, 175°
White Bright Plains	p_{bw}	15°, 195°
Red-Brown Plains	p_{rb}	-55°, 135°
Layered Plains	p_l	-7°, 165°
Dark Flows	f_d	23°, 115°
Bright Flows	f_b	13°, 149°
Undivided Flows	f_u	-37°, 165°
Bright Tholi	t_b	0°, 163°
Dark Patera Floors	pf_d	-28°, 160°
Bright Patera Floors	pf_b	13°, 142°
Undivided Patera Floors	pf_u	-26°, 158°
Lineated Mountains	m_l	-26°, 162°
Mottled Mountains	m_m	-28°, 165°
Undivided Mountains	m_u	-49°, 336°
Yellow Diffuse Deposits	d_b	19°, 141°
White Diffuse Deposits	d_w	-37°, 163°
Dark Diffuse Deposits	d_d	-40°, 272°
Red Diffuse Deposits	d_r	-22°, 161°
Green Diffuse Deposits	d_g	-20°, 160°

Table 4: Latitude-Longitude coordinates of type examples of map units shown in Figure 4 (Williams et al., submitted).

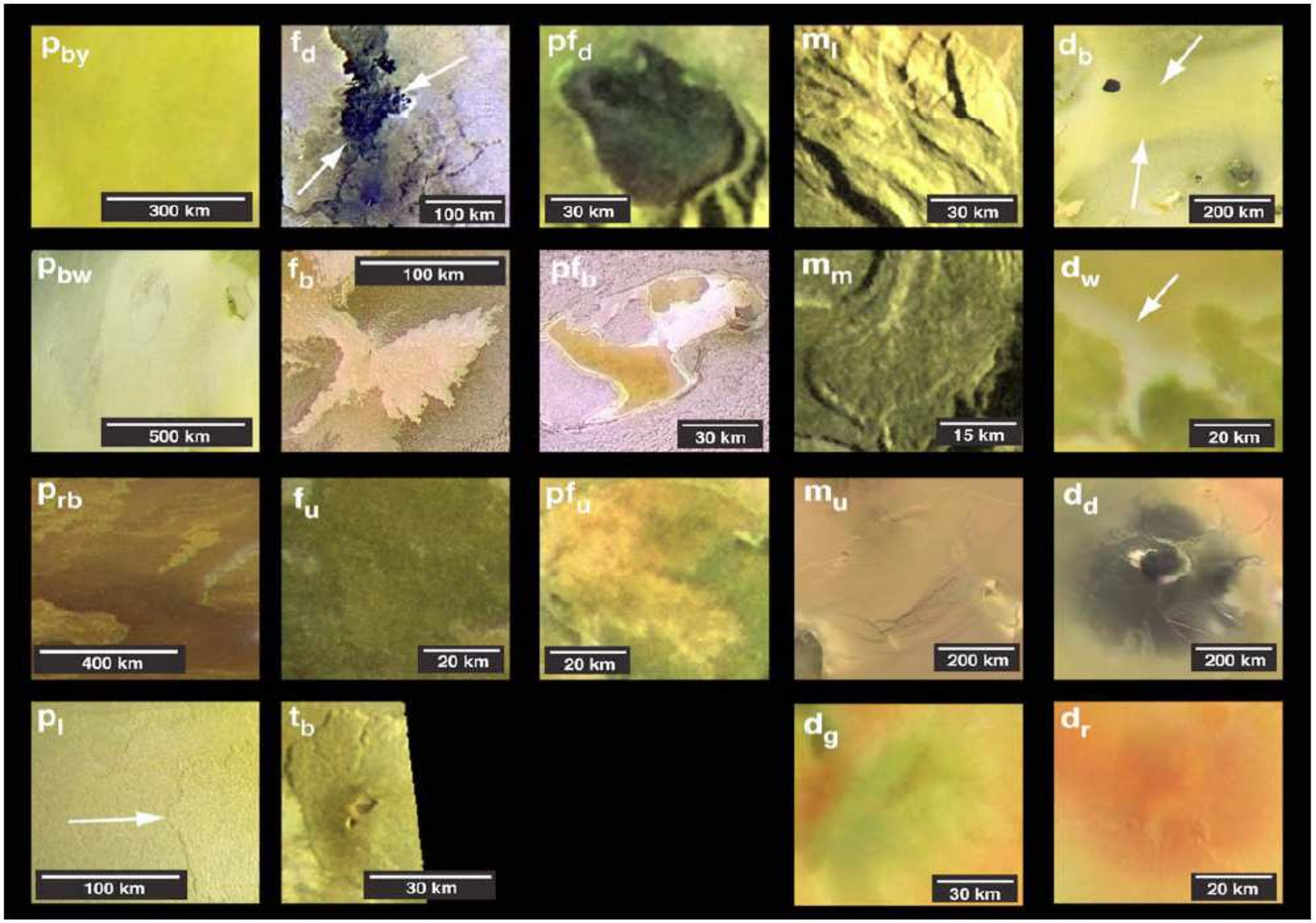
p_{by}
300 km
f_d
100 km
pf_d
30 km
m_l
30 km
d_b
200 km
p_{bw}
500 km
f_b
100 km
pf_b
30 km
m_m
15 km
d_w
20 km
p_{rb}
400 km
f_u
20 km
pf_u
20 km
m_u
200 km
d_d
200 km
p_l
100 km
t_b
30 km
d_g
30 km
d_r
20 km

Figure 4. Color type examples of material units proposed for the global geologic mapping of Io. Bright plains materials (p_b), white plains materials (p_w), red-brown plains materials (p_{rb}), layered plains materials (p_l), bright patera floor materials (p_{fb}), dark patera floor materials (p_{fd}), undivided patera floor materials (p_{fu}), bright flow materials (f_b), dark flow materials (f_d), undivided flow materials (f_u), lineated mountain materials (m_l), mottled mountain materials (m_m), tholus material (t_b), cone material (c), white diffuse material (d_w), bright diffuse material (d_b), dark diffuse material (d_d), red diffuse material (d_r), green diffuse material (d_g) (Williams et al., submitted).

recognized types of diffuse deposits appear to thinly mantle underlying materials and, in most instances, occur as circular patches around active vents. These circular patches are interpreted as the results of umbrella-like plume eruptions. This type of eruption was imaged in action by the New Horizons spacecraft's Long Range Reconnaissance Imager (LORRI) at the Tvashtar caldera complex near the north pole of Io. Two frames of this 330-km high plume were captured on February 28, 2007 (Spencer et al., 2007) from a range of 2.7 million kilometers (Figure 5).

White Diffuse deposits (d_w) occur as circular patches around active vents and also as irregular patches around grooves on mountains or in the plains. They are thought to be dominated by condensed SO_2 gas (Williams et al., submitted).

Bright Diffuse deposits (d_b), recognized around some volcanoes, can occur as circular patches around active vents and as irregular patches extending away from active vents or structural features. They generally cover larger extents than do white diffuse material and are thought to be pyroclastic deposits, likely colored by sulfur-bearing particles (Williams et al., submitted).

Red Diffuse deposits (d_r) occur as either circular deposits around active vents or as asymmetrical deposits on one side of vents. They are pyroclastic deposits, thought to

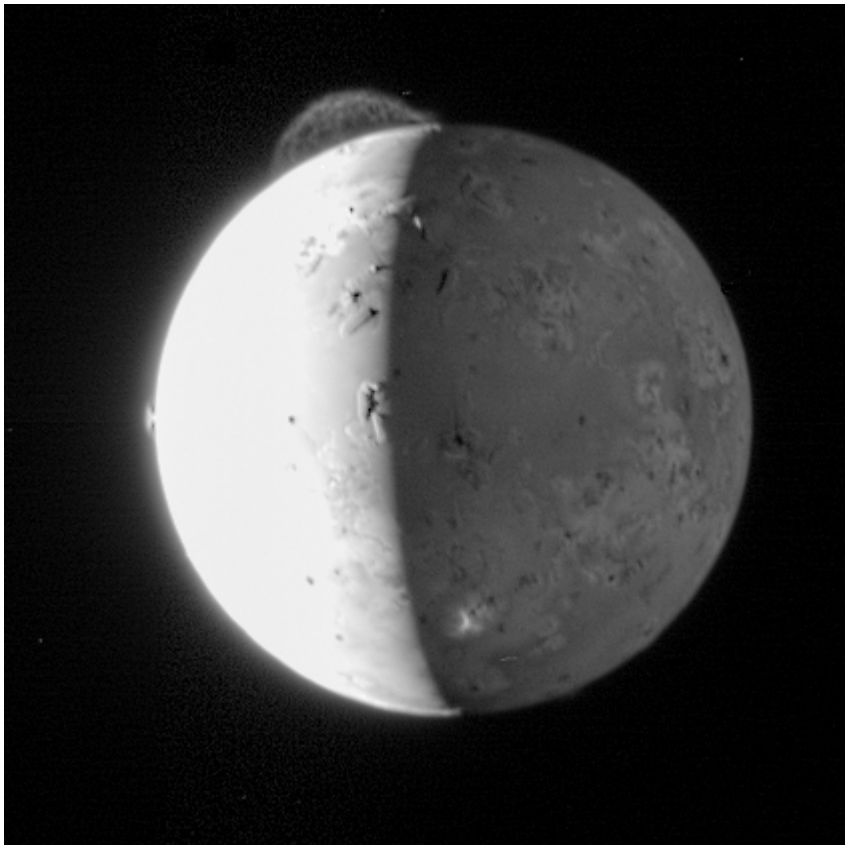

Figure 5: Tvashtar plume, imaged by New Horizons; LORRI in Feb 2007. Source: Science.NASA.gov

be rich in metastable short-chain sulfur polymers (S3, S4: Spencer et al., 2000; Williams et al., submitted).

Dark (low-albedo) Diffuse deposits (d_d) occur in the same manner that red diffuse deposits do. They have been interpreted as pyroclastic deposits derived from mafic to ultramafic silicate lavas (Williams et al., submitted).

Green Diffuse deposits (d_g) occur around active vents and underneath or near active plumes (Williams et al., 2004). They have been interpreted to be the result of the alteration coating produced by the interaction of red diffuse deposits with warm silicate lava flows (Williams et al., submitted).

2.5.2.2 Lava flow material units

After the diffuse deposits were identified, I focused on drawing the contacts of volcanic centers and their associated lava flows, which I found to be the most interesting aspect of the mapping process (Figure 4; Table 4). Many individual lobes of lava can be traced for hundreds of kilometers. For example, the longest lobe measured from images of Amaterasu patera stretches approximately 376 km.

Lava-flow material units were characterized by their albedo and color, which in turn relate to their inferred composition. Dark flows (f_d), bright flows (f_b), and undivided flows (f_u) are all characterized as smooth (hundreds of meters scale) to rough and platy (tens of 100 meters scale) lobate flows, with lengths greater than their widths. Contacts with surrounding terrain are sharp, and the variation in albedo and cross-cutting relations can be used to define age relations in some cases, as younger flows tend to be darkest (e.g. Williams et al., submitted).

Dark Flow materials (f_d), as their name suggests, have a low albedo and correspond with high-temperature hot spots, as has been noted in NIMS and PPR observations (Lopes at al., 2001; Williams et al., 2002). They are believed to be produced from mafic to ultramafic silicate eruptions (McEwen et al., 1998a; Williams et al., 2000; Keszthelyi et al., 2001; Williams et al., submitted).

Bright Flow materials (f_b) have a high relative albedo and NIMS hot spots rarely correlate with them (Williams et al., 2004). They are composed of sulfur or sulfur-rich compounds, which are much cooler than dark flows (Williams et al., submitted).

Undivided Flow materials (f_u) have an intermediate albedo and a range of colors. The contacts with surrounding terrain are less sharp than bright or dark materials. They are believed to be flows of intermediate composition and most likely source from various

older sulfurous or silicate effusive eruptions related to bright or dark materials (Williams et al., submitted). Io's volcanism will be discussed in greater detail in the next chapter.

2.5.2.3 Topographic Features

I then identified topographic features, which include mountains, scarps, ridges, topographic highs and lows, grooves and furrows, and lineaments (Figure 4; Table 4). Mountains, in a similar manner to paterae, also appear to have a grouping near the equator, and I conducted similar statistical analyses as the paterae on these features to determine any statistical significance. The results are presented later in this chapter.

Mountains, layered plateaus, and other materials delineated by scarps and other structural features were mapped using the monochrome mosaic supplement with low-sun images. From *Voyager* images, Crown et al. (1992) mapped a wide range of structural features in the subjovian hemisphere, including scarps, ridges, graben, lineaments, faults, and circular depressions (pits and patera rims). These same structures were often seen on the surface in the new mosaics, and mapped where resolvable (Williams et al., submitted). Mountain materials are summarized as follows:

Lineated Mountain material (m_l) consists of dark yellow to greenish-brown to yellow-white positive relief edifices in color images. The bounding scarps of these edifices are well-defined and the surface exhibits grooves, ridges, scarps, and lineaments. These features generally have heights of >1-2 km, based on shadow measurements or stereo observations (Williams et al., submitted). Carr et al. (1998) summarized the process for collecting shadow measurements of mountains on Io: places were sought where shadows were cast by an object onto nearby plains, which are assumed to be level for this purpose. The length of the shadow was measured and the peak height estimated

from the illumination conditions. Errors arise because of the inability to exactly determine the edge of the shadow and the part of the peak casting the shadow. Stereo image pairs were also used to determine mountain height. The pairs were obtained by taking images from different points of the same area, from which digital elevation maps (DEMs) were generated using an automated stereogrammetry program (Schenk and Bulmer, 1998). These lineated mountains are sections of tectonically formed mountains, and are probably deeper crustal material uplifted along faults (e.g. Schenk and Bulmer, 1998; Jaeger et al., 2003).

Mottled Mountain material (m_m) consists of dark yellow to greenish-brown to yellow-white positive relief edifices with mottled lobes lacking in structural features. They generally have heights of >1-2 km (Williams et al., submitted). These are likely sections of tectonically-formed mountains that have undergone displacement by mass-wasting processes (Turtle et al., 2001).

Undivided Mountain material (m_u) is difficult to categorize. They are yellow-gray to yellow-white positive-relief edifices that lack features diagnostic of either Lineated or Mottled Mountain materials. These units are commonly completely, or at least partially, covered with diffuse deposits. They generally have heights of >1-2 km. They are believed to be uplifted crustal blocks whose detailed morphology cannot be determined (Williams et al., submitted).

Bright Tholus materials (t_b) are positive-relief edifices, circular to elliptical in planform, with colors and albedo similar to Bright Plains material, with heights of >1-2km. They typically contain one or more circular central pits near the top and center of the edifices. These are volcanically derived mountains, including shield volcanoes and

composite cones that may be largely composed of silicate or sulfurous materials (Williams et al., submitted).

2.5.2.4 Patera floor materials

Patera floor materials have a range of albedos and fill volcano-tectonic depressions, although they commonly extend outside and around these paterae (Figure 4; Table 4). They come in three colors: bright (p_{fb}), dark (p_{fd}) and undivided (p_{fu}) patera floor materials. Various colors suggest different compositions, including mixes of silicates, sulfurous compounds, and relatively pure sulfur dioxide in some cases (Williams et al., 2002, 2004; Lopes et al., 2001).

Bright patera floor material (p_{fb}) is a bright pinkish-white to red-orange unit with smooth surfaces at the tens to hundreds of meters scale. *Galileo* NIMS data indicate an enhanced signature of sulfur dioxide in the white to pinkish-white material on several patera floors (Lopes et al., 2004), where the brightest material is freshest. They are thought to be sulfur-bearing lava flows, lava ponds, or lava lakes that may or may not contain significant amounts of SO_2. Surfaces may also form as coatings on cold silicate lavas in less active paterae or as melting or sublimating plains material remobilized by heat from intrusions (Keszthelyi et al., 2004; (Williams et al., submitted).

Dark patera floor material (p_{fd}) is a dark gray to black unit that has distinct contacts with the surrounding terrain. This material commonly correlates with NIMS and PPR hot spots (Williams et al., submitted). These are believed to be silicate lavas that may or may not be coated by sulfurous materials, or intermingled with various warmer silicate and sulfur flows; black surfaces are likely warm, most recently emplaced,

coalesced silicate lava flows, crusted lava ponds or lava lakes (Lopes et al., 2001; Davies et al., 2001; Radebaugh et al., 2004).

Undivided patera floor material (p_{fu}) is an intermediate gray to brown unit that has indistinct contacts with surrounding terrain, usually underlying or adjacent to bright or dark patera floor materials. These are thought to be coalesced lava flows, crusted lava ponds or lava lakes of indeterminate composition that may or may not be coated by sulfurous materials (Williams et al., submitted).

2.5.2.5 Plains materials

Finally, the regions that were left over after mapping the features described above were mapped as plains materials, which come in a variety of colors and types (Figure 4; Table 4). Plains materials cover more than 70 percent of Io's surface (Geissler et al., 1999), and appear in SSI color images as bright/yellow (p_{by}), gray-white (p_w), and red to red-brown (pr_b) color units. There are also layered plains materials (p_l).

The yellow bright plains material (p_{by}) is a unit with various shades of yellow in color images, and appears smooth and bright at global scale, appearing increasingly layered and hummocky at higher resolution. They exhibit a variety of geomorphologic structures such as scarps, grooves, pits, mesas, graben-like depressions, and channel-like features in some regions. These plains materials have been interpreted as a heterogeneous mixture of silicate and sulfur-rich materials, in the form of lava flows, pyroclastic deposits, or both, without clear margins or source regions (Williams et al., submitted).

White bright plains materials (p_{bw}) have smooth surfaces at low resolution; layered and hummocky surfaces at high resolution, and are white to white-gray in color.

Hummocky texture and mantling may occur as described above. These are a heterogeneous mixture of silicate and sulfur-rich materials, in the form of lava flows, pyroclastic deposits, or both, without clear margins or source regions, dominated by sulfur dioxide snow and frost (Douté et al., 2001, 2002) on the upper surface (Williams et al., submitted).

Red-brown plains materials (p_{rb}) have a smooth surface at low resolution, layered and hummocky surface at high resolution, and are red to red-brown in color. These are a heterogeneous mixture of silicate and sulfur-rich materials, in the form of lava flows, pyroclastic deposits, or both, without clear margins or source regions (Williams et al., submitted).

Layered plains material (p_l) are the result of portions of yellow, white, or red-brown plains materials that are isolated into layers separated from underlying material by bounding scarps. Generally lacking the lineations and steeper slopes typical of mountain materials, this unit has heights (based on shadow measurements or stereo observations) of <1-2 km. These are a heterogeneous mixture of silicate and sulfur-rich materials, in the form of lava flows, pyroclastic deposits, or both, without clear margins or source regions, typically isolated into plateaus and mesas by mass-wasting processes (Williams et al., submitted).

Williams et al. (submitted) adapted the table of Ionian hot spots detected by ground-based telescopes and all spacecraft flybys given in Lopes and Spencer (2007) and integrated it with the finalized geologic map of Io to correlate the locations of hot spots with map units. Approximately 93.5 percent of all detected hot spots occur in either dark (45.3 percent) or undivided (18.6 percent) patera floor units, or dark (20.3 percent) or

undivided (9.3 percent) lava flows. About 4.8 percent of hot spots occur in plains or other units without a clear volcanic vent, with the remaining 1.7 percent of hot spots correlating with Bright flows.

Bright flows are more abundant than dark flows. This result seems inconsistent with the understanding of Io's active volcanism, which correlates active hot spots with the darkest material units and is thought to represent silicate eruptions (Lopes-Gautier et al., 1999, 2001; Lopes et al., 2004). However, if most recent sulfur volcanism on Io is secondary sulfur volcanism (i.e., crustal silicate magma bodies melt surrounding sulfur-rich country materials that then erupt through crustal fractures as sulfur flows), as suggested by Greeley et al. (1988), then this might explain the discrepancy.

I independently mapped the entire surface of Io using ArcGIS and a compiled set of Io mosaics. Color plate 1 shows my mapping effort (attached CD).

CHAPTER 3

VOLCANISM ON IO

3.1 Introduction

Io is the most volcanically active body in the solar system, with some 150 actively erupting volcanic centers (Radebaugh et al., 2001; Lopes et al., 2004). During the early years of Io observation, the highest temperature on the surface of Io recorded from the *Voyager* spacecraft flybys was ~ 650 K in 1979, which led scientists to believe that the predominant type of volcanism was sulfurous, perhaps mobilized or driven by silicate magmas at depth (Smith et al., 1979a) (Figure 6). Their conclusion was supported by the knowledge that a significant part of the surface of Io is sulfur and sulfur dioxide, as shown by Io's distinct color palate. The *Voyager* spacecraft, however, did not have the equipment to sense small areas of higher temperatures, and it was not until 1986 that the first evidence of hotter temperatures was found (Johnson et al., 1988; McEwen et al., 1998a). Earth-based telescopes measured temperatures of ≥900 K on the surface of Io, and, with this measurement, the possibility of at least occasional eruptions of silicate magma could not be denied. This resulted in scientists rethinking the models of volcanism they had made (McEwen et al., 1998a). An immediately pre-*Galileo* model of the interior of Io was put together (Spencer and Schneider, 1996) (Figure 7). With the arrival of *Galileo* in the Jovian system in the 1990s, in addition to more accurate Earth-based measurements of infrared emissions from Io, much higher temperatures than those initially measured by *Voyager* were found to exist on the surface of Io (e.g. Johnson et al., 1998; Veeder et al., 1994).

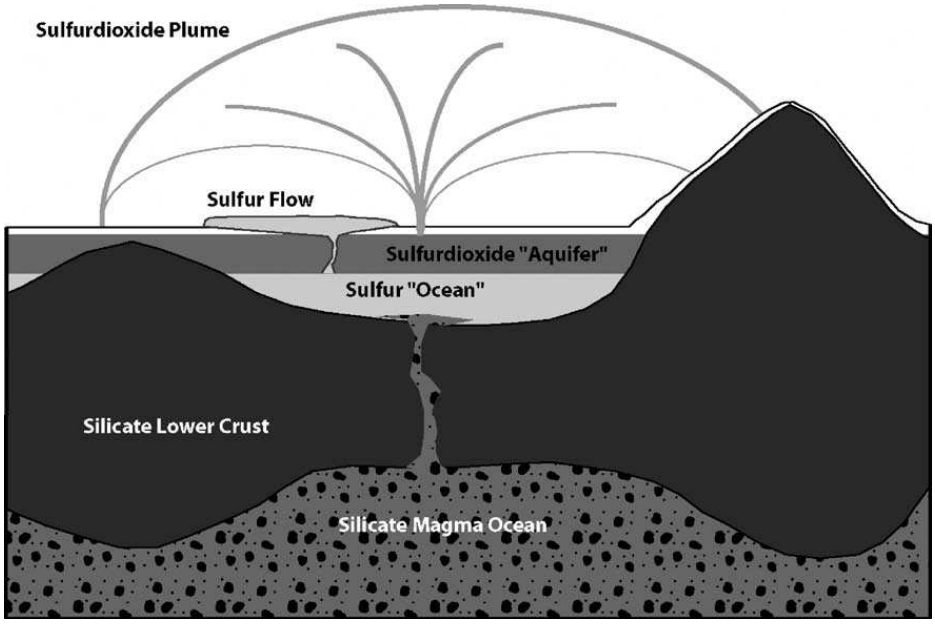

Figure 6: The accepted view of Io's interior after the *Voyager* flybys. Intense tidal heating was believed to be strong enough to completely melt sulfur at a depth of about 1 km and silicates at a depth of <20 km. It was thought that sulfur volcanism dominated, along with SO_2-rich plumes (From Smith et al., 1979; Keszthelyi et al., 2004).

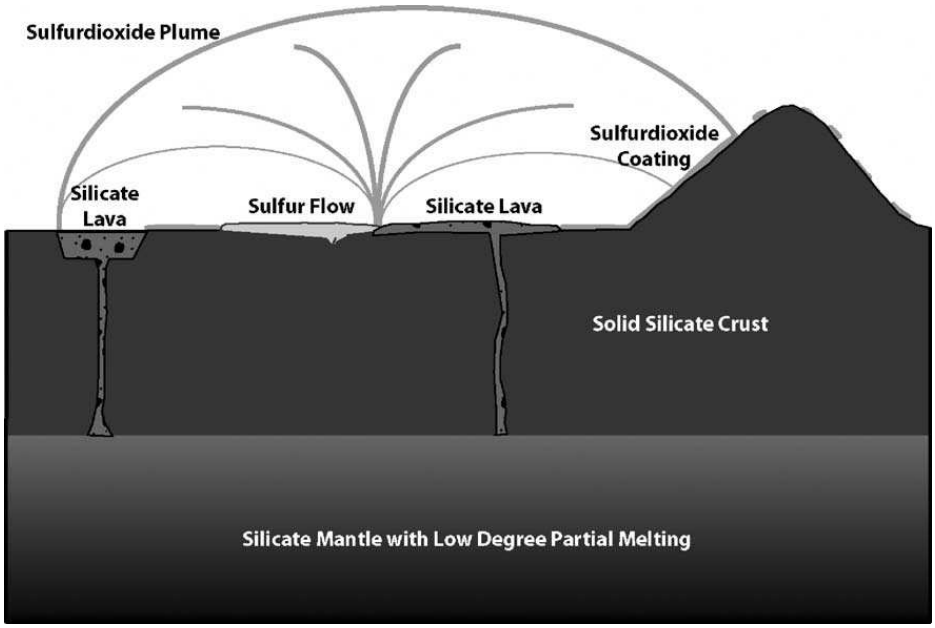

Figure 7: A generally accepted view of the interior of Io immediately before *Galileo* arrived at Jupiter. The silicate portion of Io was presumed to be mostly solid with a low degree of partial melting of the mantle, primarily in the uppermost ~ 50 km. Sulfur compounds were thought to be largely confined to the uppermost crust and in a surface deposit that covered most of the silicate rocks. Volcanism was seen to be a combination of sulfur and silicate lavas. The lithosphere was generally estimated to be ~ 30 km. (After Spencer and Schneider, 1996; Keszthelyi et al., 2004).

McEwen et al. (1998) summarized evidence supporting high-temperature silicate lavas on Io. Solid-state imaging (SSI) and near-infrared mapping spectrometer (NIMS) images were used to provide temperature estimates at hotspots, and SSI multispectral (color) images were used to infer compositional information. The maximum brightness temperatures were calculated for 13 hotspots and the results showed that these temperatures were much greater than typical terrestrial basaltic volcanism (>1200ºC or 1500 K), more consistent with either superheated mafic or ultramafic volcanism (McEwen et al., 1998a), and well in excess of the boiling point of elemental sulfur (717 K) (Lunine and Stevenson, 1985) (Table 5). In addition, *Galileo* SSI data for the Pillan eruption of the 1997 recorded eruption temperatures >1600ºC (1900 K). The *Galileo* data allowed scientists to characterize the types of volcanism on Io. These will be discussed later in this chapter.

The atmosphere of Io appears to be tenuous, but has been detected at infrared, millimeter, and ultraviolet wavelengths (Lellouch, 1996). The low hydrogen abundance in Io's plasma torus indicates that the volatiles outgassed from Io are depleted in hydrogen (Zolotov et al., 2000). The observations indicate an atmosphere composed predominantly of SO_2, with pressures on the order of 1 nanobar (10^{-9} bar). For comparison, the Earth's atmosphere at sea level is 1 atmosphere, which equates to 1.01325 bars. The atmosphere appears to be patchy, lacking uniform coverage. It may be the product of sublimation of SO_2 frost, or directly from volcanic output (Lellouch, 1996). The observed SO/SO_2 ratio in the atmosphere is 3-10 percent (Zolotov and Fegley, 1998). Data from Earth-based astronomy, Hubble Space Telescope, *Voyager*, indicate that O_2, S, Na, K, Cl, and H_2 are escaping Io. Sulfurous volatiles, but apparently no

significant quantities of silicates, are exposed to surface sputtering; no silicates are explosively ejected from Io's volcanoes at sufficient energies to escape. If the crust is made primarily of silicates, then just about as rapidly as new silicate surfaces are formed by volcanism they must be coated by volatile O_2, S, Na, K, Cl, H_2 sublimates and flows which are dominantly sulfur, sulfur dioxide, and other S-O compounds (Kargel, Delmelle, and Nash, 1999).

Several different factors influence the volcanic degassing of alkalis and chlorine on Io: the predominance of sulfur in magmatic gases, the anhydrous character of the magmas, the very high temperatures of at least some volcanic vents, and the low ambient pressure at Io's surface. The predominance of sulfur in magmatic gases on Io favors the formation of sodium sulfate and sulfide and condensation of these phases. The anhydrous nature of the magmas can enhance the amount of Cl in the gas phase because the Cl concentration in terrestrial magmatic gases is anticorrelated with the amount of water in the magmas (Webster et al. 1999). The dryness of magma source regions probably increases liquidus temperatures. In turn, the higher liquidus temperatures increase the amount of degassed volatiles because vapor pressures increase exponentially with increasing temperature. Magmatic interactions with volatile-rich deposits formed volcanically or by other processes, may also be a source of alkalis, chlorine, and sulfur in volcanic gases. Surface material enriched in alkalis may be assimilated partially by upwelling high-temperature ultrabasic melts throughout the lithosphere and recycled in subsequent eruptions (Zolotov and Fegley, 2000).

As stated, the deficiency of water in Io's magmas should lead to a higher melting temperature of mantle and lithospheric materials and a higher liquidus temperature of

magmas (Zolotov et al., 2000). This water deficiency can, in part, account for the observed high temperature magmas (McEwen et al., 1998a) and the absence of plate tectonic processes. It is also consistent with the *Galileo* SSI data (Geissler et al., 1999), which indicate a mafic/ultramafic rather than more silicic character of solidified lava flows (Zolotov and Fegley, 2000).

Hot spot name	Latitude, Longitude	Orbit	Best T	T_{min}	T_{max}
Kanehekili-S	17°S, 36°	G7	940	830	1030
		G8	1375	1195	1530
Kanehekili-N	14°S, 33°	G7	1660	1335	1930
		G8	1440	1280	1580
Janus	4°S, 39°	G7	1160	840	1380
		G8	1525	945	1900
Amirani	23°N, 116°	G8	1675	1050	>2000
Svarog	54°S, 270°	C9	1110	1095	1130
Acala	11°N, 333°	C9	1320	1200	1430
Marduk	27°S, 209°	C9	780	600	975
	27°S, 209°	E11	1500	1365	1615
Pillan	10°S, 242°	C10	930	920	945
Pillan-N	9°S, 243°	E11	1450	1330	1560
Pillan-S	11°S, 242°	E11	1300	1280	1320
Pele	18°S, 256°	E11	1275	1260	1290
Lei-Kung	37°N, 203°	E11	1440	1210	1625
Isum-N	33°N, 205°	E11	1450	1205	1655
Isum-S	30°N, 207°	E11	1325	1070	1530
–	22°N, 238°	E11	1620	1240	1915

Table 5: A sampling of hot spots and their temperatures from the *Galileo* flybys (Modified from McEwen et al., 1998a).

Keszthelyi et al. (2004) put forth a post-*Galileo* model of Io that is somewhat more like the immediately post-*Voyager* view than the immediately pre-*Galileo* view (refer to Figures 6, 7). Keszthelyi et al. (2004) suggest that the interior of Io includes a large volume of liquid and that the iron- and sulfur-rich core is molten and about half the radius of Io. The mantle is theorized to range from ~ 10 percent partial melt at its base to as much as ~ 50 percent at its top. The ascent and eruption of the mantle melts may be hindered by the strength of the solid portion of the mantle, the compressive stresses in most of the lithosphere, and a volatile-rich low-density layer in the uppermost crust. Heat from magmatic intrusions may provide the energy to mobilize volatiles in Io's subsurface, helping to produce features like paterae (Keszthelyi et al., 2004).

Certain surface features changed on Io between the *Voyager* and *Galileo* missions. Changes were also observed over a shorter five-year period by *Galileo*. Three classes of surface changes (volcanic plume deposits, patera color or albedo changes, and seepage of SO_2) occurred. Some episodic brightenings have been attributed to SO_2 seepage/regeneration of SO_2 frosts surrounding many mountain massifs, perhaps triggered by volcanic heating of frozen ices caused by activity at nearby volcanic centers.

Several volcanic centers, such as Pillan, and Gish Bar, changed color or albedo prior to producing plumes or surface changes. Many other paterae were seen to darken or brighten during the *Galileo* mission (Geissler et al., 2004). Geissler et al. (2004) attributed these changes to thermal activity that either heated the surfaces of paterae (causing existing SO_2 frost to sublimate), heated the SO_2 surrounding the paterae (liquefying ice so that it then flooded into and brightened the paterae interiors as seen at Pillan), or produced eruption of fresh lava that darkened the surfaces of the paterae.

Volcanic resurfacing and erosion or alteration erase thin surficial deposits. Substantial thicknesses are needed in order for the SO_2-rich plume deposits to be apparent at visible wavelengths. Repeated eruptions of the smaller SO_2-rich plumes likely contribute significantly to Io's resurfacing rate, whereas dust ejection is likely dominated by giant plumes that erupt less frequently. Both types of plume deposits fade on timescales of months to years through burial and alteration (Geissler et al., 2004).

3.2 Eruption Styles

It is not feasible to categorize each paterae into a narrowly defined group, as each has some characteristics that can fit into one of the three eruption styles defined by Keszthelyi et al. (2001) and Lopes et al. (2004). The first type is promethean, which involves lava flow fields emplaced as compound pahoehoe flows. The interaction between molten materials and preexisting sulfur-rich deposits at the flow fronts creates relatively small SO_2–rich plumes that rise up to 200 km from the flow fronts (McEwen et al., 2000; Lopes-Gautier et al., 2000; Kieffer et al., 2000; Douté et al., 2002, 2004; Keszthelyi et al., 2001). They are long-lived and relatively gentle effusions of lava flows (McEwen et al., 2000; Milazzo et al., 2001). Amirani and Prometheus are examples of this type of eruption. The pillanian eruption style (cf. Keszthelyi et al., 2001) is violent and intense, generally accompanied by the expulsion of pyroclastic materials along with large outbursts, > 200-km-high plumes, and rapidly emplaced flow fields. Examples of this type are Pillan and Tvashtar Catena. The third style, lokian, includes all eruptions confined within paterae with or without associated plume eruptions. Loki, Pele and Emakong are all examples of this type of activity.

Such a classification is useful, but it is important to keep in mind that the boundaries are not strict. For example, sites of promethean and pillanian activity may also have been associated with lokian activity (i.e. lava lakes) at some stage in their existence (Lopes et al., 2004). In the case of Pillan patera, fissures located directly north of Pillan, which are the continuation of extensional fractures seen in a nearby mountain, were the vents for this eruption. From these fissures, a considerable amount of lava flowed southeast and cascaded over the rim of Pillan patera. The flow was partially insulated between the vent and lava falls, probably by a disrupted crust formed on active channels (Keszthelyi et al., 2001).

3.2.1 Promethean Eruptions

Prometheus is the type example of promethean eruptions (Figure 8, 9). Amirani is the site of the longest known active lava flow in the Solar system. The eruptive center consists of a ~ 300-km-long, dark lava flow complex oriented roughly north-south. In comparison, there have been areally extensive basaltic eruptions on Earth, for example the Columbia River plateau basalts, dated at 17-6 Ma. This region has produced eruption volumes on the order of 2,000 km^3, flowing across distances of up to 600 km (Hooper, 1997). Io's lava flows' morphology and thermal signature suggest insulated tube- or sheet-fed lavas (Keszthelyi et al., 2001). This method of emplacement is also a theory for the Columbia River plateau basalts. A thermal map of these flows showed a maximum temperature of at least 1000 K (Lopes et al., 2001). The occurrence of new lava flows seen by *Galileo* at numerous locations within the Amirani and Prometheus flow fields is consistent with their interpretation as compound inflated pahoehoe, formed by a repetitive process in which lava is injected beneath an insulating crust and thickens the

flow until it breaks out to form a new lobe (Geissler et al., 2004), similar to the inflated pahoehoe emplacement model of Kilauea lava flows put forth by Hon et al. (1994). This mechanism helps explain the great lengths of the lava flows. Another aspect of this type of eruption are the relatively small plumes that are produced, and it is thought that the mobilization of volatiles that formed the Prometheus plume results from interactions of older flows with the icy surface beneath the flow field (Kieffer et al., 2000; Milazzo et al., 2001; Davies et al., 2003).

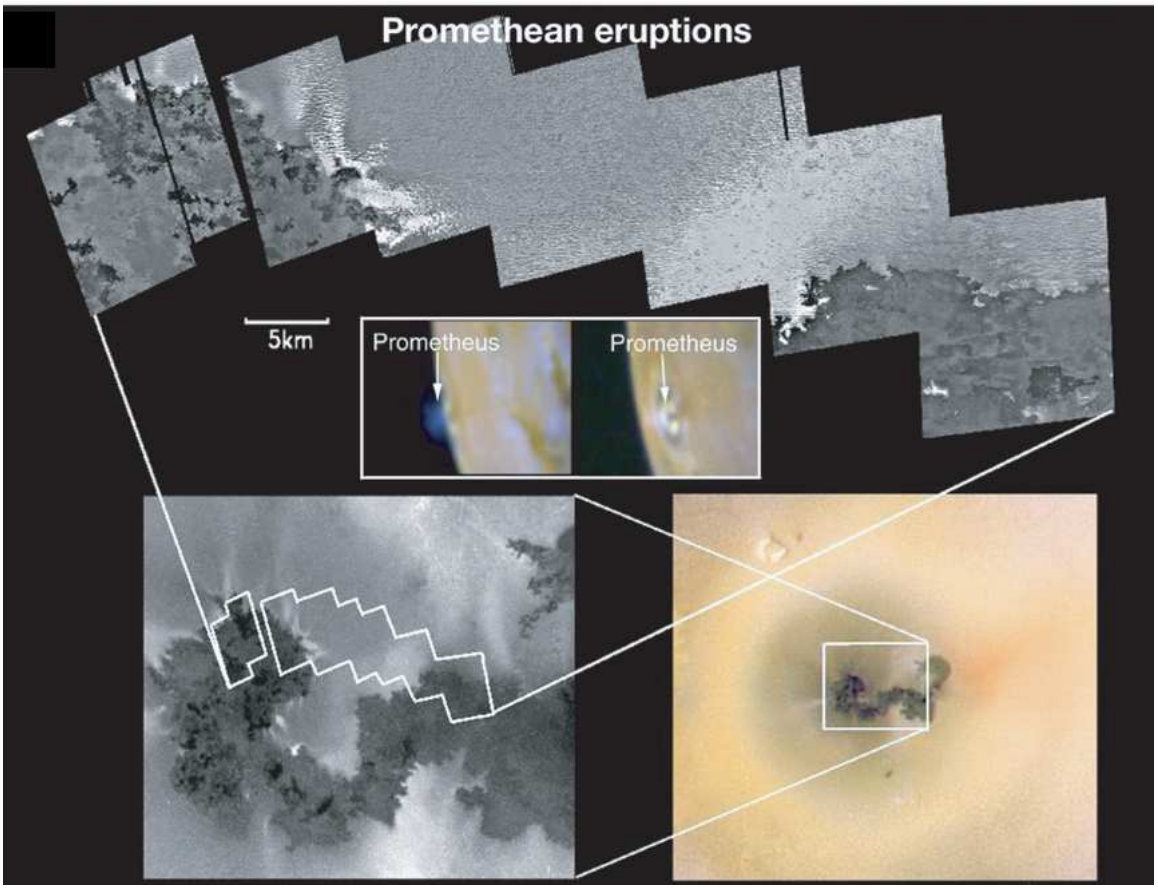

Figure 8: Promethean eruptions are relatively long-lived (months to years), and are associated with high (mafic) temperatures, relatively low (<200 km) SO_2-rich flow-front plumes, and slowly emplaced flows through multiple small breakouts (similar to Hawaiian pahoehoe flow fields). In this figure, *Galileo* SSI views of the Prometheus plume (center) are surrounded by increasingly higher resolution views of the Prometheus flow field (Lopes et al., 2005; Image credit: NASA).

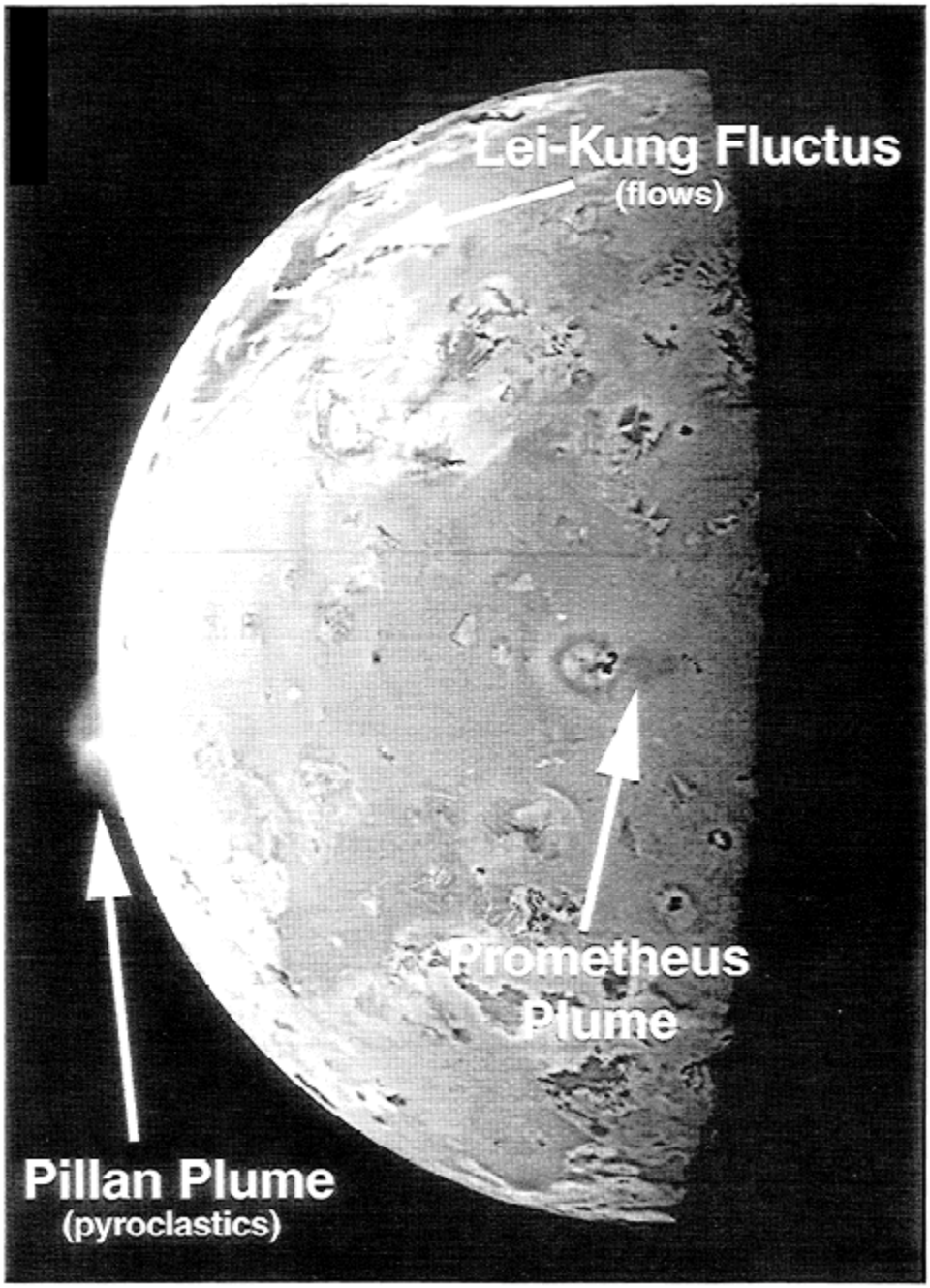

Figure 9: Pillan and Prometheus plumes, as seen by *Galileo*. This shows an ~86 km high eruption plume over Pillan patera. Resolution is 2 km/pixel. (Williams et al., 2000; *Galileo* press release PIA01081).

3.2.2 Pillanian Eruptions

Eruptive centers that produce pillanian eruptions have also exhibited other types of activity. For example, Pillan, the type example for this eruption (Figure 10), showed

less violent activity, and may have been a lava lake, before its large eruptive event in 1997 (McEwen et al., 1998; Williams et al., 2000). It is not yet known what triggers the violent pillanian eruptions.

Tvashtar catena exhibited pillanian-type eruptions in 1999-2000, but also varied in activity type, and actually has shown to exhibit all three eruption styles (Lopes et al., 2005). There was a very bright thermal emission associated with the large Tvashtar deposit that was observed by ground instruments, but not by *Galileo*. Extensive plume deposits are associated with pillanian eruptions, but these are not necessarily emplaced simultaneously with the high thermal emission phase of the eruption. For example, the extensive plume deposit at Tvashtar occurred several months after the first phase of the eruption (Keszthelyi et al., 2001).

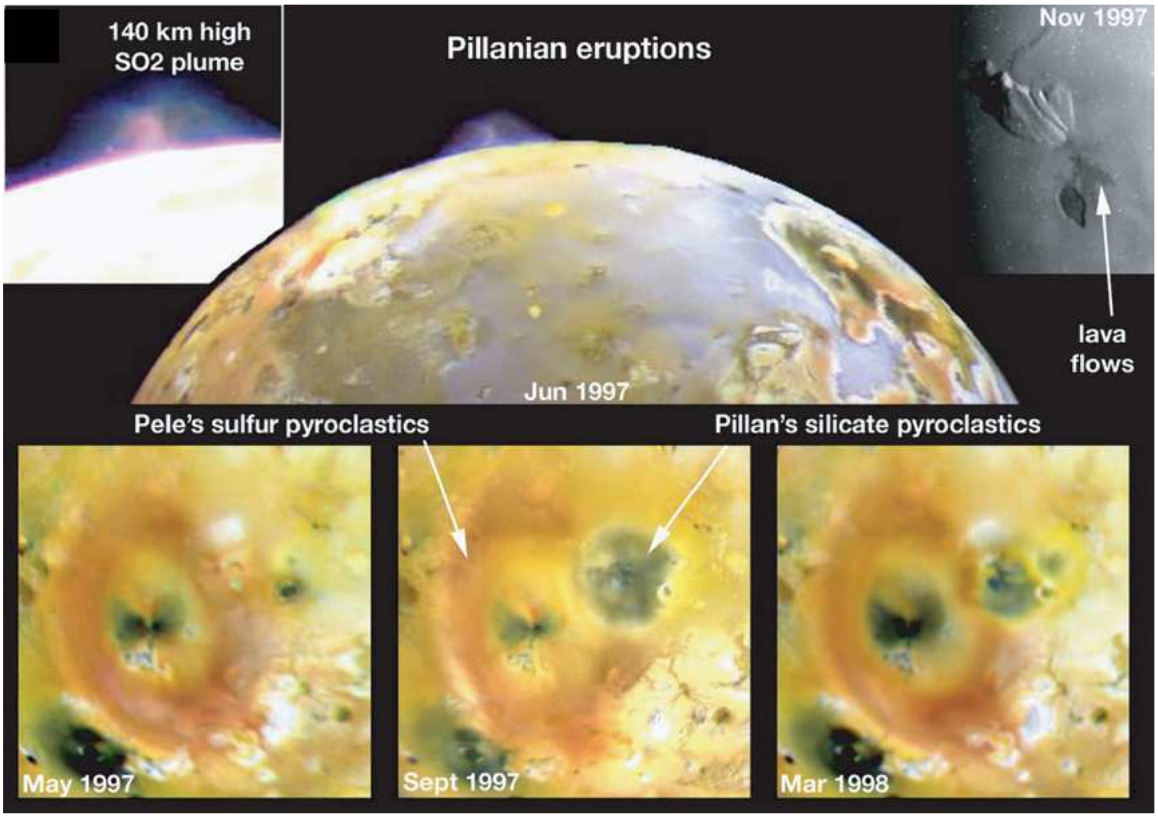

Figure 10: Pillanian eruptions occur in relatively brief (few months or less), intense outbursts that produce very high (possibly ultramafic) temperatures, plumes and rapidly-emplaced long (>50 km) lava flows. The plumes are typically >100–500 km high, are known to contain SO_2 gas, and have produced black (Pillan), red (Pele, Tvashtar) and white (Thor) rings over source vents hundreds of kilometers in diameter. These compositions are thought to be associated with silicate, sulfur and SO_2 pyroclastic materials, respectively (Lopes et al., 2005; image credit: NASA).

3.2.3 Lokian Eruptions

Lopes et al. (2004) discusses six lokian volcanic centers (possible lava lakes), three of which I will summarize here. Rathbun et al. (2002) proposed that Loki is an active lava lake that experiences complete overturns. Upon analyzing data on Loki's activity obtained over several years, which showed patterns of brightening and fading, Rathbun et al. (2002) came up with a model involving a wave of resurfacing in which silicate magma propagates around the patera, the wave being initiated when the crust on the lake founders, exposing hot material. The NIMS thermal map of Loki (Figure 11) is consistent with the model of Rathbun et al. (2002): hotter edges along the patera walls, with the hottest area observed by NIMS at the location where their model predicts, and the coolest region just to the east, where their model predicts the oldest crust is located. These NIMS results are consistent with the model of a slowly overturning lava lake (Lopes et al., 2004).

Pele patera is also thought to be an active lava lake (e.g., Howell, 1997; McEwen et al., 2000; Davies et al., 2001; Keszthelyi et al., 2001; Lopes et al 2004), the evidence for which was summarized by Radebaugh et al. (2004). This evidence includes high temperatures over long periods of observing time, no massive surrounding lava flows, curving lines of very hot materials seen in SSI images, and rapid variation of thermal output (scale of minutes) observed from Cassini imaging data, consistent with variations

observed on lava lakes on Earth (Flynn et al., 1993). The long-lived hotspot at Pele may be an ultramafic lava lake, with temperatures of at least 1600°C, that occasionally produces plume eruptions hundreds of kilometers tall, and extensive rings of sulfurous pyroclastic deposits. If indeed it is a lava lake, it is larger than any terrestrial equivalents, with a correspondingly greater effusion rate. The power and mass fluxes, however, are comparable to active terrestrial equivalents (Davies et al., 2001). The best explanation of the style of volcanism at Pele involves the presence of a lava lake, the surface of which is being constantly disrupted, as would be expected from degassing of the magma feeding the plume (Davies et al., 2000). The consistency of thermal output from Pele is indicative of Pele being a long-lived, stable, and active lava lake.

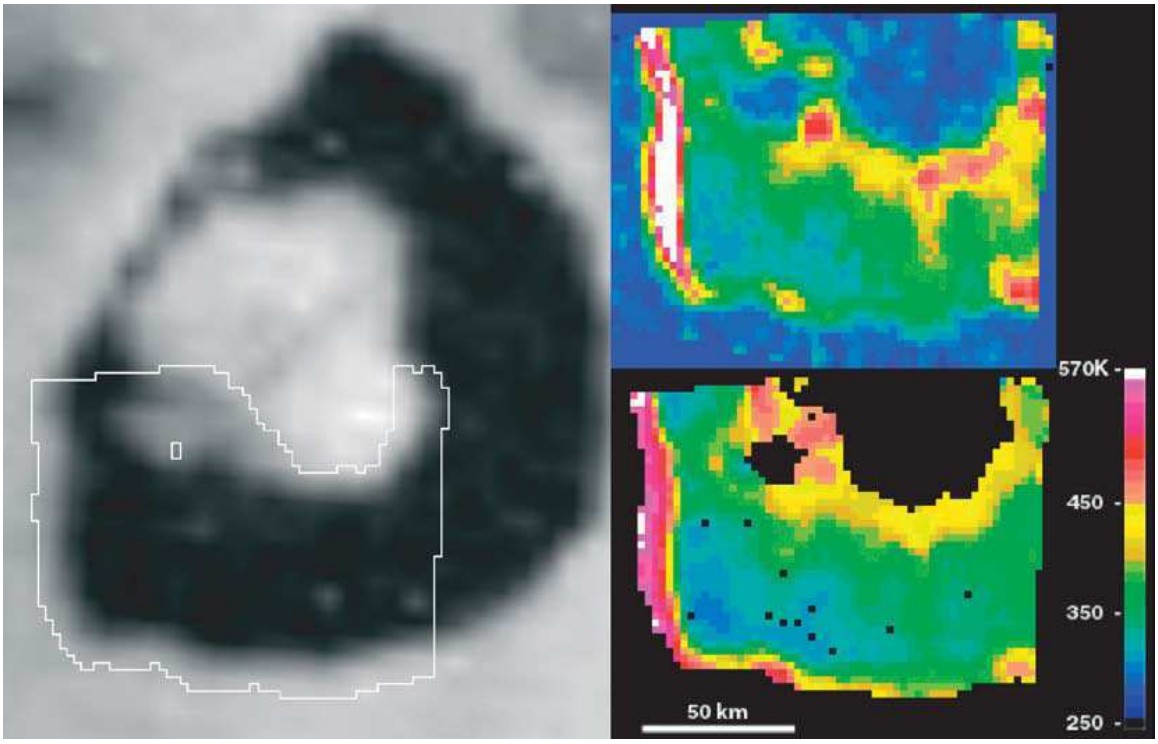

Figure 11: Lokian eruptions are confined to paterae, and occur as intermittent to periodic outbursts that are thought to represent the resurfacing of paterae floors by lava flows or overturning lava lakes. The type locality is Loki. In this montage, *Galileo* NIMS images track the temperature changes across the floor of Loki in darkness during orbit I32. The image shows a hot edge (indicated by white and red areas) next to the western patera wall. A temperature map from the NIMS

observation (lower right) shows that the highest temperatures are found near the patera walls and against the walls of the cold 'island.' The SSI image on the left, obtained earlier during the mission, illustrates the approximate outline of the areas showing thermal emission at NIMS wavelengths (Lopes et al., 2004, 2005).

3.3 Io's lava flow compositions

McEwen et al. (1998a) proposed the idea that the lavas on Io may be produced by high degrees of partial melting (~40 percent) of a mantle that has undergone little differentiation after separation of an iron-rich core, similar to the later model of Keszthelyi et al. (2004). This model is directly analogous to the formation of komatiites on Earth in Archean time and suggests that Io's interior is similar to that of early Earth. Williams et al. (2000) used komatiitic analogs and terrestrial ultramafic flow models, along with *Galileo* data, to investigate the nature of ultramafic materials that are assumed to occur at high temperature hotspots on Io.

With the assumption that the conditions on Io mimic those on early Earth, some idea of ultramafic affinity (MgO content) of Io's hotspots as a function of liquidus temperatures can be reached, with an equation modified by Williams et al. (2000), which was modified from Nisbet (1982):

$$\text{wt \% MgO} = (T_{liq} - 1000°C)/20$$

This equation is valid for terrestrial komatiites with >18 percent MgO and temperatures >1360°C. Used as an indicator of potential ultramafic affinity, this equation shows that some of the high-temperature hotspots on Io are consistent with lavas analogous to terrestrial komatiitic rocks (~12-32 wt percent MgO) (Williams et al., 2000).

Williams et al. (2000) identified a likely terrestrial komatiite analog composition to the inferred Ionian ultramafic materials. The unusual komatiites of a region in South

Africa are consistent with available *Galileo* data on temperatures and composition of potential Ionian ultramafic materials. The Commondale greenstone belt (~3.2-3.5 Ga) is located near the Swaziland border in South Africa. The komatiitic sequence is ~1.5 km thick and is composed of several hundred flow units (Williams et al., 2000). This suite of rocks is unusual for a typical terrestrial komatiite (characteristics summarized in Table 6).

The typical range of terrestrial low-SiO_2, high-MgO komatiites is represented by the Barberton and Kambalda compositions (Table 6). The Commondale komatiites, however, have a higher SiO_2 content, lower FeO content, and higher average MgO content relative to these komatiites. These differing compositions affect the liquidus temperature for the Commondale komatiites (~1610°C), which is ~ 50°C hotter than the Barberton komatiites. The higher SiO_2 and lower FeO contents of the Commondale komatiites are inferred to result in high liquidus temperatures (~1610°C), low dynamic viscosities, and low densities (~2680 kg/m^3) and in the crystallization of orthopyroxene phenocrysts (Williams et al., 1999, 2000). Orthopyroxene spinifex crystals are characteristic of the whole sequence of the Commondale komatiite, which is the only known komatiitic locality on Earth containing orthopyroxene phenocrysts. The orthopyroxenes have compositions up to 94 wt% MgO, indicative of crystallization from very Mg-rich liquids (Williams et al., 2000).

The *Galileo* SSI temperature data for the 1997 Pillan eruption recorded magma eruption temperatures of >1600°C, which is very close to the liquidus temperature of the Commondale komatiite/Io analog composition of 1611°C, as calculated by the igneous petrology program MELTS (Williams et al., 2000). In addition, orthopyroxene seems to

be abundant in association with these high-temperature eruptions. All evidence points toward the Commondale komatiite being a useful analog to Ionian high temperature

	Commondale Komatiite	Kambalda Komatiite	Barberton Komatiite	Cape Smith Kom. Basalt	Lunar Mare Basalt	Tholeiitic Basalt
Components						
SiO_2	49.8	45.0	47.9	46.9	43.6	50.9
TiO_2	0.1	0.3	0.4	0.6	2.6	1.7
Al_2O_3	7.9	5.6	4.1	9.8	7.9	14.6
Fe_2O_3	0.5	1.4	1.9	-	-	-
FeO	4.8	9.2	9.7	14.4	21.7	14.6
MnO	0.1	0.2	0.2	0.3	0.3	-
MgO	30.9	32.0	27.5	18.9	14.9	4.8
CaO	5.2	5.3	7.5	8.6	8.3	8.7
Na_2O	0.4	0.6	0.2	0.3	0.2	3.1
K_2O	0.01	0.03	0.02	0.05	0.05	0.8
Physical Properties						
T_{liq}, °C	1611	1638	1556	1419	1440	1160
T_{sol}, °C	1170	1170	1170	1150	1150	1080
ρ at T_{liq}, kg/m³	2680	2770	2760	2800	2900	2750
c, J/kg·°C	1780	1790	1740	1640	1570	1480
μ at T_{liq}, Pa s	0.22	0.08	0.20	0.74	0.40	86
L at T_{liq}, J/kg	6.84E+05	6.97E+05	6.58E+05	5.96E+05	6.06E+05	5.37E+05
k at T_{liq}, J/m s °C	0.4	0.4	0.4	0.5	0.5	0.7
h, m	10	10	10	10	10	10
u at T_{liq}, m/s	4.6	4.8	4.5	3.9	4.2*	1.7
Re at T_{liq}	5.74E+05	1.74E+06	6.31E+05	1.46E+05	3.09E+05*	5.50E+02
Pr at T_{liq}	1.0E+03	3.8E+02	8.4E+02	2.6E+03	1.3E+03*	1.9E+05
h_T at T_{liq}, J/m² s °C	260	396	277	172	217*	N/a
u_{ab} at T_{liq}, m/day	1.1	1.7	1.0	0.52	0.24*	N/a
Composition location	Commondale, South Africa	Kambalda, Western Australia	Barberton, South Africa	Katinniq, Cape Smith Belt, Canada	Apollo 12 sample 12002	Columbia River Basalt, Washington
Composition reference	this study	*Lesher and Arndt* [1995]	*Viljoen et al.* [1983]	*Barnes et al.* [1982]	*Walker et al.* [1976]	*Murase and McBirney* [1973]

T_{liq}, liquidus temperature; T_{sol}, solidus temperature; ρ, density; c, specific heat; μ, dynamic viscosity; L, heat of fusion; k, thermal conductivity; h, flow thickness; u, flow velocity; Re, Reynolds number; Pr, Prandtl number; h_T, convective heat transfer coefficient, u_{ab}, thermal erosion rate of consolidated basalt, NA, not applicable for nonturbulent flows. Read 6.84E+05 as 6.84×10^5.
*Erupted on Earth.

Table 6: Inferred liquid compositions and physical properties for several komatiitic and basaltic lavas (Williams et al., 2000).

volcanism. Adapting the model of Williams et al (1998), Williams et al. (2000) simulated the emplacement on Io's surface, and used the Commondale composition to investigate potential ultramafic flow behavior on Io and Earth.

Williams et al. (2000) concluded that due to the differing environmental conditions, several key differences must be considered between Io and terrestrial komatiite emplacement. Io's environmental differences (e.g., low-gravity, low-pressure

atmosphere) and abundant volatiles (as indicated by ubiquitous plumes and sulfurous pyroclastic deposits) suggest that magma-volatile interactions and explosive eruptions play a greater role in ultramafic volcanism on Io than occurred during komatiitic eruptions in the Earth's Precambrian era.

The presence of plumes at sites of potentially ultramafic eruptions on Io, such as Pillan and Pele (Figure 12), suggests that Io's environment enhances the potential for magma-volatile interactions to play an important role in ultramafic eruptions on Io, in contrast to Precambrian Earth where submarine, effusive emplacement was dominant (Williams et al., 2001). It is likely that the range of compositions and styles of lava emplacement on Io are as broad as the styles of emplacement of terrestrial komatiites (Williams et al., 2000). In addition to these ultramafic eruptions, plumes, driven partly by both SO_2 and S, are an important aspect of Io volcanism as well (McEwen and Soderblom 1983; Keszthelyi et al., 2004).

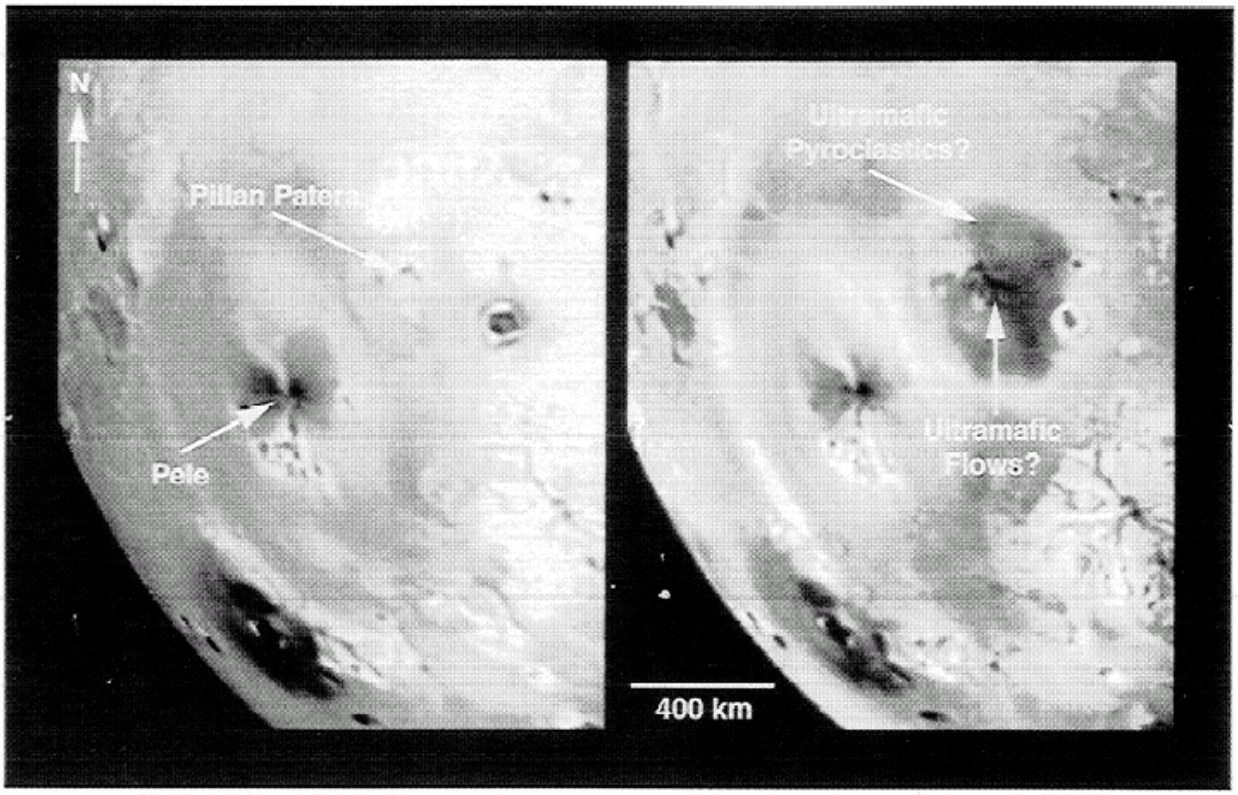

Figure 12: *Galileo* images of the Pele-Pillan region taken September 1997. The large dark spot in the right image is ~400 km in diameter and may consist of ultramafic pyroclastic deposits and lava flows from very high temperature eruptions that have occurred at Pillan (Williams, et al. 2000; *Galileo* press release image PIA00744).

CHAPTER 4

SULFUR FLOWS ON IO AND EARTH

4.1 Sulfur flows on Io

As explained in the previous chapter, bright flow material on Io has been identified as being composed of sulfur or sulfur-rich compounds. Pieri et al. (1984) hypothesized that progressive color and morphology changes in flows at Ra patera indicate a sequence of sulfur allotropes within the flows (see Figure 16). Colors and morphology are consistent with a predominantly sulfur lava erupting in the range of 470-520 K.

The persistently low temperatures observed at Emakong patera are consistent with either cooled silicates or sulfur volcanism (Lopes et al., 2004). A hot spot in this region was detected by NIMS at a resolution of ~25 km/pixel and yielded a thermal map (Figure 13), showing that the highest temperatures were 270 ± 90 K (see Lopes et al., 2001). This is consistent with cool sulfur volcanism and with the color/albedo changes seen at the Emakong volcanic system. For more on the properties of sulfur and sulfur dioxide, refer to Appendix A. The consistently low temperatures and thermal emission at Emakong indicate that either the material has a low melting temperature (sulfur) or that a molten lava lake's activity has not been vigorous during the years of Galileo observations, and the lake has remained mostly crusted over with few incandescent cracks.

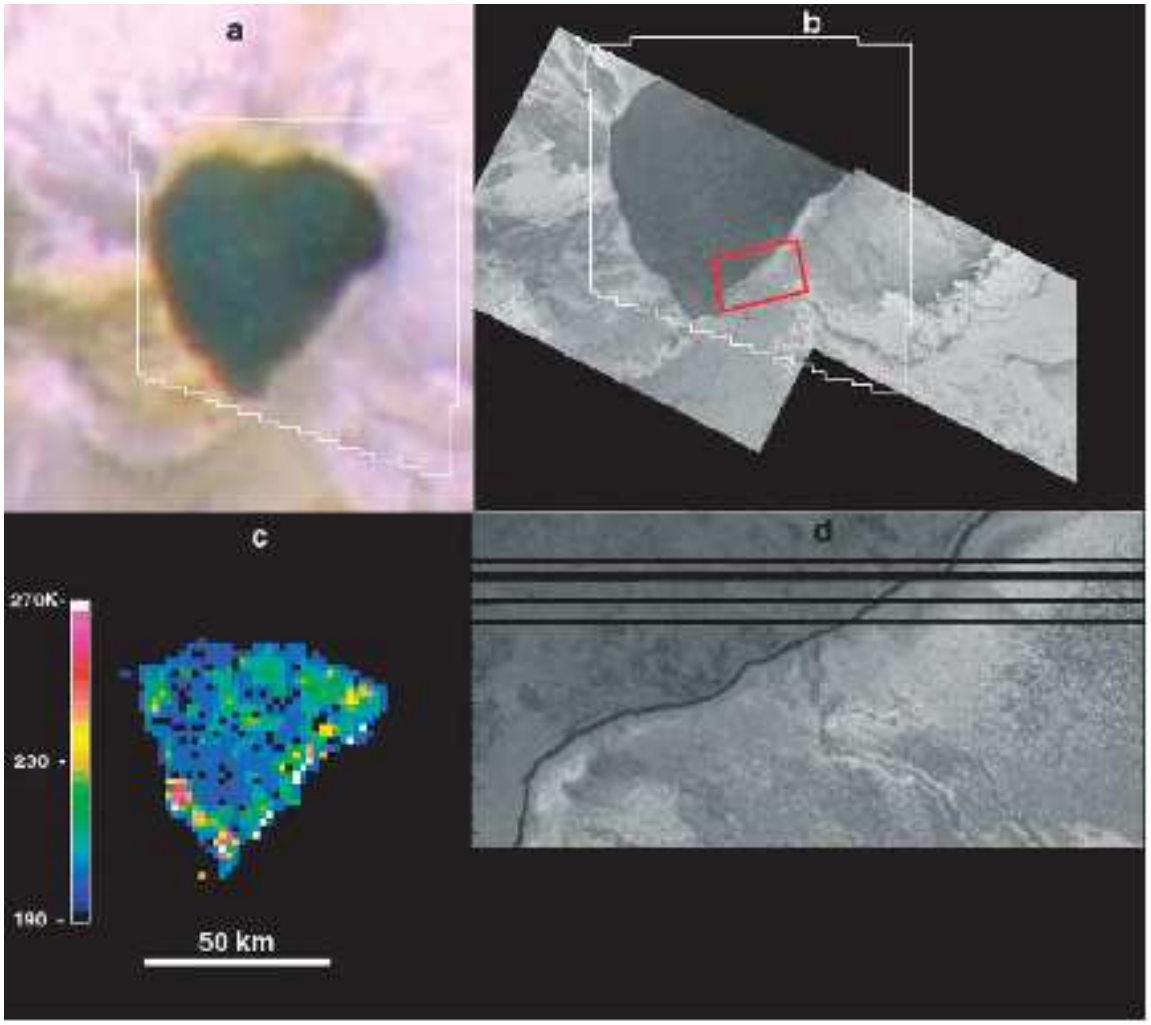

Figure 13: NIMS observed Emakong during the I32 fly-by. Emakong Patera is shown in an SSI color image from orbit C21 (a) and in clear filter SSI images obtained during the I25 fly-by (b) and the I32 fly-bys (d). The image in (d) has a different scale from the others and its location in (b) is outlined in red. The NIMS thermal map (c) shows that most of the patera floor is cool at NIMS wavelengths. The highest thermal emission is found at the edges of the patera, and coincides with the darkest areas shown in the SSI high-resolution images. SSI and NIMS data are therefore consistent with either a crusted-over lava lake, with the crust breaking up against the patera walls, or a sulfur lake (From Lopes et al., 2004).

Figure 14: Emakong patera from the mosaic map used for mapping. Scale 1:5,900,000

The temperatures of the active sulfur flows surrounding Emakong are below about 400 K (e.g., Williams et al., 2001), so if sulfur volcanism were taking place inside the patera, it would be consistent with the NIMS observations of the patera. The most intriguing aspect of the thermal map is that it shows very distinctly that the highest temperatures are close to the patera walls, as would be expected if there was a rigid crust on a lava lake that was breaking up against the patera walls. SSI and NIMS data are therefore consistent with either a crusted-over silicate lava lake or a sulfur lake (Lopes et al., 2004). Typical temperatures are between 190-270 K, cooler than pure molten sulfur.

Sulfur polymorphs have melting points of 385-393 K, which is much warmer than observed patera temperatures. Lopes et al. (2004) interpreted the colors seen at Emakong to indicate that the patera floor deposits consist of molten or partly cool sulfur and the brighter flows around the patera represent older cooled sulfur. This idea will be revisited later in this work. However, Williams et al. (2010, submitted) suggest the low percentage of hot spots that correlate with bright flows (< 2 percent of active hot spots are associated with bright flows) indicates the sulfur volcanism is not a major component of Io's volcanism.

Molten sulfur flows long distances on Io as a result of relatively low viscosities, sustained effusion resulting from continued heating of the source area, and relatively low heat loss in the Ionian environment even for thin sulfur flows (Fink et al., 1983), and apparent formation of flow tubes that effectively extend the source vent to the flow front (Greeley et al., 1984). Maasaw patera (Figure 15) has a flow field that extends approximately 344 km north to south and 230 km m west to east, covering about 44,649 km^2. Ra patera's bright flows extend 573 km E-W and 617 km N-S, covering approximately 234,775 km^2 (Figure 16). Ra patera's dark flows cover 377 km E-W and 239 km N-S.

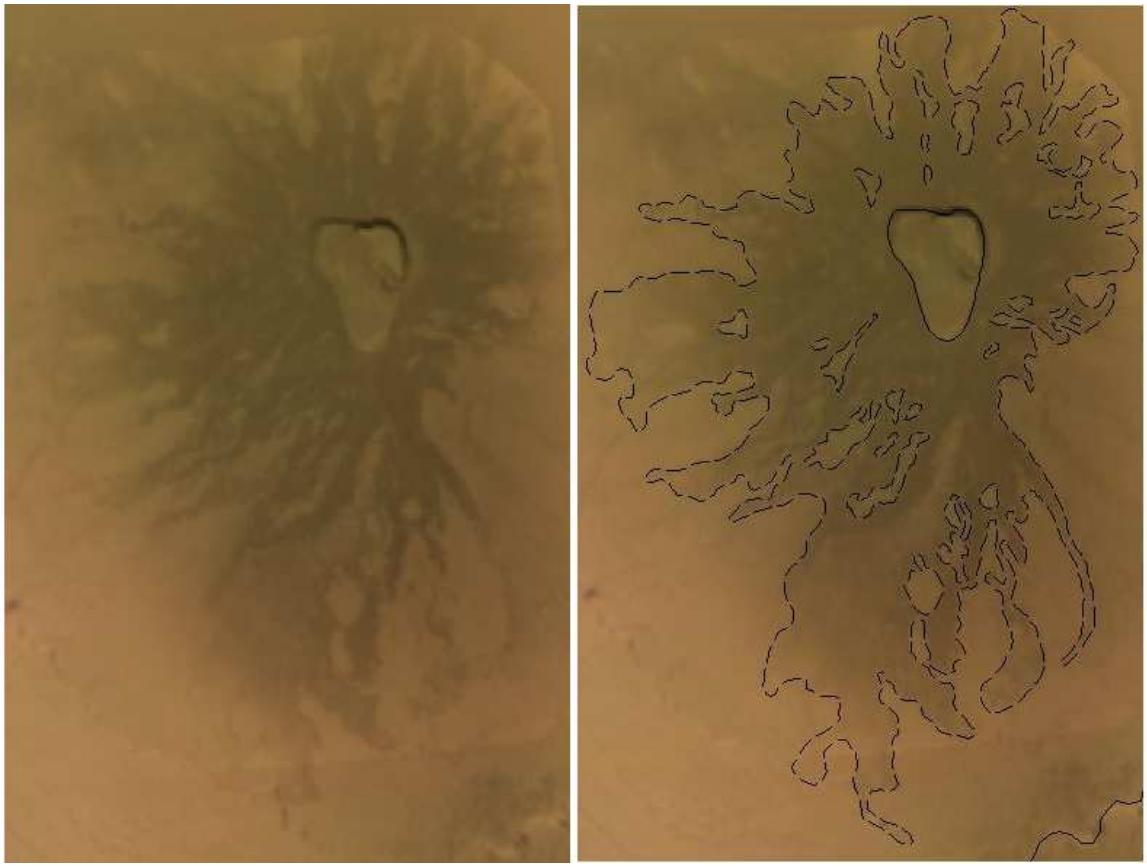

Figure 15: Dark flow material around Maasaw patera. Scale: 1:2,300,000.

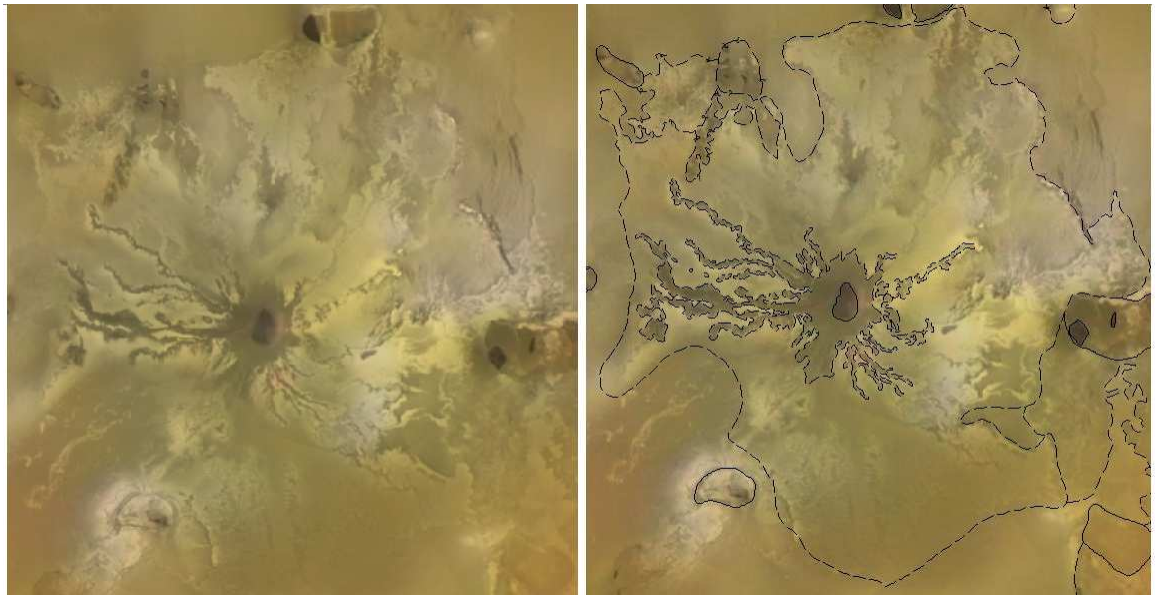

Figure 16: Bright flow material and dark flow material around Ra patera (center) Scale: 1:4,200,000. Mazda patera (right) abuts flow material from Ra patera. Bright flows are interpreted as sulfur-rich eruptive products, while dark flows are believed to be silicate in nature.

4.2 Sulfur flows on Earth

All reported natural terrestrial sulfur flows appear to have been formed by the remobilization of fumarolic deposits (Naranjo, 1985). Silicate magmas/lavas can either directly (or indirectly via shallow magma intrusion) remelt sulfur deposits. Remobilization of precipitated sulfur has been seen at Mauna Loa, Hawaii (Figure 18), and at Lastarria volcano in the Chilean Andes (Naranjo, 1985). Fumarolic sulfur is deposited near the surface and accumulates in the talus; heating by magma intrusion melts the fumarolic sulfur above its liquidus and mobilizes it to form a flow (Greeley et al., 1984).

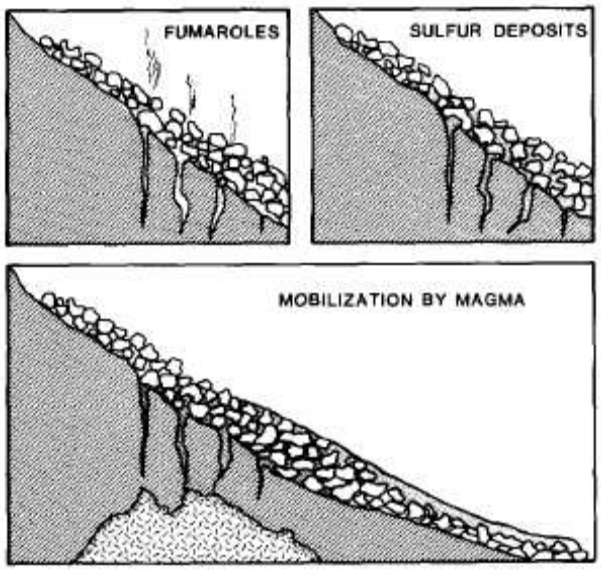

Figure 18: The origin of secondary sulfur flow in 1950 at Mauna Loa, Hawai'i (Greeley et al. 1984).

The 1950 Mauna Loa sulfur flow was about 27 m long, up to 14 m wide, and ranged in thickness from 0.10 to 0.45 m (Greeley et al., 1984). Remelting of fumarolic sulfur deposits also likely occurs at Poás and could result from heat transferred from hot gases or silicate lava bodies at depth.

4.3 Comparison

The possible sulfur flows seen on Io are much larger than equivalents on Earth (see Figures 15, 16). On Earth, most sulfur flows appear to be produced from the remobilization of previously deposited sulfur (i.e. secondary flows). Such processes may be the primary emplacement mechanism of sulfur-rich flows on Io as well, although plume deposits are widely accepted as one mechanism of volatile emplacement (Figure 17). The most striking example that plume deposits contribute to what we see on Io's surface is seen around Pele patera, and the red halo of sulfurous material that surrounds it (Figure 17).

Figure 17: Pele patera, showing plume deposits surrounding the vent (Scale: 1:11,460,000).

At Lastarria volcano, sulfur flows extended no more than about 0.25 km from the source (Naranjo, 1985). In contrast, Ra patera's bright flows (refer to Figure 15) which are sulfur-rich, extend up to 350 km from their source. This seems to mimic what we see for silicate volcanism on Earth and on Io: similar processes seem to occur, but at a larger scale on Io.

The following chapter will discuss terrestrial requirements for the formation of standing sulfur pools in volcanic systems. An effort will then be conducted to extrapolate these requirements to Io.

CHAPTER 5

TERRESTRIAL ANALOG

5.1 Introduction

Differing opinions as to the nature of volcanism on Io have been circulated throughout the scientific literature. Although sulfur lakes cannot be entirely ruled out (e.g. Emakong), the likelihood of such features existing at all has been the focus of several studies, and will be approached from a different angle with the help of a terrestrial analog. We have hints of what Emakong might hold, but we are still limited due to resolution difficulties and availability of data coverage. A terrestrial analog is therefore our best option for determining what is happening on the surface of Io.

Terrestrial analogs provide a valuable tool in studying extra-terrestrial locations. In the planetary sciences, several such analogs have been established for Mars (e.g. Allen et al., 1981; Aharonson et al., 2002; Chan et al., 2004; Chapman, 2007) to study topics such as soil composition, evolution of geomorphologic features, and volcanism. This approach has also been applied to Venus to gain insight into the formation and nature of its volcanoes (e.g. Campbell and Rogers, 1994). Terrestrial analogs have been applied to Io in the past, in order to determine the composition of erupted magmas (e.g. Williams et al., 2000) and the possible emplacement mechanisms of sulfur flows (e.g. Greeley et al., 1984). However, limited by poor resolution, Oppenheimer and Stevenson (1989) and Oppenheimer (1992) only made tentative comparisons between a terrestrial volcano (Volcán Poás) and sulfur volcanoes on Io. The goal of this chapter is to understand the nature of, and processes involved in, terrestrial volcanoes that host molten sulfur pools in their calderas. Such features are associated with crater lakes. To that end, two terrestrial

volcanoes that host crater lakes with associated sulfur pools will be represented in order to extrapolate to volcanic systems on Io. The properties of sulfur as well as precipitation amounts will play a role in the discussion.

5.2 Terrestrial Crater Lake Systems

5.2.1 Yugama crater lake, Kusatsu-Shirane Volcano

Kusatsu-Shirane is an andesite stratovolcano located 150 km northwest of Tokyo (Figure 19a); (Takano et al., 1994). Three active craters are present on the summit, Mizugama, Yugama, and Karagama from northeast to southwest (Figure 19b). Of these, Yugama is the most active, and contains a strongly acidic lake (Takano et al., 1994) which has an average diameter of 270 m and is 27 m at the deepest point (Takano, 1987). Phreatic explosions at these craters have been recorded since 1805 (Takano, 1987).

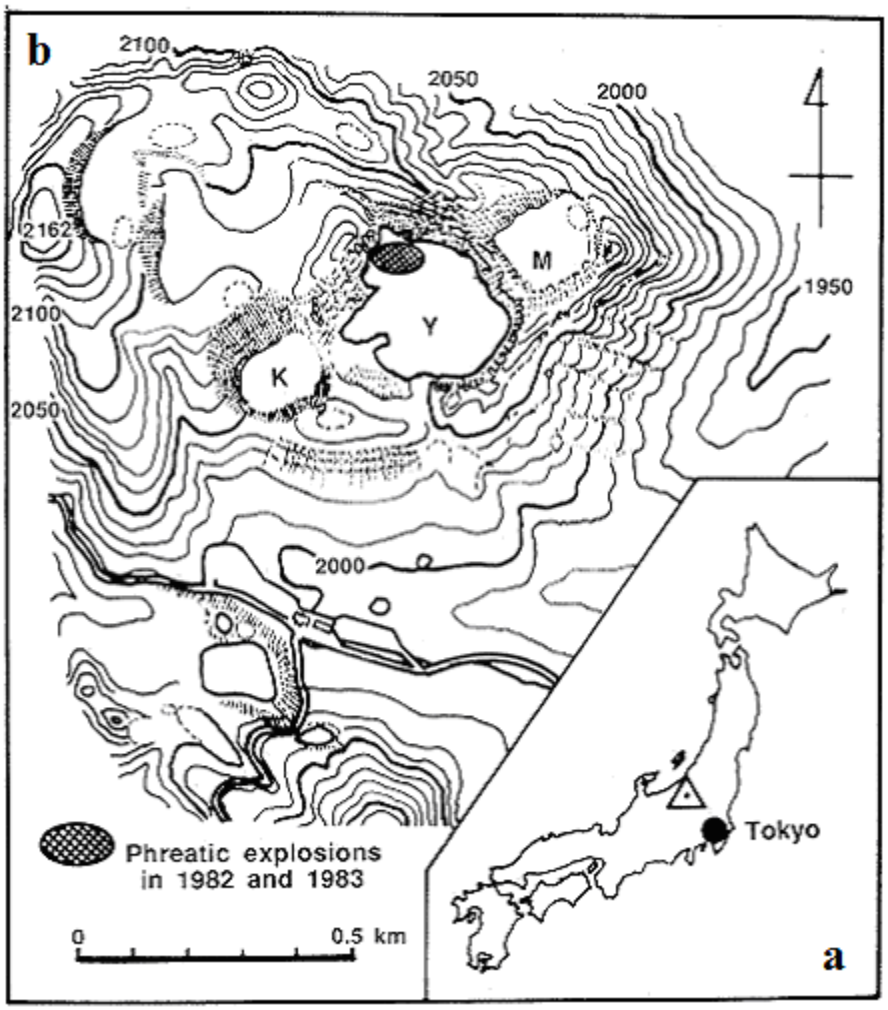

Figure 19: Geographical location map (a) and topographic map (b) of Kusatsu-Shirane volcano (Takano et al., 1987). K, M, and Y indicate the craters Karagama, Mizugama and Yugama respectively.

5.2.2 Laguna Caliente, Volcán Poás

Poás volcano is a large basaltic-andesite stratovolcano in the Cordillera Central in Costa Rica (Figure 20a). It hosts a hot, acidic crater lake (Laguna Caliente) with a shallow hydrothermal system confined within the active crater (Rymer et al., 2000). The summit of Poás consists of two caldera structures with several cones. These are the eroded remains of prehistoric calderas, including Von Frantzius to the north and Botos to the south, the latter of which contains a cold freshwater lake (Rowe et al., 1992a; Rymer

and Brown, 1984) (Figure 20b, 20c). The active crater is about 800 m in diameter, and the volcano rises 1300 m above its base at 1400 m (Prosser and Carr, 1987; Rowe et al., 1992a).

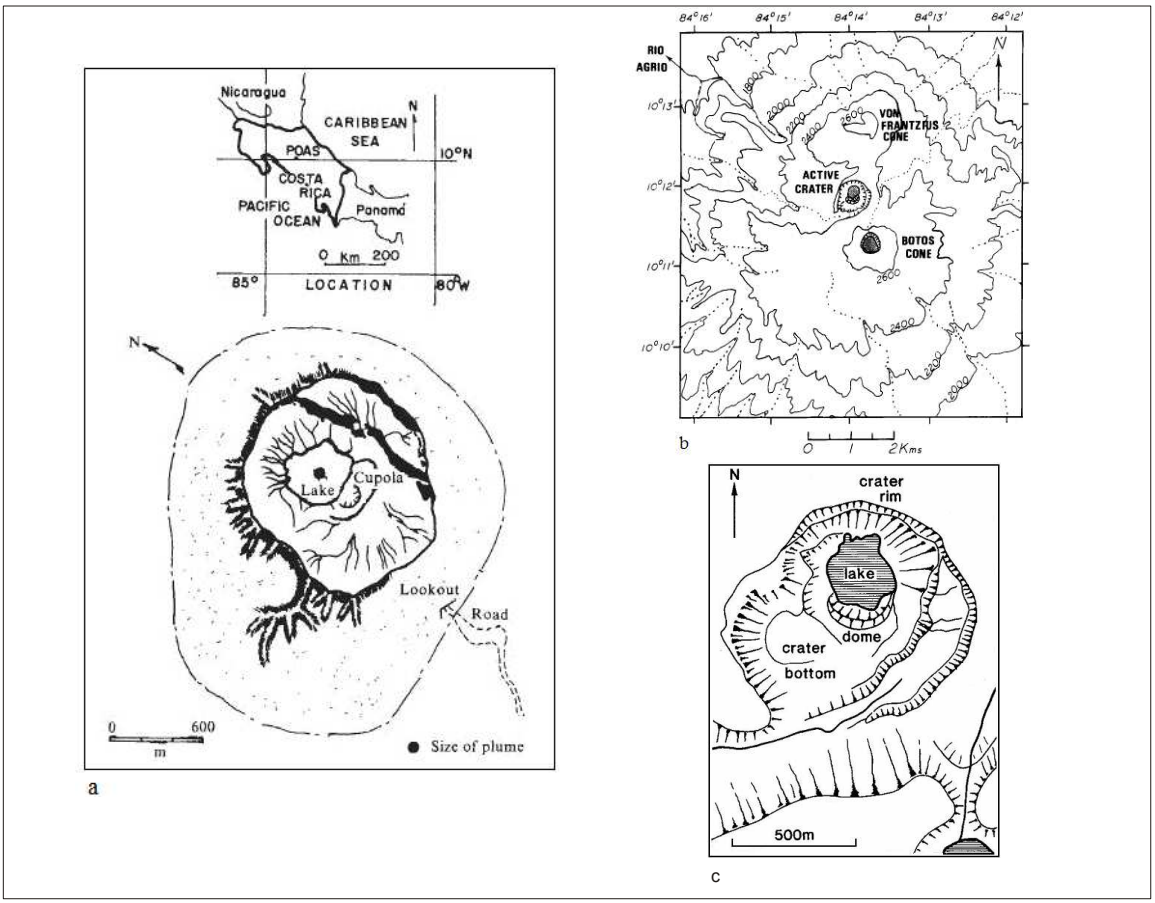

Figure 20: (a) Map location of Poás in Costa Rica; map view of the crater (Bennett and Racchicini, 1978). (b) Map of the summit region of Poás Volcano (Rowe et al., 1992a). (c) Summit morphology of Poás volcano. The area is characterized by the eroded remains of several calderas and includes an active crater with a steaming convecting lake (top center) and a prehistoric crater with a cold-water lake (bottom right) (Rymer and Brown, 1984).

The first documented instance of volcanic activity at Poás dates back to 1834, and it has been in a state of nearly continuous mild activity (Bennett and Raccichini, 1978; Oppenheimer and Stevenson, 1989), undergoing cycles of phreatic and phreatomagmatic activity focused on the crater lake (Rymer et al., 2000). Its usual activity is similar to

shallow submarine volcanism: at intervals ranging from several times a month to several times an hour, a plume erupts from the crater lake, reaching heights of a few meters to 500 m or more (Bennett and Raccichini, 1978). With the fluctuation of lake level, more violent eruptions occur. Several historic episodes of tephra, phreatic, strombolian, vulcanian and lava eruptions have occurred within the active crater, demonstrating the predominantly explosive nature of Poás (Rymer et al., 2000).

5.3 Volcanic Crater Lake Systems

Of the approximately 700 active volcanoes on Earth, roughly 12 percent have crater lakes (Rowe et al., 1992a). Crater lakes are unique in that they act as calorimeters, absorbing heat given off by intruding magma bodies. Heat flowing out of the volcanic conduit under a crater lake causes an overall increase in the temperature of the lake; trends in lake temperature therefore reflect activity of the magmatic intrusions below them (Trunk and Bernard, 2008). Lakes in craters of active volcanoes are condensers of volcanic gases and volcano-hydrothermal fluids formed in deeper zones of a volcanic edifice. Variations in chemical flux from the magma can cause significant changes in the temperature, composition and volumes of these lakes (Rouwet et al., 2004). Seismicity, deformation, changes in gravity, lake water chemistry, and lake water temperatures may indicate that an intrusion is taking place (Rowe et al., 1992 a, b; Giggenbach, 1974; Ohba et al., 2000).

In a situation with high heat output at the base of a crater lake, there must be a high water supply in order for the lake to survive (Brown et al., 1989). Water mass balance, with inputs of meteoric water and geothermal vapor or liquid and outputs of water lost by evaporation, seepage, or stream outflow determines whether a lake will

maintain its volume, grow, or shrink at any given time (Brantley et al., 1993). In order for lake water temperature to increase, the amount of heat entering the system must be greater than the amount that is exiting the system. Pasternack and Varekamp (1997) developed a simple box model to represent the heat budget of crater lakes.

$$E_{\text{cond}}^{\text{volc}} + E_{\text{rad}}^{\text{sun}} + E_{\text{volc}} + E_{\text{rad}}^{\text{atm}} = E_{\text{rad}}^{\text{lake}} + E_{\text{evap}} + E_{\text{cond}}^{\text{lake}} + E_{\text{meteoric}}$$

This shows that the sum of the conductive heat input from a shallow magma body ($E_{cond, volc}$), the short-wavelength solar flux ($E_{rad,sun}$), the enthalpy of the volcanic flux, or convective input from magmatic gases or hot brines (E_{volc}), and the long-wavelength radiative input from the atmosphere ($E_{rad,atm}$) must equal the lake surface long-wavelength radiation ($E_{rad,lake}$), heat loss due to lake surface evaporation (E_{evap}) and lake surface conduction ($E_{cond,lake}$), and heat used to warm meteoric influxes up to the lake's temperature ($E_{meteoric}$)(Figure 21). Smaller lakes can be expected to respond more rapidly to increased heat flux than large lakes because they have less thermal buffering capacity. Regardless of size, a lake cannot exist for long in any case where high thermal input requires the lake to dissipate so much heat through evaporation and radiation that precipitation cannot replace the lost mass (Pasternack and Varekamp, 1997). This is why Volcán Poás is an ideal system; rainfall is consistently high, and replenishes the crater lake on a regular basis.

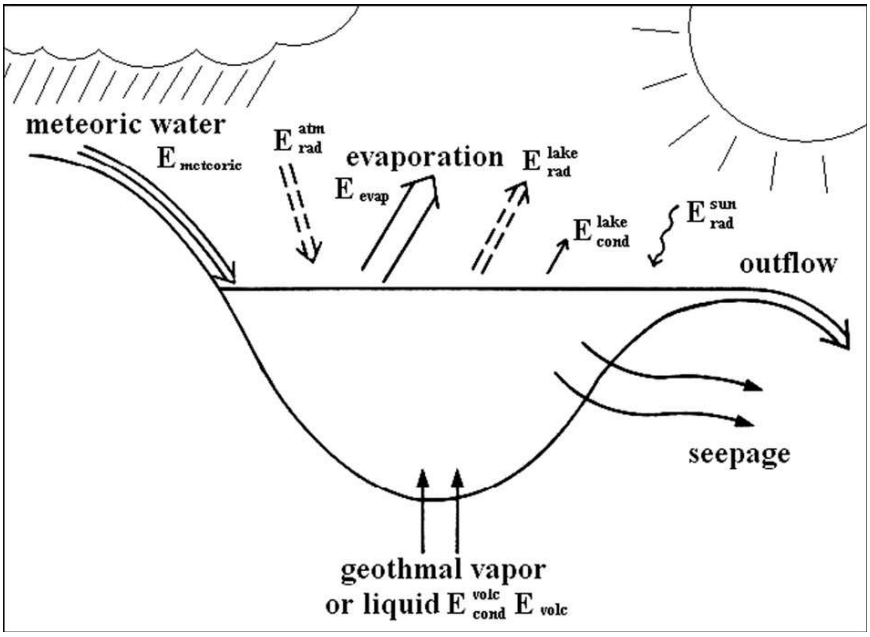

Figure 21: Diagram summarizing the mass and energy balance of crater lakes (modified from Hurst et al., 1991).

5.4 Subaqueous Molten Sulfur Pools

Those crater-lake volcanic systems with active subaqueous fumaroles and large accumulations of sulfur sediments commonly contain molten sulfur pools at the places of highest thermal activity on their lake floors (Takano et al., 1994). The process by which these molten sulfur pools exist at the bottom of crater lakes begins when volcanic lakes receive hot hydrothermal fluids by diffusive venting through bottom sediments or jetting from vents on the crater floor (Kargel et al., 1999). In such cases, sulfur can precipitate and accumulate in bottom sediment. If volcanic heat flow is high enough (i.e. enough heat from underlying magma bodies), sulfur-rich sediment may melt, creating bottom pools of molten sulfur (ρ=1.819 g/cm^3), which is denser than water at 1 g/cm^3 (Kargel et al., 1999). Laguna Caliente may store 5 x 10^8 kg of sulfur in bottom sediments (Rowe, 1994).

Evidence of such subaqueous molten sulfur pools has been observed at several locations throughout the world. Osashi (1919) first inferred the existence of molten sulfur pools at the bottom of the Yugama crater lake, as shown by sulfur spherules forming slicks on the lake surface (e.g. Osashi 1919; White et al., 1988). The spherules are formed as gas is discharged from the molten sulfur layer at the bottom of a submerged sulfur pool. When gases pass through the layer, liquid sulfur encapsulates the bubbles. As the encapsulated bubbles separate from the molten sulfur layer and enter the overlying boiling aqueous solution, the sulfur solidifies and traps the gas. The trapped gas makes the spherules buoyant (Xu et al., 2000) allowing them to rise to the surface. This phenomenon has also been seen at Laguna Caliente (Volcán Poás), as well as several other localities around the world (such as Copahue in Argentina (cf. Varekamp et al., 2001)). Visual confirmation of the existence of molten sulfur pools came when Laguna Caliente dried in 1989, exposing molten sulfur pools that were continuously disturbed by the passage of volcanic gases (Oppenheimer and Stevenson 1989; Oppenheimer 1992).

In order to provide a complete picture of the conditions at Yugama crater lake and Laguna Caliente, a discussion of gas emissions and their role in crater lake volcanic systems must first be presented. As stated earlier, those terrestrial crater lakes with active subaqueous fumaroles, and large accumulations of sulfur sediments, commonly contain molten sulfur pools at the places of highest thermal activity on their lake floors (Takano et al., 1994). Takano et al. (1994) states that these sulfur pools may play an important role in transferring heat to the lake from the heat pipe postulated to be present beneath the sulfur pool.

5.4.1 Gas Emissions and Sulfur Pools

Volcanic gases can indicate a change in the activity of volcanoes. At Yugama crater lake, the appearance of a molten sulfur pool at one vent coincided with an increase in polythionates in the lake water (Takano et al., 1994). Polythionates are sulfur oxyanions (S_xO_6, where x = 4, 5, or 6), which have been proven to herald an increase in activity and SO^{2-} and H_2S-bearing volcanic gas discharge into a hydrothermal system (Takano, 1987; Takano and Watanuki, 1990). The behavior of the sulfur pool, therefore, strongly correlates to the variation in the subaqueous discharge of volcanic volatiles (Takano et al., 1994).

These sulfur pools can dissolve volcanic gases such as SO_2 and H_2S and release them into the water. The presence of these gases in the crater lake drastically lowers the viscosity of the molten sulfur, allowing free passage of fumarolic gases and heat transfer to the lake water via convection within the molten sulfur pools (Takano et al., 1994). This lowering of viscosity may be due to the blockage of growing long-chain sulfur molecules by the dissolved gases. Oppenheimer (1992) stated that sulfur volcanism at Volcán Poás is gas driven: the initial formation of sulfur deposits results from reaction of fumarolic gases with precipitated sulfur (subsequently melting and remobilizing the latter). Fluxing gases are ultimately responsible for maintaining temperatures within liquid sulfur bodies, replenishing them, and driving the frequent, cone-building sulfur eruptions seen at Poás. Oppenheimer (1992) suggested that analogous processes could be taking place on Io albeit on a vastly greater scale; however, as water is absent on Io, the specific controls on SO_2 and H_2S must be different from those affecting Earth's equivalents.

Remelting of fumarolic sulfur deposits could result from heat transferred from hot gases or silicate lava bodies at depth. At Poás, accumulation and mobilization of liquid sulfur is greatly facilitated when the melt has a low viscosity. Because Poás is largely a gas-driven system, changes in gas temperature, as well as the extent to which rainfall recharges the lake or carries sediment over the active region, will affect the nature of sulfur manifestations. The proportion of lake sediments mixed with the sulfur is also likely to influence the rheology of the material (Oppenheimer 1992).

5.5 Precipitation at Volcán Poás

Precipitation is also a major factor in the behavior of a crater lake and its associated sulfur pool(s). A detailed record of Poás' activity is available from May 1969 to present. A summary of Poás' fluctuations in activity will be presented, with an emphasis on the role of the loss and reconstitution of the crater lake in Poás volcano's activity.

5.5.1 Hydrodynamics of the Poás System

Rainfall totals at Poás are very high (Figure 18), averaging about 3.5 m per year at the summit (Brantley et al., 1987). The lake is sensitive to variations in volcanic activity, meteoric fluxes and outflows. When these are not balanced, the lake either becomes deep and cool or becomes hot and disappears (Brown et al. 1989; Pasternack and Varekamp, 1997). Since 1980, the lake has changed from a deep tranquil aqueous body, to a rapidly convecting lake with geysers, then a sulfur-rich boiling mud pool and finally back to a deep tranquil lake (Rymer et al., 2000).

The lake plays an important role in the hydrothermal system, typically condensing ~100 kg/s of steam from floor fumaroles and transferring heat by evaporation, radiation

and conduction at the water surface (Rymer and Brown, 1989). Brown et al. (1989) attribute the lake's disappearance in 1989 to increased evaporation from the lake surface caused by an estimated doubling of power output from the summit over the period from early 1985 to late 1988. They suggest that the increase in power output was attributed to the emplacement of a small magma intrusion, inferred from microgravity measurements (Rymer and Brown, 1989, Rowe et al., 1992a). Rymer et al. (2000), however, suggest that a series of magma-filled dendritic conduits intruded beneath the lake facilitated enhanced heat and gas flux from a deeper magma feeder body.

The following section presents a summary of the power output with gas discharge and magmatic activity of Volcán Poás from 1981 to 1990. This time period is presented because it is the longest time frame on record in which the lake was at either very low levels or was gone altogether. Although gas percentages were not obtained for Poás' most active period in 1988 and 1989, they were recorded in the years leading up to this time frame. SO_2 was the major component of the gases measured. SO_2 content dropped considerably from the period 1981-1983, when lake level was low, vs. 1992, when the lake level was near normal once again. For several sampling times between 1981 and 1993, the dominant sulfur species at Poás was SO_2, with smaller concentrations of H_2S, COS and other gases (Table 7a, 7b)

Gas (in % unless otherwise noted)	07/1981	01/1982	03/1982	12/1983	11/1992
SO_2	55.79	66.4	59.8	66.1	34.16
CO_2	26.06	20.11	20.9	21.8	42.4
H_2	17.90	13.1	13.5	11.5	0.26
H_2S	0.52	0.02	0	0.246	11.65
N_2	1.98 (in air)	---	---	---	0.027
CO	0.24	0.265	0.16	0.18	0.0003
CH_4 (ppm)	84.3	---	---	---	---
He (ppm)	52	128	40	38	---
COS, carbonyl sulfide (ppm)	25.8	---	---	---	---
HCl	---	---	---	---	11.27
HF	---	---	---	---	0.26
N_2	---	---	---	---	0.27
B	---	---	---	---	0.0056

Table 7a: Data compiled by the Universidad Nacional de Costa Rica, summarized in Smithsonian Institution report (2005).

Date	SO_2 (Metric tons/day)	Source	Activity
December 1981	600	Prosser and Carr, 1987	Continuous large white vapor plume. Fumarole temperatures rose to 960 ºC from March to November 1981. Temperature of crater lake 40°C, abundant sulfur bubbles floating on its surface.
February 1982	760 ± 310	Casadevall et al., 1984	High temperatures and incandescence continued at the eroded cone at the S end of the crater lake. Water temperatures in the crater lake remained relatively high (May 1982).
December 1982	500	Stoiber et al., 1986	Fumarolic activity continued in the eroded cone at the S end of the crater lake, with temperatures ranging from 652 to 873°C. From 1981-1984 power output peaked.
February 1991	Average: 90 ± 30, Range: 50 – 160	Andres et al., 1992; Smithsonian Institution report, 2005	Crater lake level continued to drop, maximum lake depth estimated at 3m. Dome fumarole temperatures of 40-90°C.
April 2006	104	Barrancos et al., 2008	Area of the lake increased by ~ 20%. Lake temperature 54ºC, with a pH of 0.63.

Table 7b: A summary of past COSPEC measurements taken at Poás.

The measurements of SO_2 flux correlate well with activity at Poás measured by total summit power output (Rowe et al., 1992a). If power output is related to magmatic input, which in turn is related to sulfur flux, then it follows that 1991 and 2006 SO_2 fluxes should be lower than the early 1980s SO_2 fluxes (Andres et al., 1992), which they are. Throughout much of the 1980s, when the crater lake was stable, the power output of the system was estimated to be about 200 MW on average (Brown et al., 1989, 1991). However for an extended period in 1981–1983, the SO_2 flux was several hundred tons per day and dome fumarole temperatures were 800 ºC. The power output during this period exceeded 500 MW on several occasions (about 100 m plumes) (Rowe et al., 1992a). Power output peaked in 1981-1984 with a high-temperature fumarole event, and three sharp rises in lake power output preceded and accompanied periods of phreatic activity (late 1978, late 1979, mid-1987). Power output peaked at 1000 MW (creating 200-m-high plumes) in 1987–1989 during geysering episodes (Brown et al., 1991; Rymer et al., 2000). Laguna Caliente became a peak activity lake between 1984 and 1990 (Rymer et al., 2000). Power output was at a minimum just prior to the two episodes of renewed subsurface magmatic activity in 1980 and 1986 (Rowe et al., 1992a, Figure 22).

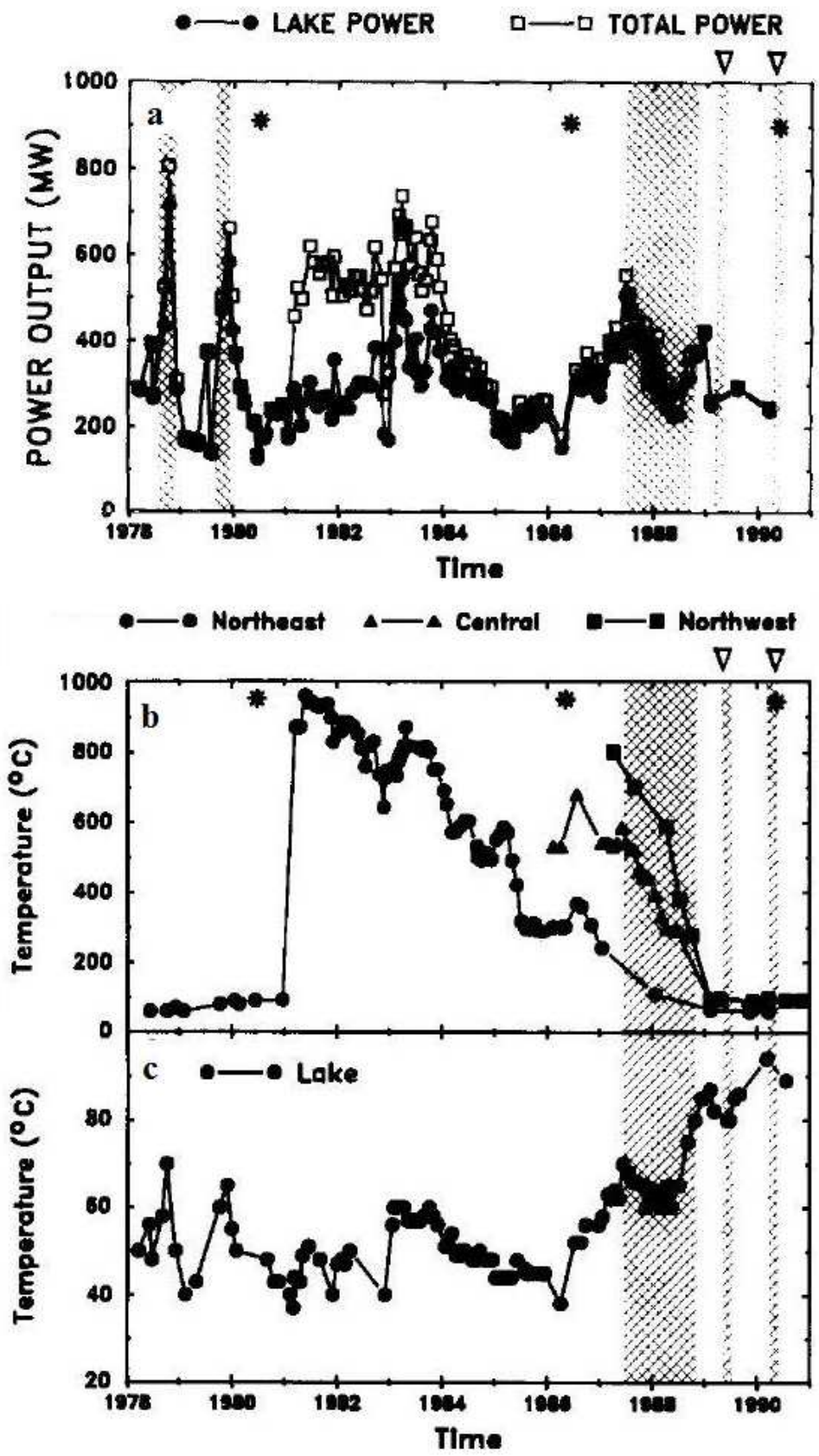
LAKE POWER
TOTAL POWER
a
POWER OUTPUT (MW)
1000
800
600
400
200
0
1978
1980
1982
1984
1986
1988
1990
Time
Northeast
Central
Northwest
b
Temperature (°C)
1000
800
600
400
200
0
c
Lake
Temperature (°C)
80
60
40
20
1978
1980
1982
1984
1986
1988
1990
Time

Figure 22: (a) Estimated lake and total summit power outputs from 1978 – 1990. Error bars, which average ± 30 and ± 45 percent of the calculated lake and total summit power outputs, are omitted for clarity (b) Temperature data for fumaroles located on northeast, central upper, and northwestern areas of the dome. (c) Crater lake temperature data (Rowe et al., 1992a).

Variations in power output through the lake surface are primarily controlled by variations in lake temperature, which in turn controls evaporation. Evaporation typically accounts for 74 percent of the power output of the lake (Rowe et al., 1992a). Although individual phreatic (geyser) eruptions have high instantaneous power outputs (10^2 to > 10^4 MW, Brown et al., 1989), integrated over time, they typically contribute < 10 percent of the total summit output (Rowe et al., 1992a).

5.5.2 Temperature variations of Poás crater lake

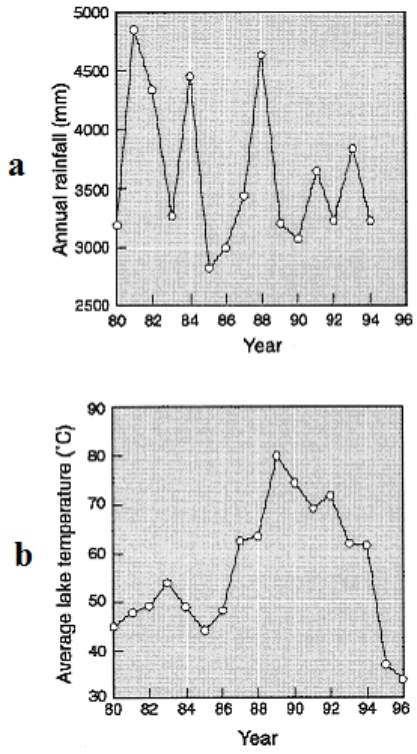

Figure 23a: Annual rainfall at the summit of Poás volcano (1985-1994); Figure 23b: Annual average temperature of Poás crater lake (1980-1996) (Rymer et al., 2000).

Figure 23a shows the average temperature of the crater lake for the same time period studied for rainfall totals as seen in Figure 23b. In order for heat to be transferred from an underlying magma body to cause an increase in temperature of a crater lake, heat must be transferred from the intrusion, through the hydrothermal system, and into the lake. Hurst et al. (1991) define four regions that are important in the transfer of heat from intrusion to lake: the magma body and its boundary layer, the volcanic conduit, a boundary layer at the top of the conduit beneath the lake (sulfur pools?), and the water at the base of the lake itself (Hurst et al., 1991). Once heat reaches the bottom of a crater lake from the magma body, it still must be transferred into the water and distributed throughout the lake volume (Kusakabe, 1996). Takano et al. (1994) states that sulfur pools may play an important role in transferring heat to the crater lake from the heat pipe postulated to be present beneath the sulfur pool, in the case of Yugama crater lake.

5.5.3 Past Activity and Crater Lake Level

Laguna Caliente became a 'peak-activity' lake during the period 1984–1990 (Rymer et al., 2000). The Smithsonian Institution report (2005) has a complete account of Poás' activity from 1969 to 2007, and the eruptive cycle at Volcán Poás in the 1980s was notable for the disappearance and subsequent reappearance of the summit crater lake. This cycle consisted of discrete phases of activity associated with a range of geophysical and geochemical signatures that heralded the increase in activity. Elevated levels of A-type seismicity (i.e. high frequency >3 Hz) in 1980 coincided with the beginning of a trend of elevated lake temperature that peaked in 1983. A significant increase in A-type seismicity again in 1986 marked the beginning of a period of increasing B-type seismicity (i.e low frequency <2Hz). The 1986–1989 event, which culminated in the

complete loss of the crater lake and explosive eruptions, was characterized by concurrent increases in micro-gravity (on the southern crater floor), B-type seismicity and lake temperature and by changes in lake geochemistry. The role of the lake as a physical and chemical buffer to the volcanic system was clearly demonstrated when its disappearance in 1989 was accompanied by enhanced eruptive activity and gas emissions with considerable local environmental impact. The lake therefore acts as both a moderator and index of volcanic processes at Poás.

Prior to 1989, when the lake disappeared, volcanic gases were discharged into the lake and became hydrated and diluted. However, once the lake disappeared, and no longer provided a buffer (Rymer and Brown, 1989), gases and particulates vented directly into the atmosphere.

By January 1988, the lake level had dropped markedly since 1987. April 1988 (Figure 24) saw phreatic explosions depositing acidic mud and sulfur. In July 1988 the lake dropped 1.5 m, from April of the same year, and the diameter reduced by 20 m. Phreatic explosions subsided to six zones of convective bubbling. Geologists at the time noted that the change from periodic explosions to continuous convective bubbling releasing heat/energy may be due to a decrease in hydrostatic pressure with lowering lake level rather than an increase of energy into the lake (Smithsonian Institution report, 2005).

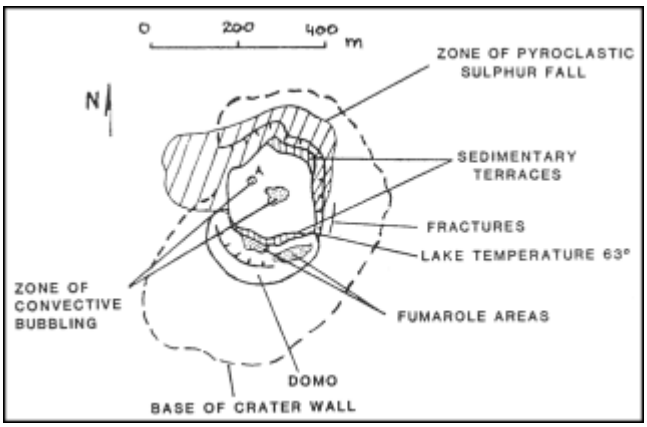

Figure 24: Sketch map of the crater of Poás on 13 April 1988. (Smithsonian Institution report, courtesy of G. Soto).

The small lake fell another 2 m in March 1989, with a cumulative decrease of 32 m since early 1987 (Figure 25).

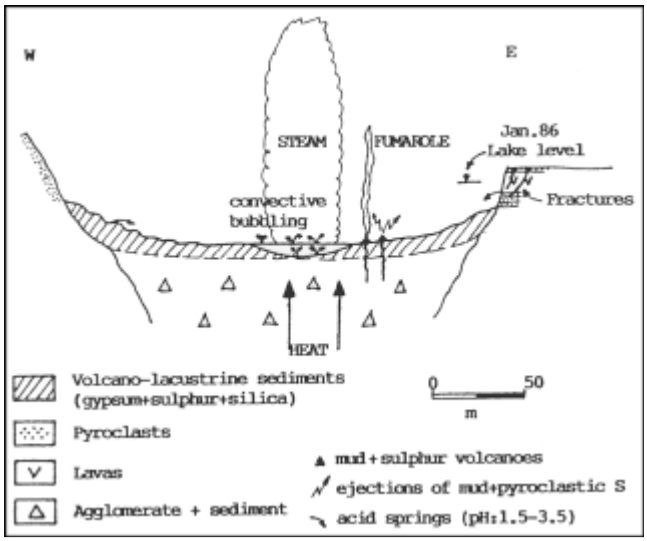

Figure 25: W-E diagrammatic cross-section of the crater at Poás illustrating March 1989 activity (Smithsonian Institution report, courtesy of Gerardo Soto).

The following is an account of the activity, summarized from the Global Volcanism Program (Smithsonian Institution report, 2005), that immediately followed the dessication of the crater lake in April 1989. Figure 26 is a sketch map of the crater's appearance during this time period. The activity culminated in an ash and dry steam

eruption (450 ºC) in April 1989 from the base of the dried crater lake. The eruption continued for 2–3 weeks, reaching a maximum

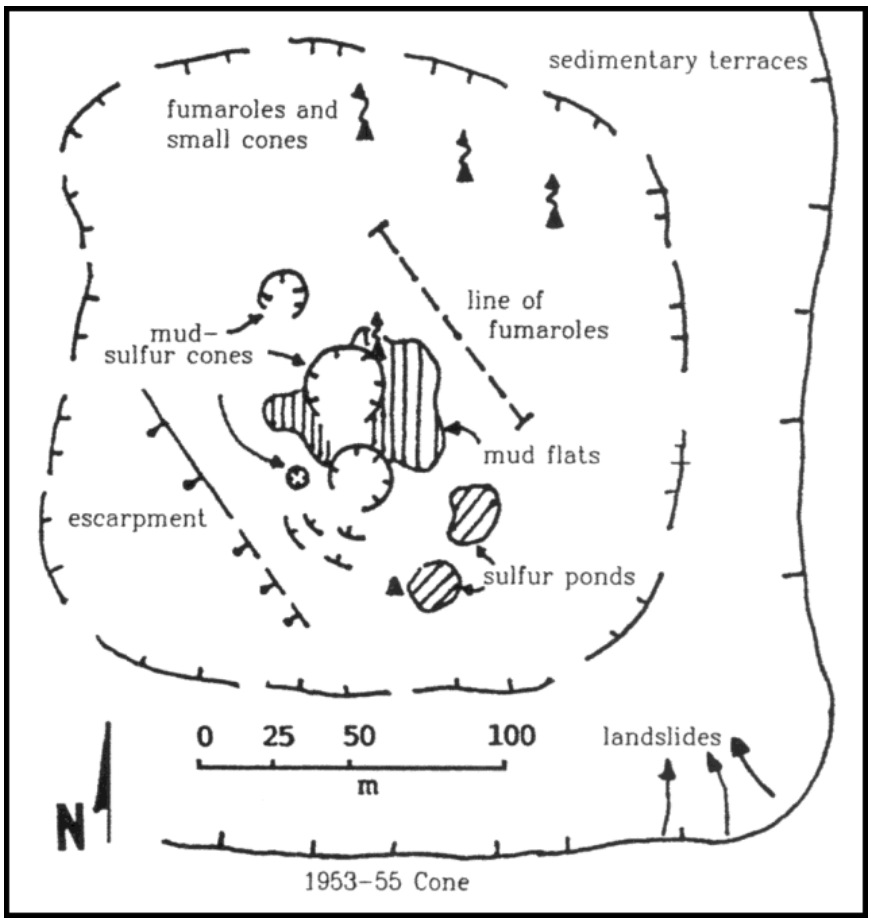

Figure 26: Sketch map of the inner crater at Poás and its features, April 1989. (Smithsonian Institution report, courtesy of G. Soto).

column height of 1.5–2 km.

The crater lake, which had been shrinking since early 1987, disappeared by April 19 of the same year. After the lake's disappearance, columns of mud erupted, rising 10-350 m, building a cone that was 15 m high and contained seven active vents by 26 April. Explosions and molten sulfur ponds dominated.

Two ponds of dark brown, very fluid, bubbling sulfur, were about 50 cm below the (former) crater lake floor in steep-sided pits, with an average temperature of 115ºC.

A terrace of solid sulfur developed at the edge of the liquid, and the sides and rims of the pits were coated by bright yellow sulfur sublimates (Figure 27).

Toward the end of May 1989, the crater partially refilled with rainwater and small ash eruptions moved to one point on the west side of the crater, where water was not present (Smithsonian Instituion report, 2005).

Figure 27: Sulfur terraces around Poás volcano in April 1987 (Smithsonian Institution report, 2005). This image does not show any sulfur pools.

Sulfur sublimates were deposited around fumarolic vents, and some of the sulfur burned, forming SO_2. Flames from the combustion of sulfur (and perhaps hydrogen) were intense above some vents. In the SE part of the crater, a molten, bubbling, sulfur lake formed and sulfur flowed across the crater floor (Smithsonian Institution report, 2005).

Activity after the April-May 1989 was strongly seasonal; during the rainy season (May-December), the crater lake began to reform, reaching a few meters depth. Mud eruptions again dominated the activity, depositing ejecta within the crater. Small ash eruptions continued only from one point on the W side of the crater where there was little water.

Several periods of sulfur flow activity occurred during 1989. The sulfur lake on the NE side of the crater produced numerous yellow sulfur flows that were up to 30 m long, a few meters wide, and a few centimeters thick. More viscous greenish-yellow sulfur/mud flows had pahoehoe morphologies. More such flows erupted again in October of the same year, and the northern section of the crater contained cones of mud and sulfur, while a molten sulfur lake was the source of occasional flows several meters long and a few centimeters thick (Figure 28).

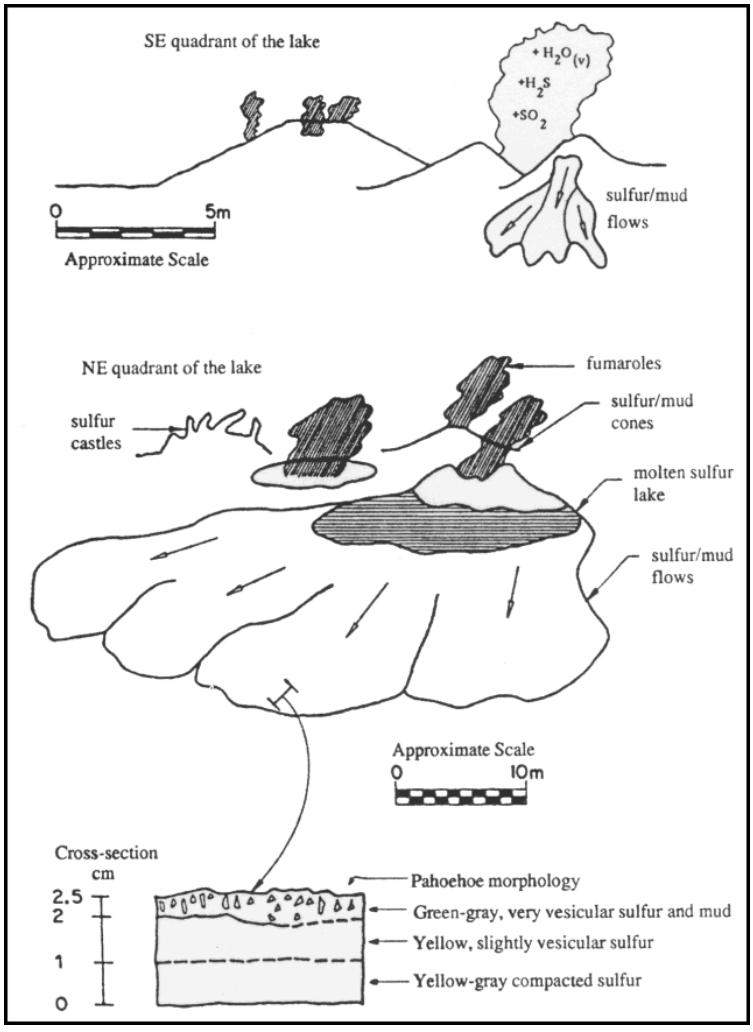

Figure 28: Sketch by Gerardo Soto of the SE (top) and NE (center) quadrants of the hot crater lake at Poás, showing gas emission, a molten sulfur lake, sulfur/mud flows, and various morphologic features as of October 1989. A cross-section of one of the sulfur/mud flows is shown at bottom (Smithsonian Institution report).

During April 1990, three shallow molten sulfur ponds with continuous convection with a mean temperature of 160ºC formed on the northeast side of the crater (Figure 29).

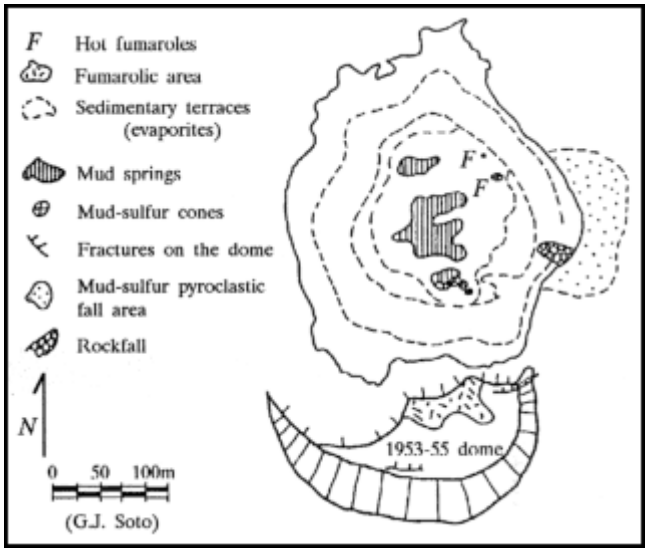

Figure 29: Sketch map of the active crater at Poás, 18 April 1990 (Smithsonian Institution report, courtesy of G. Soto).

Once the heat flux subsided after the last phreatic eruption occurred in August 1994, the crater lake began to re-establish in October 1994 (Figure 29). This apparently marked the end of the active cycle and the lake was approaching its pre-eruption level by the end of 1995 and by February 1998 had exceeded it (Smithsonian Institution report, 2005).

The volcano now appears (as of the last Smithsonian Institution report in December, 2007) to be in a state of dynamic equilibrium in which the lake is able to condense incoming volcanic gases, thus buffering variations in heat and mass flux and allowing the large body of andesitic magma beneath the active crater to de-gas with minimal effect on the local environment (Rymer et al., 2000). Thus the crater lake has acted as both a moderator and index of volcanic processes at Poás and has now moved from 'peak activity' to 'medium activity' (Pasternack and Varekamp 1997).

CHAPTER 6

SUMMARY AND CONCLUSIONS

Terrestrial Analog

A major idea in this work concerns the role of water in volcanism on Earth, and considering an equivalent on the surface of Io. Earth's most common native-sulfur-forming reactions generally involve water, which is clearly not the case on Io (Kargel et al., 1999). Eruptive activity at Poás accompanying the decline and disappearance of the crater lake in April 1989 raises the question of the role of the lake in the volcanic system, specifically water-magma interactions (Casertano et al., 1987; Brown et al., 1989; Rymer et al., 2000). The diameter of the lake lowered by 20 m in the span of a few years and phreatic explosions subsided to six zones of convective bubbling. This may be due to a decrease in hydrostatic pressure with lowering lake level, or perhaps an increase of energy into the lake (Smithsonian Institution report, 2005). In any event, the role of the lake as a physical and chemical buffer to the volcanic system was demonstrated when its complete disappearance in 1989 was accompanied by enhanced eruptive activity and gas emissions. The lake therefore acts as both a moderator and index of volcanic processes at Poás (Rymer et al., 2000).

The essential aspect of the sulfur volcanism at Poás is that it is gas-driven: the initial formation of sulfur deposits results from reaction of the fumarolic gases that then appear to have been responsible for melting and remobilizing some of the precipitated sulfur, and ultimately, for maintaining temperatures within liquid sulfur bodies, replenishing them, and driving the frequent, cone-building sulfur eruptions. Although there is still significant activity in the crater during both wet and dry periods, there is an

undeniable correlation between the intensity of activity and the presence or absence of water. The molten sulfur pools present at the bottom of the crater lake are relatively stable in the presence of water.

Oppenheimer and Stevenson (1989) believe that, in a given sulfur-rich hydrothermal/magmatic system, localized pockets of molten sulfur occur where gas temperatures exceeded the sulfur liquidus. They believed, however, that widespread melting would be inhibited when an aqueous lake is present because the temperature of the water-saturated sediments remains below the local boiling point of water. The loss of the crater lake would remove this temperature buffering system so that temperatures of sediment fluxed by hot gases can increase above the sulfur liquidus, generating much greater volumes of melt (Oppenheimer and Stevenson, 1989).

The presence of water may have prevented the temperature from getting hot enough to melt sulfur sediments at the base of the crater, but there was at least some evidence of molten sulfur when the lake was present due to the occurrence of sulfur spherules floating on the lake. The parts that were molten were stabilized by the water present above (whether by chemical balances or by hydrostatic pressure), and when the lake evaporated, even more sulfur became mobilized, and the pools became very active. This model is supported by the occurrence of some sulfur flows that were confined to the crater floor during 1989, as described in the previous chapter.

Takano et al. (1994) had a different theory in their work involving geochemical studies of molten sulfur pools at Yugama crater lake. They stated that the behavior of sulfur pools strongly correlates with the variation in the subaqueous discharge of volcanic volatiles. Heat escaping from the underlying magma body keeps the sulfur pools molten

and passage of gases continues even when the lake is desiccated. However, Takano et al. (1994) postulate that, in the absence of water and with a decrease in sulfur viscosity, sulfur cannot be molten even with high temperatures. Gases in water lower the viscosity of already molten sulfur, so if there is no medium in which such gases can be dissolved on Io, the viscosity may be too high for sulfur pools to exist. The behavior of the sulfur pool, therefore, appears to strongly correlate with the variation in the subaqueous discharge of volcanic volatiles (Takano et al., 1994).

Sulfur pools and crater lakes seem to have a symbiotic relationship. Takano et al (1994) continue, stating that these subaqeous sulfur pools can dissolve volcanic gases such as SO_2 and H_2S and release them into the water. Subsequently, the gases present in the lake lower the viscosity of molten sulfur, allowing even more free passage of gases and transferring heat to the lake. In addition, liquid sulfur bodies could be maintained for long periods as a result of the positive feedback cycle of the passage of fumarolic gases, which can inhibit the growth of crusts and keep viscosities down. This is interrupted when, for example, the crater lake level lowers due to an intruding magma body, or due to seasonal changes in precipitation.

Remelting of fumarolic sulfur deposits could result from the transfer of heat from hot gases or silicate lava bodies at depth. Accumulation and mobilization of liquid sulfur would be greatly facilitated if the melt had a low viscosity, as was the case at Poás, which would bracket likely temperatures. Liquid sulfur bodies could be maintained for long periods as a result of the passage of fumarolic gases, which can inhibit the growth of crusts and replenish evaporative losses by condensation of fresh sulfur (Oppenheimer, 1992).

When the lake dried up in April 1989, increased activity shortly followed, indicating that sulfur pools in confined magmatic/hydrothermal systems are not completely stable without the intermediary of water.

The available temperature evidence from Io indicates that there are few if any hot spots with the required temperatures to be evidence of sulfur pools. The temperatures are either too high (silicate volcanism) or too cool to be standing sulfur pools (ex. Emakong patera with temperatures of 270+/-90 K). Typical temperatures are between 190-270 K, cooler than pure molten sulfur. Sulfur polymorphs have melting points of 385-393 K, which is much warmer than observed patera temperatures (Lopes et al., 2004). Sulfur boiling in a vacuum, as a result of a magmatic intrusion, cannot get hotter than ~500 K (Lunine and Stevenson, 1985). As the liquidus of sulfur is only 388 K, it is likely that sulfur in close proximity to hot spots, or a silicate eruption, would be mobilized as flows (Clow and Carr, 1980).

Williams et al. (2010, submitted) adapted the table of Ionian hot spots detected by ground-based telescopes and all spacecraft flybys given in Lopes and Spencer (2007) and integrated it with the finalized geologic map of Io to correlate the locations of hot spots with map units. 93.5 percent of all detected hot spots occur in either dark (45.3 percent) or undivided (18.6 percent) patera floor units, or dark (20.3 percent) or undivided (9.3 percent) lava flows. About 4.8 percent of hot spots occur in plains or other units without a clear volcanic vent, with the remaining 1.7 percent of hot spots correlating with Bright flows. The low percentage of the latter features suggests that sulfur volcanism is currently not a major component of Io's active volcanism.

I propose that, in the absence of high enough temperatures (such as in the case of an impending volcanic eruption, or an intermediary such as water), the viscosity of sulfur is too high for standing pools to exist on the surface of Io. The remobilization of precipitated sulfur appears to be integral in forming the large sulfur flows seen around some paterae on Io. Lopes et al. (2004) interpreted the colors seen at Emakong as patera floor deposits consisting of molten or partly cool sulfur and the brighter flows around the patera represent older cooled sulfur. However, from the mapping effort to which I contributed (Williams et al., 2010 submitted), the low percentage of hot spots that correlate with bright flows (<2 percent of active hot spots are associated with bright flows) indicates that sulfur volcanism is likely not a major component of Io's volcanism. On the issue of the role of sulfur or silicate volcanism at Emakong, further high resolution spectral and thermal observations by future missions are required.

Sulfur dioxide, which is prevalent on Io, may play the same role as water does on Earth in providing a physical and chemical buffer to molten sulfur. With increasing temperature, due to a magmatic intrusion for example, the sulfur dioxide deposits would be dissipated, allowing sulfur to flow freely. Heated above its critical temperature (430.12K), sulfur dioxide can only exist as a vapor regardless of pressure. Currently, paterae are likened to caldera structure; this concept, however, suggests that paterae on Io may be more analogous to terrestrial crater lakes than calderas.

REFERENCES CITED

Allen, C.C., Gooding, J.L., Jercinovic, M, and Keil, K., 1981, Altered volcanic glass: a terrestrial analog to the soil of Mars: Icarus, v. 45, iss. 2, p. 347-369.

Aharonson, O., Zuber, M.T., Rothman, D.H., Schorghofer, N., Whipple, K.X., 2002, Drainage basins and channel incision on Mars: Proceedings of the National Academy of Sciences, v. 99, no.4, p. 1780-1783.

Anderson, J. D., Sjogren, W. L., Schubert, G., 1996, *Galileo* Gravity Results and the Internal Structure of Io: Science, v. 272, no. 5262, p. 709-712.

Andres, R.J., Barquero, J., and Rose, W.I., 1992, New measurements of SO_2 flux at Poás Volcano, Costa Rica: Journal of Volcanology and Geothermal Research, v. 49, p. 175-177.

Becker, T. and P. Geissler, 2005. *Galileo* global color mosaics of Io, In Lunar and Planetary Science XXXVI, Abstract #1862, Lunar and Planetary Institute, Houston (CD-ROM).

Bennett, F.D., and Raccichini, S.M., 1978, Subaqueous sulphur lake in Volcán Poás: Nature, no. 271, pp. 342-344.

Blaney, D.L., Johnson, T.V., Matson, D.L., and Veeder, G.J., 1995, Volcanic Eruptions on Io: Heat Flow, Resurfacing, and Lava Composition: Icarus v. 113, iss. 1, p. 220-225.

Brantley, S.L., Borgia, A., Rowe, G., Fernandez, J.F., and Reynolds, J.R, 1987, Poás volcano crater lake acts as a condenser for acid metal-rich brine: Nature, v. 330, p. 470-472.

Brantley, S.L., Ágústsdóttir, A.M., Rowe, G.L., 1993. Crater lakes reveal volcanic heat and volatile fluxes. GSA Today 3 (7), 175–178.

Brown, G., Rymer, H., Dowden, J., Kapadia, P., Stevenson, D., Barquero, J., Morales, L.D., 1989, Energy budget analysis for Poás crater lake: implications for predicting volcanic activity: Nature v. 339, 370–373.

Burns, J. A. and Matthews, M.S., Satellites. Tucson, AZ: University of Arizona Press, 1986, 1032 p.

Campbell, B.A., and Rogers, P.G., 1994, Bell Regio, Venus: integration of remote sensing data and terrestrial analogs for geologic analysis: Journal of Geothermal Research, v. 99, no. E10, p. 21153-21171.

Carr, M.H., 1986, Silicate volcanism on Io: Journal of Geophysical Research, v. 91,

p. 3521-3532.

Carr, M.H., A.S. McEwen, K.A. Howard, F.C. Chuang, P. Thomas, P. Schuster, J. Oberst, G. Neukum, and G. Schubert, 1998, Mountains and calderas on Io: Possible implications for lithosphere structure and magma generation, Icarus, v. 135, 146-165.

Chan, M.A., Beitler, B., Parryl, W.T., Ormo, J., and Komatsu, G., 2004, A possible terrestrial analogue for haematite concretions on Mars: Nature, v. 429, p. 731-734.

Chapman, M. G., and Smellie, J. L., Mars interior layered deposits and terrestrial sub-ice volcanoes compared; observations and interpretations of similar geomorphic characteristics, The geology of Mars; evidence from Earth-based analogs. Eds. F. Bagenal, F. Nimmo, C. Murray, D. Jewitt, R. Lorenz, and S. Russell: Cambridge, United Kingdom: Cambridge University Press, 2007, p. 178-210.

Clary, M. C.; Klaasen, K. P.; Snyder, L. M.; Wang, P. K., 1979, 800 x 800 charge-coupled device/CCD/camera for the *Galileo* Jupiter orbiter mission: Recent advances in TV sensors and systems; Proceedings of the Seminar, San Diego, Calif. Bellingham, Wash., Society of Photo-Optical Instrumentation Engineers, p. 98-108.

Clow, G.D., and Carr., M.H., 1980, Stability of sulfur slopes on Io: Icarus, vol. 44, p. 268-279.

Crown, D.A., R. Greeley, R.A. Craddock, and G.G. Schaber, 1992, Geologic map of Io: U.S. Geological Survey Miscellaneous Investigations Series Map I-2209, as part of the Atlas of Jovian Satellites, scale 1:15,000,000 Geologic Series.

Davies, A.G, Lopes-Gautier, R., Smythe, W.D., Carlson, R.W., 2000, Silicate Cooling Model Fits to *Galileo* NIMS Data of Volcanism on Io: Icarus, v. 148, iss. 1, p. 211-225.

Davies, A.G., Keszthelyi, L.P., Williams, D.A., Phillips, C.B., McEwen, A.S., Lopes-Gautier, R.M., Smythe, W.D., Soderblom, L.A., and Carlson, R.W., 2001, Thermal signature, eruption style, and eruption evolution at Pele and Pillan on Io: Journal of Geophysical Research, v. 106, p. 33,079-33,103.

Douté, S., Lopes, R., Kamp, L.W., Carlson, R., Schmitt, B., and the *Galileo* NIMS Team, 2002, Dynamics and Evolution of SO_2 Gas Condensation around Prometheus-like Volcanic Plumes on Io as Seen by the Near Infrared Mapping Spectrometer: Icarus, vol. 158, iss. 2, p. 460-482.

Douté, S, Lopes, R., Kamp, L.W., Carlson, R., and the *Galileo* NIMS Team, 2004, Geology and activity around volcanoes on Io from the analysis of NIMS spectral images: Icarus, vol. 169, p. 175-196.

Fegley Jr., B., and Zolotov, M.Y., 2000, Chemistry of sodium, potassium, and chlorine in volcanic gases on Io: Icarus v. 148, p. 193-210.

Fink, J.H., Park, S.O., and Greeley, R., 1983, Cooling and deformation of sulfur: Icarus, v. 56, p. 38-50.

Flynn, L.P., Mouginis-Mark, P.J., Gradie, J.C., Lucey, P.G., 1993, Radiative Temperature Measurements at Kupaianaha Lava Lake, Kilauea Volcano, Hawaii: Journal of Geophysical Research, v. 98, no. B4, p. 6461-6476.

Geissler, P.E., A.S. McEwen, L. Keszthelyi, R. Lopes-Gautier, J. Granahan, and D.P. Simonelli, 1999, Global color variations on Io: Icarus, v 140, p 265-282.

Geissler, P.E., McEwen, A.S., Phillips, C.B., Keszthelyi, L.P., Turtle E.P., Milazzo, M., Lopes-Gautier, R.M., Simonelli, D.P., Williams, D.A., 2000, New results on Io's color and composition. Abstracts of paper submitted to the Lunar and Planetary Science Conference, v. 31, Abstr. No. 1968.

Geissler, P.E., A.S. McEwen, C.B. Phillips, L.P. Keszthelyi, and J.S. Spencer, 2004, Surface changes on Io during the *Galileo* mission: Icarus, v. 169.

Giggenbach, W., 1974. The chemistry of crater lake, Mt. Ruapehu (New Zealand) during and after the 1971 active period. New Zealand Journal of Science 17, 33–45.

Greeley, R., Theilig, R., Christensen, P., 1984, The Mauna Loa sulfur flow as an analog to secondary sulfur flows (?) on Io: Icarus, v. 60, p. 189-199.

Greeley, R., Spudis, P.D., and Guest, J.E., 1988, Geologic map of the Ra Patera area of Io. Geological Survey Miscellaneous Investigations Series Map I-1949, scale 1:2,000,000, Geologic Series.

Hon, K., Kauahikaua, J., Denlinger, R., Mackay, K., 1994, Emplacement and inflation of pahoehoe sheet flows: observations and measurements of active lava flows on Kilauea volcano, Hawaii: Geological Society of American Bulletin, v. 106, iss. 3, p. 351-370.

Howell, R.R., 1997, Thermal emission from lava flows on Io: Icarus, v. 127, iss. 2, p. 394-407.

Hooper, P.R., 1997, The Columbia River flood basalt province: Geophysical monograph, v. 100, p. 1-27.

Hurst, A.W., Bibby, H.M., Scott, B.J., McGuinness, M.J., 1991, The heat source of Ruapehu Crater Lake; deductions from the energy and mass balances: Journal of Volcanology and Geothermal Research v. 46, 1–20.

Jaeger, W.L., 2003, Orogenic tectonism on Io: Journal of Geophysical Research, v. 108, no. E8, p. 5093, doi:10.1029/2002JE001946.

Johnson, T. V. Cook II, A. F., Sagan, C. Soderblom, L. A., 1979, Volcanic resurfacing rates and implications for volatiles on Io: Nature, v. 280, p. 746-750.

Johnson, T.V., Morrison, D., Matson, D.L., Veeder, G.J., Brown, R.H., and Nelson, R.M., 1984, Volcanic hot spots on Io: Stability and longitudinal distribution: Science v. 226, p. 134-137.

Johnson, T.V., Matson, D.L., Blaney, D.L., Veeder, G.J., and Davies, A.G., 1995, Stealth plumes on Io: Geophysical Research Letters, v. 22, p. 3293-3296.

Kargel, J.S., Delmelle, P., and Nash, D.B., 1999, Volcanogenic sulfur on Earth and Io: composition and spectroscopy: Icarus, v. 142, p. 249-280.

Keszthelyi, L., McEwen, A.S., Phillips, C.B., Milazzo, M., Geissler, P., Turtle, E.P., Radebaugh, J., Williams, D.A., Simonelli, D.P., Breneman, H.H., Klaasen, K.P., Levanas, G., and Denk, T., 2001, Imaging of volcanic activity on Jupiter's moon Io by *Galileo* during the *Galileo* Europa Mission and the *Galileo* Millennium Mission : Geology and geophysics of Io: Journal of Geophysical Research, v. 106, no. E12, p. 33025-33052.

Keszthelyi, L., Jaeger, W.L., Turtle, E.P., Milazzo, M., and Radebaugh, J., 2004, A post-*Galileo* view of Io's interior: Icarus, v. 169, p. 271-286.

Keszthelyi, L., Jaeger, W., Milazzo, M., Radebaugh, J., Gerared-Davies, A., and Mitchell, K.L., 2007, New estimates for Io eruption temperatures: Implications for the interior: Icarus, vol. 192, iss. 2., pp. 491-502.

Kieffer, S.W., 1982, Dynamics and thermodynamics of volcanic eruptions: Implications for the plumes of Io: in Satellites of Jupiter, (edited by D. Morrison), Univ. of Ariz. Press, Tucson, p. 647-723.

Kieffer, S.W., Lopes-Gautier, R., McEwen, A., Smythe, W., Keszthelyi, L., and Carlson, R., 2000, Prometheus: Io's wandering plume: Science v. 288, p. 1204-1208.

Kivelson, M. G., K. K. Khurana, R. Lopes, E. Turtle, 2001, Polar passes by Io: Limits on the internal field and sources of field-aligned currents in the polar cap: Eos Transactions AGU 83, P22A-03.

Klaasen, K.P., Breneman, H.H., and Simon-Miller, A.A., 2003, Operations and calibration of the solid-state imaging system during the *Galileo* extended mission at Jupiter: Optical Engineering, v. 42, iss. 2, p. 494.

Kusakabe, M., 1996. Hazardous crater lakes. In: Scarpa, R., Tilling, R.I. (Eds.),

Monitoring and Mitigation of Volcano Hazards. Springer, Berlin, pp. 573–598.

Lellouch, E., 1996, Urey Prize lecture. Io's atmosphere: not yet understood: Icarus, v. 124, iss. 1, p. 1-21.

Lopes, R.M.C., Kamp, L.W., Douté, S., Smythe, W.D., Carlson, R.W., McEwen, A.S., Geissler, P.E., Kieffer, S.W., Leader, F.E., Davies, A.G., Barbinis, E., Mehlman, R., Segura, M., Shirley, J., and Soderblom, L.A., 2001. Io in the near infrared: NIMS results from the *Galileo* fly-bys in 1999 and 2000: Journal of Geophysical Research, v. 106, p. 33,053-33,078.

Lopes, R.M.C., Kamp, L.W., Smythe, W.D., Mouginis-Mark, P., Kargel, J., Radebaugh, J., Turtle, E.P., Perry, J., Williams, D.A., Carlson, R.W., Douté, S., and the *Galileo* NIMS and SSI Teams, 2001, Lava lakes on Io? Observations of Io's volcanic activity from *Galileo* NIMS during the 2001 fly-bys: Icarus v. 169, p. 140-174.

Lopes-Gautier R., Douté, S., Smythe, W.D., Kamp., L.W., Carlson, R.W., Davies, A.G., Leader, F.E., McEwen, A.S., Geissler, P.E., Kiefer, S.W., Keszthelyi, L., Barbinis, E., Mehlman, R., Segura, M., Shirley, J., and Soderblom, L.A., 2000, A Close-Up Look at Io from *Galileo*'s Near-Infrared Mapping Spectrometer: Science, v. 288, no. 5469, p. 1201-1204

Lunine, J.I., Stevenson, D.J., Physics and chemistry of sulfur lakes on Io: Icarus, v. 64, p. 345-367.

Matson, D.L., G.A. Ransford, and T.V. Johnson 1981. Heat flow from Io (J1): Journal of Geophysical Research, v. 86, p. 1664-1672

McEwen, A.S., D.L. Matson, T.V. Johnson, L.A. Soderblom 1985. Volcanic hot spots on Io: Correlation with low-albedo calderas: Journal of Geophysical Research, v. 90, p. 12,345-12,377.

McEwen, A.S., and 14 coauthors, 1998a, High-temperature silicate volcanism on Jupiter's moon Io: Science, v. 281, p. 87-90.

McEwen, A.S., and 13 coauthors, 1998b, Active volcanism on Io as seen by *Galileo* SSI: Icarus, v. 135, p. 181-219.

McEwen, A.S., and 25 coauthors, 2000, *Galileo* at Io: Results from high-resolution imaging: Science, v. 288, p. 1193-1198.

Milazzo, M.P., Keszthelyi, L. P., and McEwen, A.S., 2001, Observations and initial modeling of lava-SO_2 interactions at Prometheus, Io: Journal of Geophysical Research, v. 106, iss. E12, 33,121–33,127.

Moore, H.J., 1987, Geologic map of the Maasaw Patera area of Io, U.S. Geol. Surv. Misc. Invest. Series Map I-1851, 1:1,003,000, Reston, VA.

Naranjo, J.A., 1985, Sulphur flows at Lastarria volcano in the north Chilean Andes: Nature, v. 313, p.778-780.

NASA Press Release Image PIA00744.

Nash, D.B., Carr, M.H., Gradie, J., Hunten, D.M., and Yoder, C.F., 1986, Io. In Satellites (J.A. Burns and M.S. Matthews, Eds.), pp. 629-688, Univ. of Arizona Press, Tucson.

Nash, D.B., and Moses, J.I., 1988, Vacuum weathering of sulfur – temperature effects and applications to Io. Geophysical Research Letters, v. 15, p. 697-700.

Osashi, R., 1919, On the peculiar sulfur spherules produced in a crater lake of the volcano Shirane, in the province of Kozuke, Central Japan: Journal of the Mining College**,** Akita University, no 1, p 1-10.

Ohba, T., Hirabayashi, J., Nogami, K., 2000. D/H and 18O/16O ratios of water in the crater lake at Kusatsu–Shirane Volcano, Japan. Journal of Volcanology and Geothermal Research 97, 329–346.

Oppenheimer, C., and Stevenson, D., 1989, Liquid sulphur lakes at Poás volcano: Nature, v. 342, p. 790-793.

Oppenheimer, C., 1992, Sulfur eruptions at Volcán Poás, Costa Rica: Journal of Volcanology and Geothermal Research, v. 49, p. 1-21.

O'Reilly, T.C. and G.F. Davies, 1981, Magma transport of heat on Io: A mechanism allowing a thick lithosphere: Geophysical Research Letters, v. 8, p. 313-316.

Pasternack, G.B., and Varekamp, J.C., 1997, Volcanic lake systematics 1. Physical constraints: Bulletin of Volcanology, v 58, p. 528-538.

Phillips, C.B. 2000. *Voyager* and *Galileo* views of volcanic resurfacing on Io and the search for geologic activity on Europa. Ph.D. dissertation, 269 pp., Univ. of Arizona, Tucson.

Pieri, D.S., M. Baloga, R.M. Nelson, and C. Sagan, 1984, Sulfur flows of Ra Patera, Io: Icarus, v. 60, p. 685-700.

Prosser, J.T; Carr, Michael J., 1987, Poas Volcano, Costa Rica: geology of the summit region and spatial and temporal variations among the most recent lavas: Journal of Volcanology and Geothermal Research, v. 33, no. 1/3, p. 131-146.

Radebaugh, J, Keszthelyi, L.P., McEwen, A.S., Turtle, E.P/ Jaeger, W., and Milazzo, M., 2001, Paterae on Io: A new type of volcanic caldera? Journal of Geophysical Research: v. 106, no. E12, p. 33,005-33,020.

Radebaugh, J., Jaeger, W.L., Keszthelyi, L.P, Turtle, E.P., Milazzo, M.P., Perry, J., McEwen, R., Davies, A.G., Geissler, P., 2004, Relationships between paterae, mountains, and hotspots on Io from a global database. Lunar and Planetary Science XXXV.

Rathbun, J.A., J.R. Spencer, A.G. Davies, R.R. Howell, and L. Wilson 2002. Loki, Io: A periodic volcano, Geophysical Research Letters. Vol. 29 (10), doi: 10.1029/2002GL014747.

Rathbun, J.A., Spencer, J.R., Tamppari, L.K., Martin, T.Z., Barnard, L., and Travis, L.D., 2004, Mapping of Io's thermal radiation by the *Galileo* photopolarimeter–radiometer (PPR) instrument: Icarus, l. 169, iss 1, p. 127-139.

Rouwet, D., Taran, Y.A., Varley, N.R., 2004, Dynamics and mass balance of El Chichón crater lake, Mexico: Geofísica Internacional, v. 43, no. 3, p. 427-434.

Rowe G.L., Brantley, S.L., Fernandez, M., Fernandez, J.F., Borgia, A., Barquero, J., 1992a, Fluid-volcano interaction in an active stratovolcano: the crater lake system of Po is volcano, Costa Rica: Journal of Volcanology and Geothermal Research, v. 49, p. 23-51.

Rowe, G.L., Ohsawa, S., Takano, B., Brantley, S.L., Fernandez, J.F., Barquero, J.,1992b, Using crater lake chemistry to predict volcanic activity at Poás volcano, Costa Rica. Bulletin of Volcanology 54, 494–503.

Rymer, H., Cassidy, J., Locke, C.A., Barboza, M.V., Barquero, J., Brenes, J., and Van der Laat, R., 2000, Geophysical studies of the recent 15-year eruptive cycle at Poás volcano, Costa Rica: Journal of Volcanology and Geothermal Research, v. 97, p. 425-442.

Sagan, C. 1979. Sulfur flows on Io: Nature v. 280, p. 750-753.

Schaber, G.G., Arthur, D.W.G., 1980, Io; preliminary mapping of geologic units. NASA Technical Memorandum, Report: NASA TM-8235, no. 82385, p. 40-42.

Schaber, G.G., 1982, in Satellites of Jupiter Tucson, AZ, University of Arizona Press, 1982, p. 556-597, 942, 943

Schenk, P.M., and Bulmer, M.H., 1998. Origin of mountains on Io by thrust faulting and large-scale mass movements. Science, v. 279, p. 1514-1517.

Phillips, T., "Alien Volcano" NASA. 9 March, 2007

<http://science.nasa.gov/headlines/y2007/09mar_alienvolcano.htm>

Shoemaker, E.M., and Hackman, R.J. 1962. Stratigraphic basis for a lunar time scale. In The Moon (Z. Kopal, Z. and Z.K. Mikhailov, Eds.), p. 289-300, Academic Press, London.

Smith, B.A., Soderblom, L.A., Beebe, R., Boyce, J., Briggs, G., Carr, M., Collins, S.A., Cook II, A.F., Danielson, G.E., Davies, M.E., Hunt, G.A., Ingersoll, A., Johnson, T.V., Masursky, H., McCauley, J., Morrison, D., Owen, T., Sagan, C., Shoemaker, E.M., Strom, R., Suomi, V.E., and Veverka, J., 1979a, The Galilean satellites and Jupiter: *Voyager* 2 imaging science results: Science, v. 206, no. 4421, p. 927-950.

Smith, B. A.; Shoemaker, E. M.; Kieffer, S. W.; Cook, A. F., II, 1979b, The role of SO_2 in volcanism on Io: Nature, v. 280, p. 738-743.

"Poás Index of Monthly Reports" Smithsonian Museum of Natural History. Smithsonian Institution Global Volcanism Program Report. Last revised December, 2007. http://www.volcano.si.edu/world/volcano.cfm?vnum=1405-04=&volpage=var.

Spencer, J.R., Schneider, N.M., 1996, Io on the eve of the *Galileo* mission: Annual Review of Earth and Planetary Sciences, v. 24, p. 125-190.

Spencer, J.R., J.A. Rathbun, L.D. Travis, L.K. Tamppari, L. Barnard, T.Z. Martin, and A.S. McEwen, 2000, Io's thermal emission from the *Galileo* Photopolarimeter-Radiometer, Science v. 288, p. 1198-1201.

Spencer, J.R., Stern, S.A, Cheng, A.F., Weaver, H.A., Reuter, D.C., Retherford, K., Lunsford, A., Moore, J.M., Abramov, O., Lopes, R.M.C., Perry, J.E., Kamp, L., Showalter, M., Jessup, K.L., Marchis, F., Schenk, P.M., Dumas, C., 2007, Io volcanism seen by New Horizons: A major eruption of the Tvashtar volcano: Science, v. 318, no. 240, p. 240-243.

Tanaka, K.L. (Compiler), 1994, The Venus Geologic Mappers' Handbook, 2nd Edition, US Geological Survey Open-File Report 94-438, 66 p.

Takano, B., 1987, Correlation of Volcanic Activity with Sulfur Oxyanion Speciation in a Crater Lake: Science, v. 235, no. 4796, p. 1633-1635.

Takano, B., Saitoh, H., and Takano, E., 1994, Geochemical implications of subaqueous molten sulfur at Yugama crater lake, Kusatsu-Shirane volcano, Japan: Geochemical Journal, v. 28, p. 199-216.

Takano, B., Watanuki, K., 1990, Monitoring of volcanic eruptions at Yugama crater lake by aqueous sulfur oxyanions: Journal of Volcanology and geothermal research, v. 40., no. 1, p. 71-87.

Thomas, P.C., Davies, M.E., Colvin, T.R., Oberst, J., Schuster, P., Neukum, G., Carr, M.H., McEwen, A., Schubert, G., Belton, M.J.S., and the *Galileo* Imaging Team, 1998, The shape if Io from *Galileo* limb measurements: Icarus, v. 135, no. IS985987, p. 175-180.

Trunk, L., Bernard, A., 2008, Investigating crater lake warming using ASTER thermal imagery: case studies at Ruapehu, Poas, Kawah Ijen, and Copahue volcanoes: Journal of Volcanology and Geothermal Research, v. 178, iss. 2, p. 259-270.

Turtle, E.P., Jaeger, W.L., Keszthelyi, L.P., McEwen, A.S., Milazzo, M., Moore, J., Phillips, C.B., Radebaugh, J., Simonelli, D., Chuang, F., Schuster, P., and the *Galileo* SSI Team, 2001, Mountains on Io: High-resolution *Galileo* observations, initial interpretations, and formation models: Journal of Geophysical Research, v. 106, no. E12, p. 33,175-33,199.

Turtle, E.P., L.P. Keszthelyi, A.S. McEwen, J. Radebaugh, M. Milazzo, D. Simonelli, P. Geissler, D.A. Williams, J. Perry, W.L. Jaeger, K.P. Klaasen, H.H. Breneman, T. Denk, C.B. Phillips, and the *Galileo* SSI Team, 2004, The Final *Galileo* SSI Observations of Io: Orbits G28-I33: Icarus, v. 169.

Varekamp, J.C., Ouimette, A.P., Herman, S.W., Bermúdez, A., and Depino, D., 2001, Hydrothermal element fluxes from Copahue, Argentine: a "beehive" volcano in turmoil: Geology, v. 29, no. 11, p. 1059-1062.

Veeder, G.J., Matson, D.L., Johnson, T.V., Blaney, D.L., Goguen, J.D., 1994, Io's heat flow from infrared radiometry, 1983-1993: Journal of Geophysical Research, v. 99, no. E8, p. 17,095-17,165

Webster, J. D., Kinzler, R.J., and Mathez, E.A., 1999, Chloride and water solubility in basalt and andesite melts and implications for magmatic degassing: Geochimica et Cosmochimica Acta 63, 729–738.

Wilhelms, D.E., 1972, Geologic mapping of the second planet, U.S. Geol. Surv., Interagency Report, Astrogeology, 55.

Wilhelms, D.E., 1990, Geologic mapping, in Planetary Mapping, edited by R. Greeley and R.M. Batson, Cambridge Univ. Press, New York, 208-260.

Williams, D.A., J. Radebaugh, L.P. Keszthelyi, A.S. McEwen, R.M.C. Lopes, S. Douté, and R. Greeley, 2002, Geologic mapping of the Chaac-Camaxtli region of Io from *Galileo* imaging data: Journal of Geophysical Research, v. 107, no. E9, p. 5068, doi:10.1029/2001JE001821.

Williams, D.A., P.M. Schenk, J.M. Moore, L.P. Keszthelyi, E.P. Turtle, W.L. Jaeger, J. Radebaugh, M.P. Milazzo, R.M.C. Lopes, and R. Greeley, 2004, Mapping of the Culann-Tohil region of Io from *Galileo* imaging data: Icarus, v. 169.

Williams, D.A., Keszthelyi, L.P., Crown, D.A., Jaeger, W.L., Geissler, P.E., Schenk, P.M., and Becker, T.L., Techniques for the Global Mapping of Io using *Voyager* and *Galileo* datasets: Icarus (in press).

Williams, D.A., Keszthelyi, L.P., Crown, D.A., Yff, J.A., Jaeger, W.L., Schenk, P.M., Geissler, P.E., and Becker, T.L.: Volcanism on Io: New insights from global xgeologic mapping. Manuscript submitted to USGS planetary geologic mapping program for publication.

Xu, Y; Schoonen, M. A. A., Nordstrom, D. K., Cunningham, K. M., Ball, J. W., 2000, Sulfur geochemistry of hydrothermal waters in Yellowstone National Park, Wyoming, USA; II, Formation and decomposition of thiosulfate and polythionate in Cinder Pool: Journal of Volcanology and Geothermal Research, v. 97, iss. 1-4, p. 407-423.

Zolotov, M.Y., and Fegley Jr., B., 1998, Volcanic production of sulfur monoxide (SO) on Io: Icarus, v. 132, iss. 2, p. 431-434.

Zolotov, M.Y., and Fegley Jr., B., 2000, Volcanic degassing of hydrogen compounds on Io: Annual Lunar and Planetary Science Conference, March 13-17, Abstract no. 1186.

Appendix A

Properties of Sulfur and Sulfur Dioxide

Composition, including minor impurities in elemental sulfur, appears to be one of the important mechanisms responsible for color variations on Io. MacIntyre et al. (2000) conducted an experiment to investigate the effects on the color and spectral reflectance of sulfur caused by minor impurities. They used insights from reflectance spectra as well as the compositions of natural volcanogenic sulfur on Earth. Lab experiments consisted of sulfur specimens quenched from the molten state and containing controlled quantities of impurities. Their results showed that iron (as fine-grained inclusions of pyrite) produces green sulfur similar to that found naturally in some terrestrial volcanic crater lakes (MacIntyre et al., 2000).

These are somewhat similar to locations on Io. Other impurities added to sulfur (such as selenium and especially tellurium, chemically bonded or interacting with sulfur) and then quenched produced reddish or orange sulfur (MacIntyre et al., 2000). As little as one percent of these impurities may produce marked changes in the spectral reflectance and color of sulfur (Kargel et al., 2000).

The speciation (including oxidation state and molecular form) of sulfur, mineral stabilities, and exact reaction pathways of impurities depend on whether the system includes water (Kargel et al., 1999). Formation of impure sulfur does not require the involvement of water, but it likely does involve SO_2, the prevalent gas on Io (Kargel et al., 1999). Volcanic-hydrothermal systems on Earth that are rich in sulfur illustrate the potential for extreme concentrations of certain trace elements to a degree that they notably affect the sulfur already present (Kargel et al., 1999). On Io, the concentration mechanisms may be different, but contamination still appears to occur. Regions of extremely high temperatures on Io may mobilize a larger number of moderately volatile

elements in the vapor phase (such as arsenic), thereby generating greater chemical variety of heavy-metal sulfide sublimates (Kargel et al., 1999). Many of these sulfides may be intimately associated with sulfur sublimates and sulfur lavas.

Behavior of Sulfur

Molten sulfur exhibits varying behavior as a function of temperature (Figure A-1). Most molten substances (e.g. silicate magma) are fluid at high temperatures and become more viscous as they cool and approach their solidification point. Sulfur behaves differently, however. At 159.4°C (432 K), pure liquid sulfur undergoes a sudden increase in viscosity (Meyer, 1976) from ~10^{-2} to ~10^{2} Pa s, transforming a low-viscosity, fast-moving flow into a high-viscosity, slow-moving flow (Harris et al., 2000). High viscosity at temperatures over 159.4°C would virtually block the free passage of gases through a given liquid sulfur pool in pure sulfur (Takano et al., 1994).

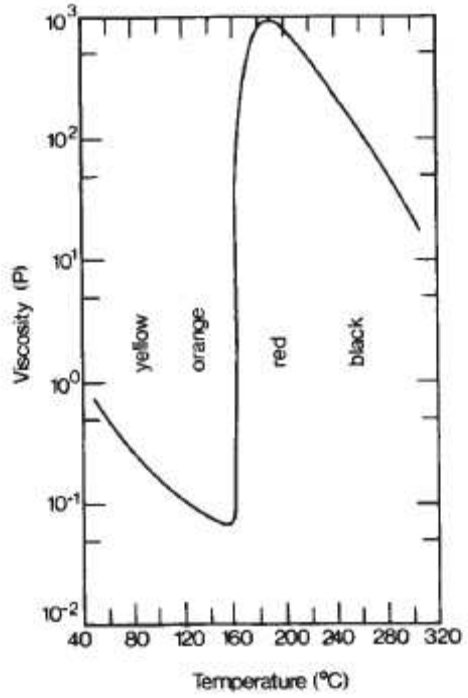

Figure A-1: The variation of viscosity and color of liquid sulfur with temperature (Naranjo, 1985).

The color and viscosity of sulfur is primarily a function of temperature, and both features are important in sulfur flow observations on Io's surface. Yellow α- and β-sulfur allotropes melt at 112.8–115.1 °C (385 – 388 K) and 114.6 – 119.6 °C (387 – 393 K), respectively (Meyer, 1976). With increasing temperature, the melt turns orange at ~133 °C (406K), red-orange at ~161 °C (434K), red at ~171 °C (444 K), and brown-black at ~221 °C (494 K), before reaching its boiling point of 444.6 °C (717 K) (Meyer, 1976; Pieri et al., 1984). Inversely, initially hot sulfur might start off chocolate-brown and turn red, orange and yellow as it cools.

Trace amounts of impurities, such as carbon, potassium or sodium, will change the color of sulfur to greens, tans and grays (Kargel et al., 1999). Minor impurities can also produce changes in the viscosity of molten sulfur and the elasticity of solid sulfur in the lab (see next section). Impurities might have a role in determining the morphology of Io's sulfur flows. The distribution and abundance of impurities likely relates to sublimation and volcanic processes. Chemical and spectral zonation around major volcanic vents on Io is also a possibility (Kargel et al., 1999).

Impurities and Io

Arsenic-bearing sulfur is discussed in Chapter 4 and arsenic is a likely impurity in Io's sulfur, as is selenium (Kargel et al., 1999). Chlorine has been detected on Io (Kuppers and Schneider, 2000; Lellouch et al., 2003). In pure form, S_2Cl_2 forms a yellow–red liquid and melts at 193 K, although when elemental sulfur is in excess, higher liquidus temperatures result (Lopes et al., 2004). Fumarolic selenides, tellurides, antimonides, halides, sulfates, and oxides also may occur on Io in considerable amounts (Kargel et al., 1999). In addition, Nash and Howell (1989) found evidence of the

presence of condensed H_2S on Io's surface. They add that it is sparse and variable, but can be widespread on the surface. These impurities contribute to the phase stabilities and liquid temperatures in complex sulfurous systems (Lopes et al., 2004). On Earth, the formation of native sulfur and of arsenic-bearing sulfur generally involves aqueous systems, such as in Yugama crater lake (Takano et al., 1994). In Io's case, there are other ways in which sulfur can form, and arsenic can concentrate in sulfur, in the absence of water. Both sulfur and arsenic are moderately volatile elements, with or without the presence of water, evidenced by heating experiments done on lunar samples in both wet and dry conditions (cf. Gibson and Hubbard, 1972). Takano et al. (1994) state that H_2S, arsenic (As), and SO_2 dramatically reduce the viscosity of liquid sulfur, especially above 159ºC (432K). At 187ºC (460K), the viscosity of pure sulfur is 920 poise, while that of H_2S-saturated sulfur is 0.51 poise at the same temperature. Similarly, the viscosity of sulfur with 0.2 percent As is much lower than pure sulfur. At temperatures higher than 159ºC (432K), which usually link to increasing volcanic activity at Yugama crater lake, viscosity would decrease noticeably.

Vacuum Experiments

Io is thought to have a surface atmospheric pressure with an upper limit of ~10^7 atm (10^4 Torr), comparable to a good laboratory vacuum (Nash, 1987). Nash (1987) conducted lab experiments to study the effect of vacuum sublimation (solid evaporation) on the surface texture and optical properties of the residual solid sulfur to compare to how the various colors of sulfur are produced on Io (Nash, 1987; Figure A-1).

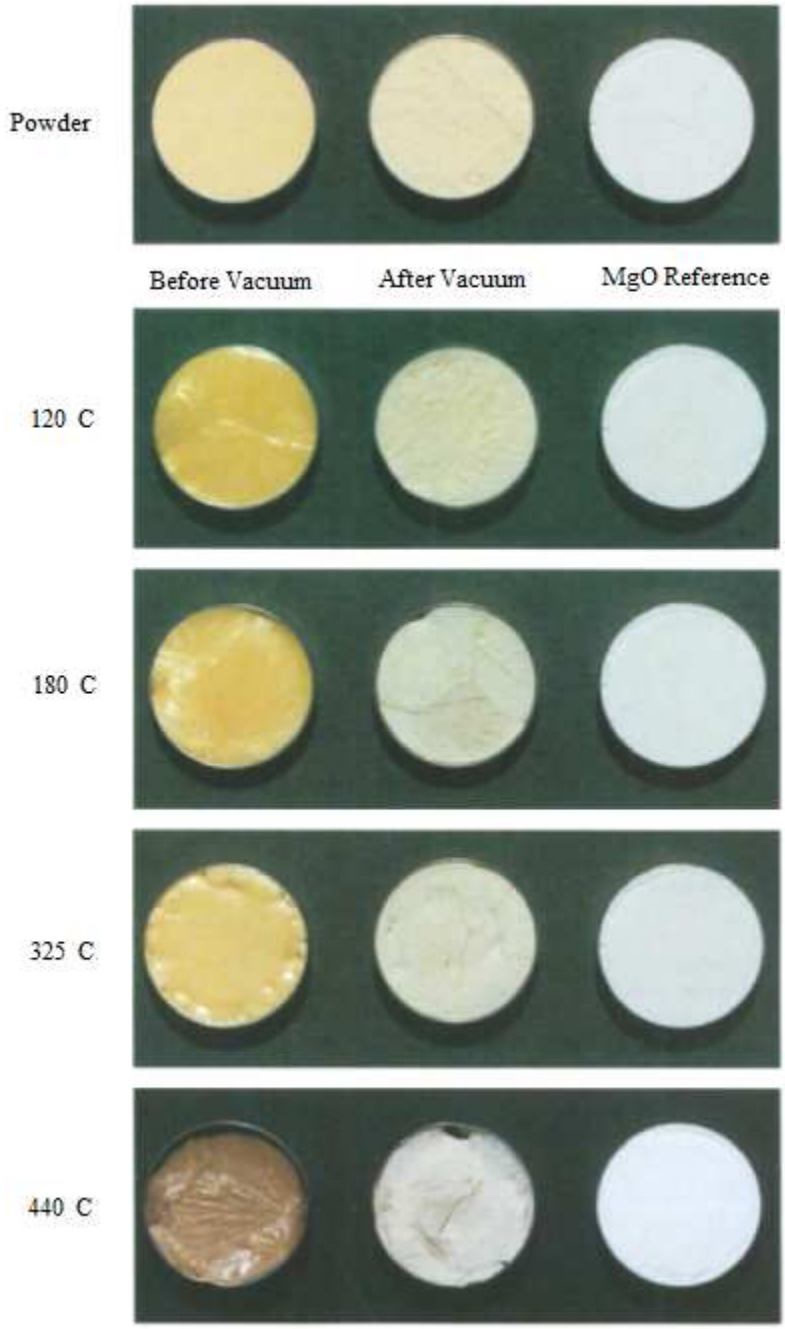

Figure A-1: Color of sulfur melt freezes and unmelted powder before and after vacuum sublimation. All samples are 1.9 cm in diameter. Each pair is compared to fresh smoked MgO, which is pure white, for color reference. Each picture shows a sulfur melt freeze at four different temperatures. (Note: These are reproductions of color photographs and do not accurately represent completely the 'true' color of the samples) (Modified by Nash 1987).

These pictures do not show the effects of impurities, however, and previous work with seleniferous sulfur show that colored forms of impure sulfur may be thermodynamically stable even to low temperatures, whereas pure sulfur in the lab or occurring naturally is white unless quenched or irradiated to a metastable colored form (Kargel et al., 1999).

Sulfur Dioxide

High-temperature hot spots are abundant on Io. Approximately 20 areas larger than 10^4 m^2 with temperatures exceeding ~1000 K are present across the globe at any given time. Sulfur boiling in a vacuum cannot get much hotter than about 500K (Lunine and Stevenson, 1985), so these particular hot spots cannot be due to pure sulfur volcanism (McEwen et al., 1997). An important property to note about sulfur dioxide is that, when heated above its critical temperature (157.12°C or 430.12K), it can only exist as a vapor regardless of pressure.